Genetic Mouse Models of Liver Disease: Potential Roles of Zhx2 (Afr1) and Afr2 in Damage and Regeneration

Courtney P. Turpin

University of Kentucky, courtney.turpin12@gmail.com

Author ORCID Identifier:

https://orcid.org/0000-0001-6299-8062

Digital Object Identifier: https://doi.org/10.13023/etd.2021.352

Right click to open a feedback form in a new tab to let us know how this document benefits you.

GENETIC MOUSE MODELS OF LIVER DISEASE:
POTENTIAL ROLES OF ZHX2 (AFR1) AND AFR2
IN DAMAGE AND REGENERATION

_____

DISSERTATION
_____

A dissertation submitted in partial fulfillment of the
requirements for the degree of Doctor of Philosophy in the
College of Medicine
at the University of Kentucky

By

Courtney Paige Turpin

Lexington, Kentucky

Director: Dr. Brett T. Spear, Professor of Microbiology, Immunology, and Molecular
Genetics

Lexington, Kentucky

2021

ABSTRACT OF DISSERTATION

GENETIC MOUSE MODELS OF LIVER DISEASE:
POTENTIAL ROLES OF ZHX2 (AFR1) AND AFR2
IN DAMAGE AND REGENERATION

The liver is the largest internal organ in mammals and responsible for carrying out various processes, including lipid and carbohydrate metabolism, detoxification of chemicals, and production of serum proteins. Liver damage, which can be caused by a variety of agents including viral infection, environmental toxins, alcohol and excessive dietary fats, can cause dysregulation of these critical functions, leading to worsening liver pathophysiology and impacting health. However, the liver has the remarkable ability to regenerate when damaged. Hepatocytes, which comprise a majority of liver cells, are relatively quiescent under healthy conditions. Upon injury, remaining hepatocytes can proliferate to recover from liver damage while performing their metabolic functions. Unfortunately, persistent injury can progressively lead to hepatitis, fibrosis, and ultimately end-stage liver disease, cirrhosis, and liver cancer. Overall, liver disease is the fifth leading cause of death worldwide and a growing healthcare problem in the United States and other western countries. A better understanding of liver regeneration could be used clinically to treat a wide range of liver diseases.

Studies in different mouse strains have provided genetic models to understand aspects of liver gene regulation and liver disease. Two regulators of the liver-derived serum protein alpha-fetoprotein (AFP), alpha-fetoprotein regulator 1 and 2 (Afr1 and Afr2), have been implicated to play a role in liver disease and regeneration. AFP is normally expressed in the fetal liver, silenced at birth, and reactivated in liver regeneration and liver cancer. Based on the unusually high AFP expression in adult BALB/cJ mice, our lab identified *Zinc Fingers and Homeoboxes 2* (*Zhx2*) as the gene responsible for the Afr1 trait. BALB/cJ mice contain a natural mutation in the *Zhx2* gene. Additional studies have shown that Zhx2 is involved in several liver diseases, including diet-induced fatty liver disease and hepatocellular carcinoma. In addition to these traits, BALB/cJ mice have been shown to have increased liver fibrosis after chronic treatment with the hepatotoxin carbon tetrachloride (CCl_4). The locus responsible for this trait, called Hepatic fibrosis 1 (Hfib1), was mapped to the same region of Chromosome 15 (Chr15) as Zhx2, but the Hfib1 gene has not been identified.

During liver regeneration after acute treatment with CCl_4, it was found that liver AFP mRNA levels were much higher in C3H/HeJ mice than in C57BL/6J mice. The locus that controls this strain-specific difference in AFP reactivation was called *Afr2*; C3H/HeJ and C57BL/6 mice are thought to contain the $Afr2^a$ and $Afr2^b$ alleles, respectively. The Afr2 locus has been mapped to Chr2, but the *Afr2* gene has not been identified.

This dissertation tested the hypothesis that Zhx2 is responsible for the Hfib1 trait in BALB/cJ mice. Using BALB/cJ mice and C57BL/6J mice with a targeted mutation in the Zhx2 gene, my data indicates that Zhx2 is not responsible for the Hfib1 trait. Mice with low Zhx2 expression did not have more significant inflammation, liver damage, or

fibrosis than mice with wild-type Zhx2 levels. These data suggest that another gene, presumably within the same region as Zhx2, is responsible for the Hfib1 phenotype in BALB/cJ mice. I also analyzed the Afr2 trait across several different strains of mice. My studies indicate that the strains 129X1/SvJ, C3H/HeJ, and DBA/2J contain the $Afr2^a$ allele, whereas mice in the C57 lineage (C57BL/6J, C57BL/6N, C57BL/10) contain the $Afr2^b$ allele. I also demonstrate that F1 offspring of 129X1/SvJ mice and C57BL/6J mice display an intermediate AFP reactivation phenotype, suggesting that the $Afr2^a$ and $Afr2^b$ alleles are co-dominant. These data provide the framework for future studies to identify the *Afr2* gene. Taken together, my results indicate that regulators of gene expression within the liver, as defined by differences within mouse strains, can provide insight into liver disease and regeneration.

KEYWORDS: Zinc Fingers and Homeoboxes 2, Alpha-fetoprotein, Afr2, Liver disease, Liver regeneration, Gene regulation

Courtney Paige Turpin
(Name of Student)

07/15/21
Date

GENETIC MOUSE MODELS OF LIVER DISEASE:
POTENTIAL ROLES OF ZHX2 (AFR1) AND AFR2
IN DAMAGE AND REGENERATION

By

Courtney Paige Turpin

Dr. Brett T. Spear
Director of Thesis

Dr. Howard Glauert
Director of Graduate Studies

07/15/21
Date

DEDICATION

To my parents and sister.

ACKNOWLEDGMENTS

TABLE OF CONTENTS

LIST OF TABLES

LIST OF FIGURES

CHAPTER 1. INTRODUCTION

1.1 <u>The Liver</u>

The liver is the largest internal organ in mammals and carries out numerous functions, including multiple metabolic processes such as glucose metabolism and lipid homeostasis. The liver is a primary location for converting glucose into glycogen for energy storage, enabling it to be utilized later [1], and is the setting for glycolysis, the process of breaking down glucose to generate ATP for energy [2]. The liver is also responsible for producing the key enzymes responsible for gluconeogenesis, including phosphoenolpyruvate carboxykinase (PEPCK), glucose-6-phosphatase, and fructose 1,6-biphosphate [3]. The liver is also the site for producing serum proteins, including numerous transport proteins such as albumin and alpha-fetoprotein (AFP) [4, 5].

The liver also is essential for both lipid production and breakdown. Hepatocytes within the liver can generate lipid from excess glucose by converting the pyruvate produced during glycolysis into acetyl-CoA. The process of *de novo* lipogenesis (DNL) can use this acetyl-CoA to create fatty acids [3, 6, 7]. β-oxidation within the hepatocytes can break down lipids for energy. β-oxidation reduces the lipid chain to make acetyl-CoA within the mitochondria or peroxisomes, which can then be used for ATP production [3, 6, 7].

The liver has an essential role in the metabolism and detoxification of numerous endogenous and exogenous compounds. Many enzymes within the liver are responsible for this process, categorized as Phase I, II, and III metabolizing enzymes. Phase I enzymes include those that have a primary role in oxidizing xenobiotics for subsequent breakdown [8, 9]. Cytochrome P450s (Cyp) are a family of proteins that are classified in

this group and are responsible for approximately 75-95% of the breakdown of the compounds that enter the liver from the bloodstream [10, 11]. Although this process has a vital role in eliminating toxic compounds, some of the metabolites from these reactions are more toxic than the original compounds [12, 13]. For example, environmental chemicals such as carbon tetrachloride (CCl_4) can be converted by *Cyp2E1* into highly reactive radical products trichloromethyl ($CCl_3\cdot$) and trichloromethyl peroxyl ($CCl_3OO\cdot$), both of which can cause oxidative damage to cellular components [12, 14]. Cyps can metabolize compounds into carcinogens, like Diethylnitrosamine (DEN), which can cause initiate tumorigenesis in the liver [15]. This occurs after *Cyp2E1* metabolizes DEN into the metabolite methyldiazohydroxide, which can create methylated guanine, creating DNA adducts [13]. In addition, Phase II metabolizing enzymes function as transferases and include the enzymes glutathione-s-transferases (GST), UDP-glucuronosyltransferases (UGT), sulfotransferases (SULT), among others [16]. Phase II enzymes can metabolize processes such as removing free radicals, conjugating to compounds to help with excretion, and metabolizing certain endogenous and exogenous compounds [9]. Phase III metabolizing enzymes serve as transporters for small and large compounds, including the transporters multidrug resistance-associated protein (MRP), P-glycoprotein (P-gp), and organic anion transporter (OAT) [17]. These transporters are important for shuttling nutrients and metabolites to targeted areas [18].

1.2 Liver Structure and Zonality

Liver functions depend on the overall liver structure and the various cell types that comprise this organ. Hepatocytes, which comprise roughly 80% of total liver volume and ~60% of liver cells, carry out a majority of liver functions, including carbohydrate,

lipid, and drug metabolism processes [2, 19]. The resident macrophages, called Kupffer cells, make up the largest population of macrophages in the body. Kupffer cells are essential for innate immune responses both locally and throughout the body [20, 21]. In addition to the Kupffer cells, other immune cells include NK, neutrophils, and dendritic cells that are important for responding to liver injury [22]. The hepatic stellate cells are generally quiescent pericytes that serve as the body's primary location for Vitamin A storage. However, persistent liver damage results in the activation of stellate cells into myofibroblasts, which produce several extracellular matrix proteins that contribute to liver fibrosis [23]. Liver sinusoidal endothelial cells line the blood vessels, playing an important role in regulating blood flow [24]. Cholangiocytes line the bile ducts and are critical for delivering bile acids from the liver to the GI tract [25].

The liver architecture is organized into repeating hexagonal units called lobules. At the middle of each lobule is the central vein, whereas each axis of the hexagon consists of a portal triad, which is comprised of a portal vein, hepatic artery, and bile duct [26] (Figure 1.1 A). On average, the distance between the central veins and portal triads spans roughly 15 hepatocytes. Blood enters the liver through the portal vein and hepatic artery rich in nutrients from the GI tract and oxygen from the heart, respectively. The blood then travels through a sinusoidal space between plates of hepatocytes lined by a layer of endothelial cells. During this time, the exchange of materials between the bloodstream and hepatocytes occurs [27] (Figure 1.1 B).

Many functions within the liver are managed, in large part, by a phenomenon called metabolic zonation. Hepatocytes within the liver carry out distinct functions based on their location within the liver lobule. The region surrounding the portal triad, called

zone 1 or the periportal region, contains hepatocytes that perform oxygen-dependent processes such as lipolysis, glucogenesis, and cholesterol synthesis [28, 29]. The region surrounding the central vein, called zone 3 or pericentral region, contains hepatocytes that carry out glycolysis and lipogenesis [28, 30] (Figure 1.1 C). Thus, the expression of subsets of hepatic genes is based on their location within the lobule [31]. Pericentrally expressed genes are involved in glycolysis (glyceraldehyde-3-phosphate dehydrogenase, glucose-6-phosphate isomerase), glutamine synthesis (glutamine synthetase), and drug metabolism (*Cyp2e1*) [30, 32]. In addition, periportal hepatocytes express genes crucial for gluconeogenesis (phosphoenolpyruvate carboxykinase, tyrosine aminotransferase), fatty acid oxidation (acetyl-CoA carboxylase), and bile acid formation (carnitine palmitoyltransferase 1) [29, 33-35]. Genes expressed in zone 2, which is intermediate between zones 1 and 3, are not known to have roles in specific metabolic processes but have recently been speculated to play a role in liver homeostasis [36]. Although some genes display strict or gradient zonal expression, some genes are not zonally expressed [28, 34]. A significant contributor to liver zonation is Wnt/β-catenin signaling. Active β-catenin protein is normally only found in pericentral hepatocytes; this restricted expression is due to certain Wnt proteins that are synthesized by endothelial cells surrounding the central veins. When the β-catenin gene is deleted in hepatocytes, pericentral genes are no longer expressed and liver regeneration is diminished [32]. In contrast, deletion of the Adenomatous Polyposis Coli (APC) gene, which is part of a complex that phosphorylates β-catenin in the periportal hepatocytes, leading to its degradation, results in expression on pericentral genes in all hepatocytes [33]. In a 2019

single-cell transcriptomics paper, reductions in zonal expression were found to be due to reductions in Wnt secretion and signaling [28].

1.3 Liver Injury and Disease

The adult liver is usually a quiescent organ under healthy conditions with very low cell turnover. However, hepatocytes can be damaged or killed by various agents, leading to liver disease. These agents include viral infection [primarily Hepatitis B Virus (HBV) and HCV], excessive alcohol consumption, obesity-related fatty acid accumulation, environmental toxins, pharmaceutical drugs, and autoimmune disorders. The liver normally recovers from acute damage with minimal impact on liver function, as described below, but persistent damage can lead to progressive liver disease. Persistent damage, such as HBV infection, can lead to inflammation that, if it persists, may lead to permanent damage and worsen liver function [37]. Chronic alcohol consumption can also lead to advanced liver disease. In 2017 the mortality rates for alcoholic liver cirrhosis were 6.8 per 100,000 people [38]. In recent years, obesity rates have been steadily rising, increasing many obesity-related diseases. Obesity can lead to a condition known as non-alcoholic fatty liver disease (NAFLD), which has rapidly become one of the most common causes of liver disease in the United States and other western countries. It is estimated that approximately 31% of adult Americans have some form of NAFLD [39]. Some autoimmune disorders, including autoimmune liver disease, primary sclerosing cholangitis, and primary biliary cirrhosis, can also cause patients to develop hepatitis that can further diminish liver function [40]. Immune cells can lose self-tolerance and target hepatocytes of immunocompromised patients, leading to worsening liver damage if persistent environmental or internal stimuli continue [41].

Liver disease can range in a spectrum of severity. Hepatic steatosis, the initial stage of liver disease, is hallmarked by lipid accumulation within the hepatocytes [42]. This increase in lipid droplets is associated with developing NAFLD, alcoholic, and drug-induced fatty liver disease [42]. Non-alcoholic fatty liver-caused steatosis develops as the result of multiple factors. The "multi-hit hypothesis" proposes that disease starts with an accumulation of lipids dependent on insulin resistance development [43]. The first hit results from insulin resistance and is associated with increases in DNL in the liver leading to elevated fatty acid production [44]. The secondary hit is when steatosis develops inflammation, a condition known as steatohepatitis. Oxidative stress is a crucial player in this second hit, causing the accumulation of proinflammatory cells and activation of stellate cells, which combine to promote fibrosis [45]. Alcoholic fatty liver disease can also cause steatosis and steatohepatitis by reducing β-oxidation, increasing fatty acid synthesis, and reducing fatty acid clearance [46]. Although cases are rare, drug-induced fatty liver can happen in various ways depending on the drug. Drugs can cause microvesicular steatosis by reducing β-oxidation, macrovesicular steatosis through triglyceride accumulation, and drug-induced steatohepatitis by increasing reactive oxygen species content [47].

Steatosis and steatohepatitis are often asymptomatic and can be reversed if the damaging agent is eliminated. More recent studies indicate that fibrosis can also be reversed through the removal of harmful stimuli. However, when damaging stimuli persist, inflammation and fibrosis can lead to a worsening of liver disease. Fibrosis is initially triggered by the amassing of inflammatory cells to the liver. These inflammatory cells produce chemokines, including transforming growth factor-beta (TGF-β), platelet-

derived growth factor (PDGF), and tumor necrosis factor-alpha (TNF-α), that activate

quiescent hepatic stellate cells [48, 49], which synthesize and secrete extracellular matrix

proteins such as collagen 1a1 (Col1a1) and alpha-smooth muscle actin (α-SMA) [50].

These components contribute to the build-up of fibrotic tissue in the liver. Continued

accumulation of fibrous materials can lead to cirrhosis. Liver cirrhosis, also known as

end-stage liver disease, is not reversible and results in an increased amount of damage

that disrupts the liver's normal functioning [51]. Cirrhosis is life-threatening, and

although certain drugs can reduce the progression of cirrhosis, the only real treatment is a

liver transplant.

The inflammatory environment of the cirrhotic liver promotes the development of

transformed cells that can lead to cancer. Liver cancer is one of the leading causes of

cancer deaths in the world [52, 53]. Although viral causes of liver cancer are decreasing,

cases associated with NAFLD are dramatically increasing. Hepatocellular carcinoma

(HCC) is a malignancy of the hepatocyte that comprises the most significant amount of

liver cancer cases [54]. Other lesser occurring instances include cancers of

cholangiocytes (cholangiocarcinoma) and blood vessels, but those result in far fewer

cases per year. Cancer of the liver and bile duct rank as the 5th highest cancer death in

American men and 7th in American women in 2021 [55], and liver cancer is projected to

be the second leading cause of cancer deaths by 2030 [56].

The liver is unique among internal organs in that it has the remarkable ability to

regenerate after damage. In times of damage, the liver activates signaling pathways to

restore liver mass. The healthy liver is relatively quiescent, and there is a low level of

hepatocyte loss and renewal. However, hepatocytes can replenish themselves by

activating signaling systems required for cellular regeneration via the re-entry of hepatocytes into the cell cycle when there is significant cell loss. In a rodent partial hepatectomy model, in which 70% of the liver is surgically removed, hepatocytes activate signaling molecules essential for hepatocyte proliferation, including Notch 1 and epidermal growth factors (EGF), within an hour [57, 58]. Following hepatocyte proliferation, the hepatocyte produces growth factors that stimulate angiogenesis and proliferation of other resident cells of the liver [59]. As a result, the liver can regenerate to its normal mass in response to the loss of liver cells within 7-10 days.

The liver can also regenerate in response to other models of liver injury, including those caused by hepatotoxins such as CCl_4. These types of liver damage are often zonal due to the zonal expression of liver enzymes and usually requiring a different regeneration response than partial hepatectomy. In most liver diseases or after any hepatocyte damage, regeneration is required. Initially, after damage, the remaining hepatocytes must receive signals to initiate their re-entry into the cell cycle. Priming the hepatocytes initializes this proliferation, which results in increased c-jun and c-myc signaling and production of the inflammatory cytokines TNF-α and interleukin-6 (IL-6) [60, 61]. This cascade of events enables the transition of quiescent hepatocytes to proliferative hepatocytes. After the initial priming phase, growth factors, including hepatocyte growth factor (HGF) and endothelial growth factor (EGF), are released, causing hepatocytes to enter the cell cycle [62, 63]. Hepatocytes can regenerate to replace damaged or apoptotic cells and then undergo the termination phase once the liver regains its normal size. Although there are many unknowns regarding the termination of hepatocyte regeneration, TGF-β signaling has a role in stopping hepatocyte proliferation

[64]. Through this multi-phased process, the liver can orchestrate the regeneration and repair of lost hepatocytes so that the liver can maintain metabolic functions when regaining normal liver size.

1.4 Models of Liver Disease

Animal models of liver disease have helped to elucidate disease mechanisms and potential therapeutic treatments, although many experimental models do not fully recapitulate liver disease in humans. Mouse models for NAFLD focus on either a genetics-based or a diet-based approach [65]. Alcohol liver disease (ALD) requires the administration of ethanol orally or through intragastric infusion [66]. One of the most commonly used liver fibrosis models requires administering the hepatotoxin CCl_4. As noted previously, the metabolism of CCl_4 by hepatic *Cyp2e1* produces free radicals causing significant damage and death of hepatocytes. A single dose of CCl_4 leads to transient damage, whereas ongoing treatment over six weeks leads to continual damage and regeneration and activation of stellate cells, ultimately resulting in fibrosis [67]. Another commonly used fibrosis model is bile duct ligation, a surgical method of liver damage and fibrosis caused by accumulating bile acids within the liver; an attractive aspect of this model is that it often mimics human liver disease [68]. Alternatively, diets used for NAFLD models like Methionine Choline Deficient diet (MCD) and high-fat (HF) diets can also cause liver damage, including fibrosis [69]. DEN is often used as a model for HCC, causing DNA damage that results in tumor development [13]. There is considerable debate in the liver field regarding different animal models and their ability to fully recapitulate all aspects of liver disease progression in humans.

9

1.5 Inbred mouse strains

Mice have been bred for interesting behavioral characteristics and coat colors for thousands of years [70]. More recently, mice have been bred for phenotypic traits that can be of use in biomedical research for studying human disease [70]. Through thousands of years of breeding, many strains and substrains have been developed which can possess unique characteristics [71] (Figure 1.2). One commonly studied difference between substrains is the difference between C57BL/6J and C57BL/6N mice. When the sequencing of these two mice was compared, 34 single nucleotide polymorphisms and 15 structural variants were identified [72]. C57BL/6J mice have a mutation in the nicotinamide nucleotide transhydronase, which has been found to contribute to impaired glucose tolerance and insulin secretion [73]. Research characterizing unique phenotypes between mouse strains can be used as a tool to identify genes that could be involved in disease.

1.6 Alpha-fetoprotein (AFP)

Alpha-fetoprotein (AFP) is a serum transport protein produced by hepatocytes in the developing fetal liver; in fact, AFP is the earliest known marker of hepatocytes as they differentiate from the foregut endoderm during development. AFP is highly similar in both structure and function to albumin, which is also expressed in the liver and is the major serum transport protein in adult mammals [53]. Comparisons of albumin and AFP genes indicate that they are evolutionarily related and have the same structure as other members of this gene family, which also includes alpha-albumin, Alpha-fetoprotein related gene, and vitamin D binding protein [74]. In addition to the fetal liver, AFP is expressed in the yolk sac and, to a lesser extent, in the lower gastrointestinal tract levels

[75]. AFP is the most abundant protein synthesized in the fetal liver, but its expression drops off dramatically within the first several weeks after birth [76]. AFP levels typically remain low in the healthy adult liver, but AFP expression transiently increases in the regenerating liver after liver damage and is often reactivated in liver cancer, including HCC. AFP serum levels often correlate with liver disease and HCC severity enabling the use of serum AFP as an important biomarker. [77]. In most models of toxic liver injury that requires hepatocyte regeneration, AFP levels were found to significantly increase [78]. In human cell culture lines, more significant cell proliferation and growth are associated with increased AFP expression [79]. Furthermore, poorer HCC prognosis and an increased chance of reoccurrence correlated with higher AFP levels [80]. Studies investigating AFP expression in the liver have found different mouse strains that have traits of AFP expression during development and disease, as described further below.

1.7 Alpha-fetoprotein regulator 1 (Afr1)/Zinc fingers and homeoboxes 2 (Zhx2/Afr1)

Due to high AFP levels in HCC, Olsson et al. analyzed serum AFP levels in 27 different strains of inbred mice; this study found that adult BALB/cJ mice had significantly higher AFP serum levels than all other mouse strains studies, including several other BALB/c substrains [81]. The elevated AFP levels in the postnatal liver of BALB/cJ mice were due to a recessive, monogenic trait, and the locus that controlled this trait was called in called alpha-fetoprotein regulator 1 (Afr1) [81]. After Tilghman and colleagues cloned the AFP gene, they showed increased liver AFP mRNA levels correlated with increased serum AFP [82]. Blankenhorn et al. found that the Afr1 locus was located on mouse Chromosome 15 close to the c-Myc gene [83]. Our lab further localized Afr1 to a small region of Chromosome 15, and analysis of genes in this region

found that a hypomorphic mutation in BALB/cJ Zinc fingers and homeoboxes 2 (Zhx2) gene was responsible for the Afr1 trait [84, 85]. The Zhx2 protein contains two zinc fingers and four homeodomains, suggesting that it functions as a transcription factor. This led us to propose that Zhx2 contributes to postnatal silencing of the AFP gene, and the Zhx2 mutation in BALB/cJ mice results in incomplete AFP repression [84]. In addition to AFP, Zhx2 represses the expression of other fetal liver genes that are often reactivated in liver disease and HCC, including Glypican 3 (Gpc3) and the long noncoding RNA (lncRNA) H19 [84, 86].

Zhx2 mutation serves as a possible candidate for several phenotypic traits that are seen in BALB/cJ mice (Figure 1.3). The lab of Jake Lusis found that BALB/cJ mice, when given a high-fat diet, had fewer atherosclerotic plaques than other mouse strains [87]. This trait, named Hyperlipidemia 2 (Hyplip 2), was mapped by quantitative trait locus QTL analysis to a region of chromosome 15 where Zhx2 is located. In a collaboration between our lab and the Lusis lab, it was found that the Zhx2 mutation in BALB/cJ mice was responsible for the Hyplip2 phenotype [88]. Our lab determined that BALB/cJ mice, when given a high-fat diet, showed higher lipid content in the liver and increased inflammation compared to mice with a wild-type Zhx2 gene [89]. These findings indicate that Zhx2 controls the developmental expression of target genes as well cardiovascular disease and diet-induced liver injury.

In the chronic CCl_4 liver fibrosis model, BALB/cJ mice were found to have greater liver damage, as judged by fibrotic injury, than other mouse strains [90, 91]. Using QTL analysis, this study concluded that the fibrosis phenotype was associated with several hepatic fibrosis (Hfib) loci. The most significant QTL, called Hfib1, was

localized to the same region of chromosome 15 as Zhx2. Since our lab showed that the *Zhx2* gene is mutated in BALB/cJ mice, this led us to hypothesize that Zhx2 is responsible for the Hfib1 trait and serves as a potential candidate for the increased fibrosis seen in BALB/cJ mice.

1.8 Alpha-fetoprotein regulator 2 (Afr2)

In an early study of liver regeneration using CCl_4, it was found that C3H/HeJ mice had significantly higher increased AFP expression compared to C57BL/6J [82]. This difference in AFP activation was a monogenic trait governed by a locus called alpha-fetoprotein regulator 2 (Afr2). The Afr2^a allele in C3H/HeJ mice was dominant over the Afr2^b allele found in C57BL/6J mice. Curiously, other genes that are targets of Zhx2, including H19 and Gpc3, also appear to be regulated by Afr2. The Afr2 locus was mapped to a region on mouse chromosome 2 [92], although it should be noted that this study, in contrast to earlier studies, suggested that the Afr2^a and Afr2^b alleles were co-dominant. Several candidate genes for Afr2 fall within this region of Chromosome 2 (Figure 1.4), but it is currently unknown what gene is responsible for the Afr2 phenotype.
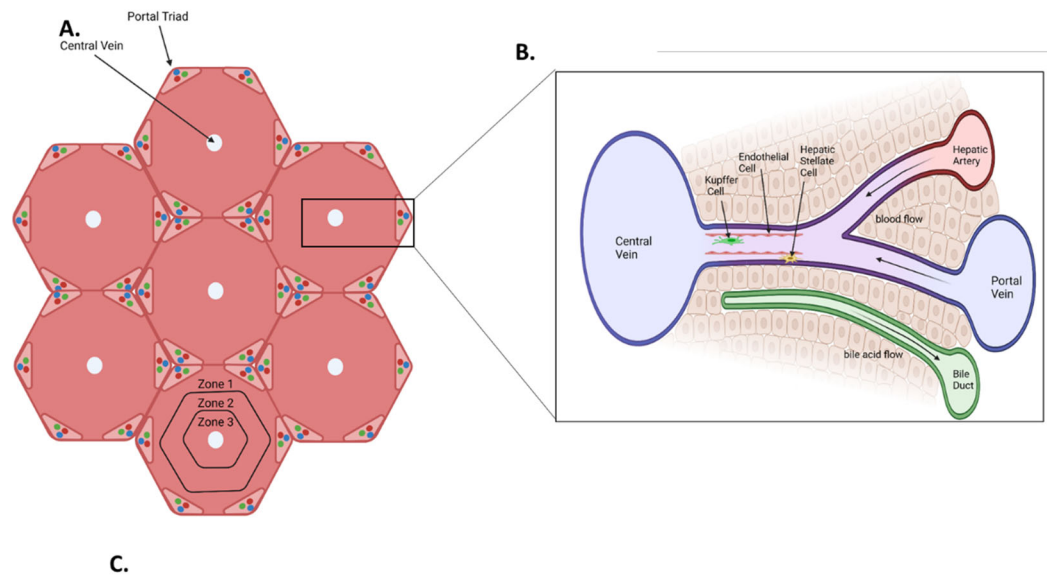
Figure 1.1 Liver Structure and Function.

(A). Layout of the liver lobule with six portal triads surrounding a single central vein.

Hepatocytes in the lobule are located in zone 1 (periportal region), zone 2, or zone 3

(pericentral region (B). Labeled image of how the liver lobule works, with blood flowing

from portal vein/hepatic artery, past the major cells of the liver, to the central vein; bile

flows in the opposite direction and exits the liver through the bile duct. Created with

BioRender.com
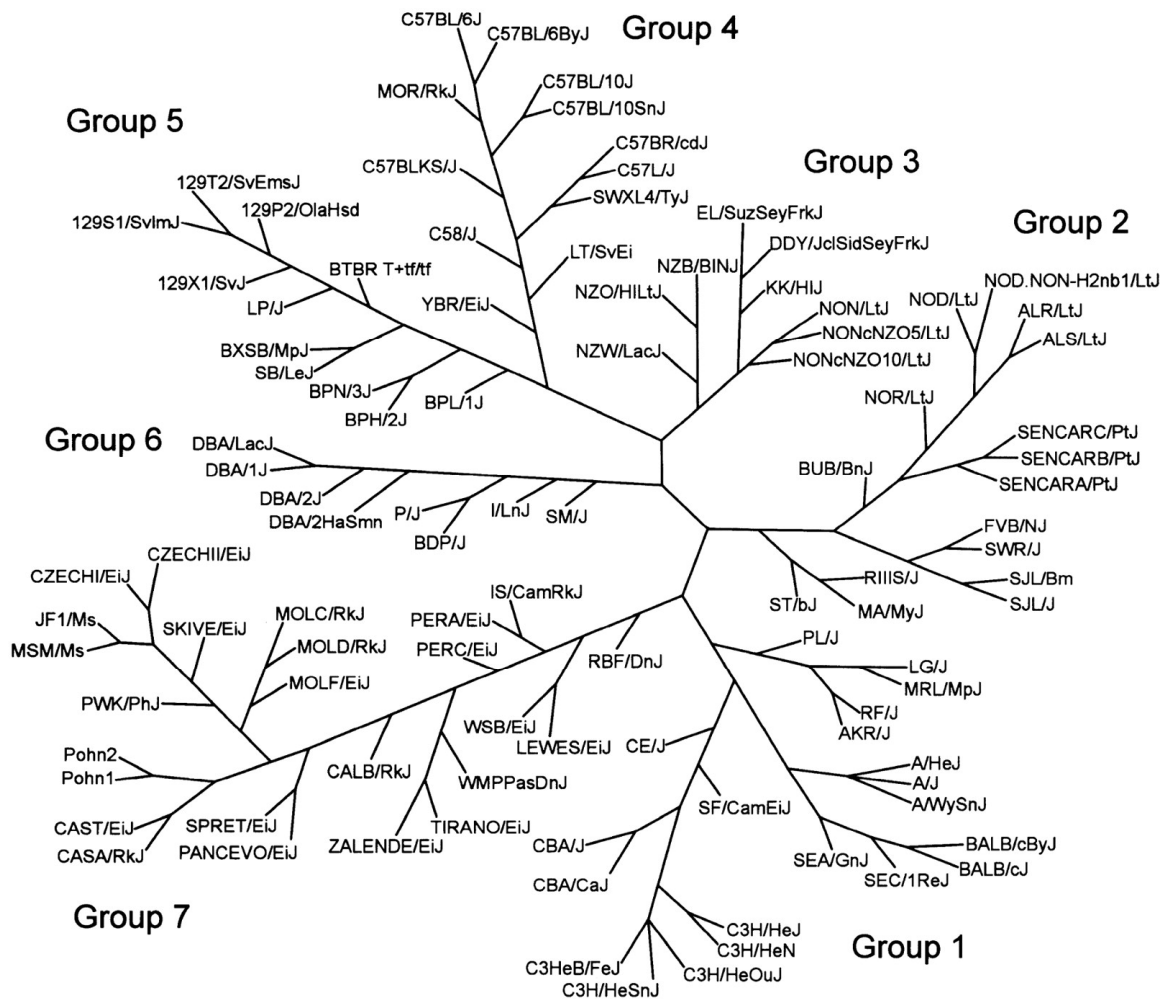
Figure 1.2 Phylogenetic tree of inbred mouse strains.

Figure from Petkov PM, Ding Y, Cassell MA, Zhang W, Wagner G, Sargent EE, Asquith S, Crew V, Johnson KA, Robinson P, Scott VE, Wiles MV. An efficient SNP system for mouse genome scanning and elucidating strain relationships. Genome Res. 2004 Sep;14(9):1806-11. doi: 10.1101/gr.2825804. PMID: 15342563; PMCID: PMC515327.
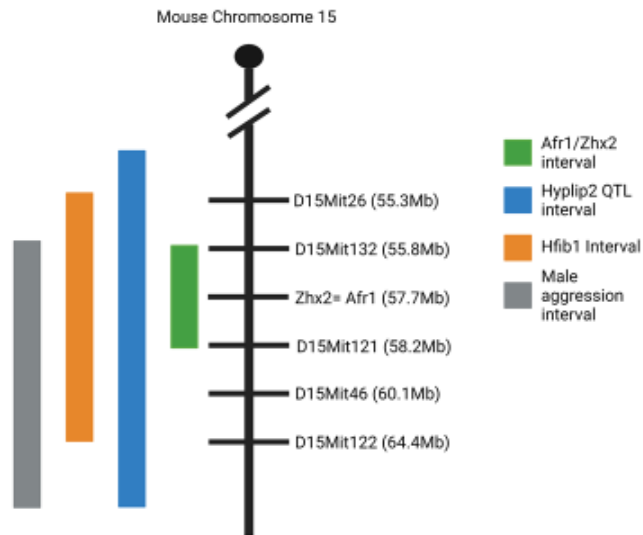
Figure 1.3 The Zhx2 gene co-localizes with several traits that are seen in BALB/cJ mice.

Quantitative trait analysis (QTL) mapping of the Zhx2/Afr1 interval responsible for increased AFP levels in BALB/cJ mice to a region on mouse chromosome 15 (green). Other phenotypic traits, including Hyplip2 (Blue), Hfib1 (Orange), and Male aggression (Gray), have been mapped to intervals overlapping the Zhx2 mutation. Created with BioRender.com.
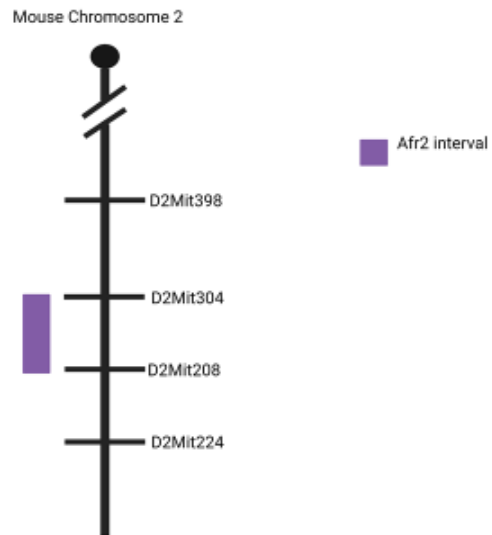
Figure 1.4 Mapping of Afr2 interval on chromosome 2.

Quantitative trait analysis (QTL) mapping of the Afr2 interval responsible for differing

AFP reactivation responses in liver regeneration in C3H/HeJ and C57BL/6J mice to a

region on mouse chromosome 2 (Purple). Created with BioRender.com

CHAPTER 2. MATERIALS AND METHODS

2.1 Mice

Mice were housed in the University of Kentucky Division of Laboratory Animal Research (DLAR) facility and were kept according to approved Institutional Animal Care and Use Committee (IACUC) protocols. Mice were purchased from The Jackson Laboratory, obtained from the Knockout Mouse Project (KOMP), or bred in-house. The mice were maintained on a 14/10 light/dark cycle and had access to ad libitum food and water.

2.2 Generating BALBcJ$^{Afr1/Afr1}$ and BALBcJ$^{WT/Afr1}$ mice

Male BALB/cJ mice, homozygous for the Zhx2^{Afr1} allele, were bred to female BALB/cByJ mice that were homozygous for wildtype Zhx2 allele (Zhx2^{WT}). Female offspring of this mating (BALB/cJ$^{WT/Afr1}$) were backcrossed to male BALB/cJ mice to obtain male and female BALB/cJ$^{Afr1/Afr1}$ and BALB/cJ$^{WT\,/Afr1}$ F$_2$ offspring. At 8-weeks of age, F$_2$ mice were administered carbon tetrachloride (CCl$_4$) injections as described below.

2.3 Generating Zhx2$^{WT/Afr1}$ and Zhx2$^{KO/Afr1}$ mice

Zhx2$^{Fl/Fl}$ mice were initially purchased from the Knockout Mouse Project Repository (KOMP) at the University of California- Davis. These mice had loxP sites flanking Zhx2 exon 3, which contains the entire Zhx2 protein-coding region. When exon three was deleted, it resulted in a complete deletion of the Zhx2 protein. Male BALB/cJ mice (BALB/cJ^{Afr1}) were bred to C57BL/6 mice heterozygous for the null mutation in the Zhx2 gene (Zhx2$^{WT/KO}$) to obtain male and female Zhx2$^{WT/Afr1}$ and Zhx2$^{KO/Afr1}$ offspring.

Mice were maintained until 8-weeks of age before starting CCl₄ injections as described below.

2.4 Afr2 Pilot Study

Male mice from six strains: 129X1/SvJ, C3H/HeJ, DBA/2J, C57BL/6J, C57BL/6NJ, and C57BL/10SnJ were obtained from the Jackson Laboratory and used to determine AFP activation during liver regeneration. Mice were maintained until 6-weeks of age before receiving a single dose of CCl₄ or mineral oil (MO), as described below.

2.5 Generating 129x1SvJxBL/6J

Breeding pairs of 129X1/SvJ and C57BL/6J mice were set up to generate male and female F1 offspring. Mice were maintained until 8-weeks of age before receiving a CCl₄ or MO injection.

2.6 Genotyping

When pups were approximately 14 days of age, mice were ear-tagged for experimental identification, and the removed ear skin was digested overnight at 55°C in 500 µL of tail lysis buffer (100 mM Tris-HCl pH 8.5, 5 mM EDTA, 0.2% SDS, 200 mM NaCl, 100 µg/mL Proteinase K). After digestion, samples were briefly vortexed, 500 µL of isopropanol was added, and samples were thoroughly mixed to precipitate the DNA. The DNA was pelleted by centrifugation at 13,000 g for 5 minutes, and the supernatant was decanted. The pellet was then washed with 500 µL of 75% EtOH and centrifuged at 13,000 g for 5 minutes, and the supernatant was again decanted. Tubes were inverted on a paper towel to dry for 30 minutes. Pellets were resuspended in 100 µL sterile ddH₂O. For BALB/cJ genotyping, 2 µL of DNA was added to a PCR mixture including 10 µL 2x

Dream Taq (Thermo Scientific), 7.4 µL of ddH$_2$O, 0.3 µL of the forward primer, and 0.3 µL of the reverse primer. Three PCR reactions were used to determine BALB/cJ genotyping by pairing primers for Afr1 and ETn3Flank to determine BALB/cJ^{WT} (no product for BALB/cJ^{Afr1}, amplicon 392 bp for BALB/cJ^{WT}), Afr1, and Afr2 to determine BALB/cJ^{Afr1} (amplicon 269 bp for BALB/cJ^{Afr1}, no product for BALB/cJ^{WT}), and ETn3Flank and Afr3 to determine BALB/cJ^{Afr1} (amplicon 786 bp for BALB/cJ^{Afr1}, no product for BALB/cJ^{WT}). For Zhx2 genotyping, 2 µl of DNA was added to a PCR mixture, including 10 µL of 2x Dream Taq (Thermo Scientific), 0.3 µL of Zhx25F primer, 0.3 µL of LAR3 primer, and 0.3 µL Zhx25R primer, and 7.1 µL water. The amplicons for Zhx2 genotyping will be 230 bp for the Zhx2 floxed allele (Zhx2^{KO}) and 385 bp for the wild-type Zhx2 allele (Zhx2^{WT}). Samples for BALB/cJ and Zhx2 genotyping underwent the same PCR protocol: 95°C for 3 minutes, 40 cycles of 95°C for 30 seconds, 55°C for 30 seconds, and 72°C for 40 seconds, and a final 72°C for 5 minutes. Primer sequences are listed in Table 2.1. The resulting product was mixed with 5 µL of 6x loading dye, and 10 µl was loaded on a 1% agarose gel along with 3ul of Gene Ruler 100bp Plus (Thermo Scientific). Samples were run at 150V for 30 minutes and visualized using an Amersham Imager 600 (GE).

2.7 Model for liver fibrosis (CCl$_4$)

At eight weeks of age, mice were selected to be injected intraperitoneally with 0.5 mL/kg of carbon tetrachloride (CCl$_4$) that was diluted 1:10 in mineral oil; control mice received mineral oil (MO) alone, prepared weekly. Each injection was performed with a 28G insulin syringe (Becton Dickinson). Mice were injected twice weekly for a total of 6

weeks (12 injections). Forty-eight hours after the final injection, at 7:00 AM, unfasted mice were euthanized.

2.8 Model for acute liver damage and regeneration (CCl4)

When mice were at 6 or 8 weeks of age, mice were injected intraperitoneally with 50 µL of a solution containing 2.5mg/kg CCl4 dissolved in MO or MO alone, as described above. Seventy-two hours after injection, at 10:00 AM, unfasted mice were euthanized.

2.9 Euthanasia and Tissue Collection

At the end of each animal study, individual mice were weighed and euthanized in a CO_2 chamber (30-70% cage volume/minute), followed by cervical dislocation. Blood was collected by cardiac puncture using a 1mL syringe with a 26G needle and allowed to clot for approximately one hour. Serum was obtained by centrifuging the blood sample at 13,000g for 3 minutes, and the clear supernatant was transferred to a new tube. The mouse liver was excised from the abdominal cavity, weighed, and cut into smaller sections. Sections were selected and placed in a cassette and placed in formalin for 3 days. After 3 days, cassettes were briefly washed in ddH_2O and stored in 70% ethanol until being paraffin-embedded. Liver sections were also frozen at -80°C in OCT for sectioning or frozen at -80°C in tubes for RNA and DNA extraction.

2.10 RNA extraction/cDNA/qPCR

Frozen liver sections that were stored at -80°C were weighed before RNA extraction. Tissue samples (~50 mg) were homogenized using a pestle in 200 µl RNAzol (Molecular Research Center Inc.). An additional 800 µL of RNAzol was added and

pipetted to mix. Sterile ddH$_2$O (400 μL) was added to the mixture, which was then mixed

vigorously for 15 seconds. After incubation at room temperature for 15 minutes, the

samples were centrifuged at 13,000 g for 15 minutes at 4°C. After centrifuging, the

sample tubes contained clear supernatant and a dark pellet. Careful to not disturb the

pellet, the supernatant (1.2 mL) was transferred to two tubes (600 μL/tube), followed by

the addition of equal parts of isopropanol. The solution was mixed and stored at 4°C for

approximately 1 hour, followed by centrifugation at 13,000 g for 10 minutes, and the

supernatant was decanted. The resulting pellet was washed twice with 75% ethanol,

centrifuged at 8,000 g for 5 minutes, and decanting ethanol in between washes. The pellet

was dried for approximately 15-30 minutes, and the RNA pellet was dissolved in sterile

100 to 200 μL of ddH$_2$O. RNA concentrations were determined using a Nanodrop

(Thermo Scientific). An aliquot of RNA was added to sterile ddH$_2$O to obtain a final

RNA concentration of 1 ug/10μl of ddH$_2$O. RNA was converted into cDNA using High-

Capacity cDNA Reverse Transcription Kit (Applied Biosystems). RNA (1 μg/10μL) was

combined with 2 μL of 10x buffer, 2 μl of random primers, 0.8 μL dNTPs, 1 μL of

reverse transcriptase, and 4.2 μL of ddH$_2$O. The mixture was placed into 0.2 mL PCR

tubes and subjected to the following PCR using a SimpliAmp Thermal Cycler (Applied

Biosystems): 25°C for 10 minutes, 37°C for 2 hours, 85°C for 5 minutes. Quantitative

Real-Time PCR (qPCR) assays were conducted using the following reagents: 10 μL of

SYBR Green PCR Supermix (Bio-Rad), 0.5 μL of 10 μM forward and reverse primers, 8

μL sterile ddH$_2$O, and 1 μL cDNA. qPCR was conducted using the CFX96 Real-Time

System (Bio-Rad) and was subjected for the following PCR: 95°C for 3 minutes, 40

cycles of 95°C for 10 seconds and 60°C for 45 seconds, followed by a melt curve, and

analyzed using the CFX Manager software (Bio-Rad). Oligonucleotide primer sequences are listed in Table 2.2. Transcript CT values were normalized to serine/arginine-rich splicing factor 4 (SFRS4), a splicing factor and housekeeping gene, and analyzed using the $\Delta\Delta$CT method [93]. SFRS4 has been found to be a more consistently expressed housekeeping gene compared to GAPDH in advanced liver diseases like HCC [94].

2.11 Histology

All histology was performed by the COBRE Pathology Research core or the Markey Cancer Center Biospecimen Procurement and Translational Pathology Shared Resource Facility. Formalin-fixed tissue samples were paraffin-embedded. Paraffin-embedded blocks were cut at 6-micron thickness on a microtome. Sections were adhered to slides and stained for Hematoxylin and Eosin, Sirius Red, or Masson Trichrome. Sirius Red was used for staining collagen and amyloid [95] and Masson Trichrome stains type I collagen [96]. Sirius red staining has been shown to have red fluorescence [97]. Sirius Red was quantified by using fluorescent microscopy and analyzed on ImageJ using mean fluorescence measurement.

2.12 TGF-β ELISA

Serum TGF-β levels were determined using the R&D Systems Quantikine ELISA TGF-β kit (DB100B) per the manufacturer's instructions. Serum samples were first activated by adding 40 µL of serum to a polypropylene tube along with 20 µL of 1N HCL. The sample was mixed and incubated for 10 minutes at room temperature. Samples were then neutralized by adding 20 µL of 1.2 N NaOH/0.5 M HEPES and mixed. After neutralization, the samples were further diluted with calibrator diluent: 40-fold dilution for mineral oil samples (5 µL in 195 µL) or 80-fold dilution for CCl$_4$ samples (2.5 µL in

197.5 µL). The ELISA plate was loaded with 50 µL of assay diluent and 50 µL of standard, controls, and activated samples. The plate was gently mixed, covered, and incubated at room temperature for two hours. After incubation, the ELISA plate was aspirated and washed four times with wash buffer, blotting on paper towels in between. After washing, 100 µL of TGF-β conjugate was added to each well, covered, and incubated for two hours at room temperature. The plates were then washed four times with wash buffer, blotting on paper towels in between. After the plate was blotted dry, 100 µL of the substrate solution was added, and the plate was protected from light for 30 minutes for color development. One hundred microliters of stop solution were added to each well to block further color development, and the optical density was measured at 450 nm and 560 nm as wavelength correction. The concentrations were calculated based on the standard curve and then multiplied by their dilution factor.

2.13 ALT Assay

Serum Alanine Aminotransferase (ALT) levels were assessed using an Alanine Aminotransferase Activity Kit (Sigma Aldrich) per the manufacturer's instructions. Samples were prepared by diluting 10 µL of MO-treated serum samples in 10 µL of ALT Assay Buffer or 5 µL of CCl_4-treated serum samples in 15 µL of ALT Assay Buffer into a 96-well microplate. This was followed by the addition of 100 µL of master reaction mix (86 µL ALT Assay Buffer, 2 µL Fluorescent Peroxidase Substrate, 2 µL ALT Enzyme Mix, 10 µL ALT Substrate). Samples were protected from light and incubated at room temperature for 3 minutes, followed by an initial reading at 560 nm. Samples were then incubated at 37°C and read again after 2, 5, 8, and 10 minutes. The final reading is the

last reading in which none of the samples exceed the standard curve. Calculations to determine ALT levels were performed as per the manufacturer's instructions.

2.14 AFP ELISA

Alpha-fetoprotein (AFP) serum levels were measured using the R&D Systems Quantikine ELISA Alpha-fetoprotein/AFP kit (MAFP00) according to the manufacturer's instructions. Serum samples were diluted 200-fold in calibrator diluent before use in the ELISA. Fifty microliters of assay diluent were added to the plate along with 50 µL of standard or diluted sample. The plate was covered and incubated at room temperature for 2 hours on a horizontal orbital microplate shaker at 500 rpm. After incubation, wells were aspirated and washed four times with wash buffer, blotting dry on paper towels between each wash. After the final blotting, 100 µL of Mouse AFP conjugate was added, and the plate was incubated for 2 hours at room temperature on the horizontal orbital microplate shaker. The plate was then aspirated and washed four times with wash buffer, blotting dry on paper towels between each wash. Next, 100 µL of substrate solution was added, and the plate was protected from light for 30 minutes as the color developed. To stop color development, 100 µL of stop solution was added to each well, and the optical density was read at 450nm and 560nm for wavelength correction. The concentrations were calculated based on the standard curve and multiplied by 200 to determine AFP levels in the undiluted serum samples.

2.15 Hydroxyproline

Hydroxyproline assays were conducted using the Hydroxyproline Colorimetric Assay Kit (BioVision). Samples were prepared by homogenizing 10mg of frozen liver tissue in 100 µL of ddH$_2$O. Tissue homogenate (~100 µL) was added to a glass tube with

a Teflon-lined cap, and 100 µL of concentrated HCl (12N) was added. The samples were hydrolyzed for 3 hours at 120°C. After hydrolysis, 40 µL of sample and the standard per manufacturer's instructions was added to a transparent flat-bottomed 96-well plate and dried in a 60°C oven for approximately 1 hour. While drying, hydroxyproline kit reagents were warmed to room temperature, and both the Chloramine T reagent and DMAB Reagent were prepared per the manufacturer's instructions. Chloramine T reagent (100 µL) was added to each standard and sample well and incubated at room temperature for 5 minutes. DMAB reagent (100 µL) was then added to each well. The plate was covered and incubated at 60°C for 1.5 hours. The plate was read on the GloMax Microplate reader (Promega) at 560 nm. The concentration was determined using the standard curve and calculated using the manufacturer's instructions.

2.16 Statistics

All data is represented as a mean +/- standard deviation. Descriptive statistics and Normality tests were performed on each data set using GraphPad Prism 9. A two-tailed t-test or one-way ANOVA with multiple comparisons of means was calculated using GraphPad Prism 9 when appropriate. Post-hoc tests were selected based on the distribution of the data. A p-value of less than 0.05 was considered significant. Outliers were detected using Grubbs' test using GraphPad Prism outlier calculator and not included in analysis.
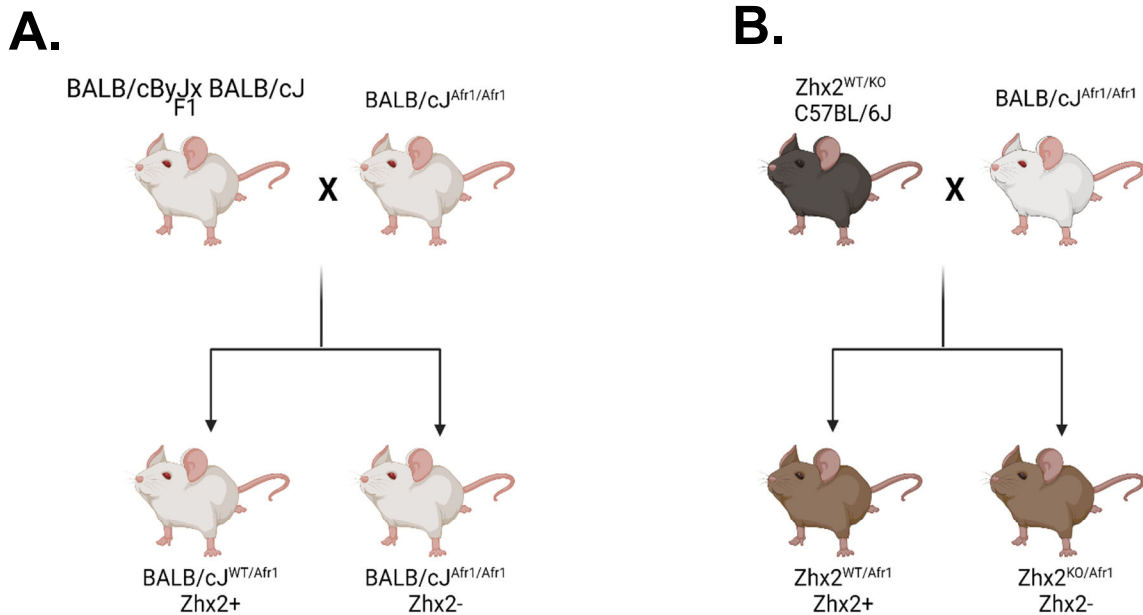
Figure 2.1 Breeding schematic for the Hfib1 project.

BALB/cJ mice that were homozygous for the Afr1 mutation were bred to F1 mice (BALB/cJ$^{Afr1/Afr1}$x BALB/cByJ$^{WT/WT}$) to obtain male and female mice that express normal Zhx2 levels (BALBcJ$^{WT/Afr1}$) and low Zhx2 levels (BALB/cJ$^{Afr1/Afr1}$) (A). BALB/cJ mice that were homozygous for the Afr1 mutation were bred to heterozygous Zhx2$^{WT/KO}$ on a C57BL/6J background to obtain male and female mice that express normal Zhx2 levels (Zhx2$^{WT/Afr1}$) and low Zhx2 levels (Zhx2$^{KO/Afr1}$) (B). Created on BioRender.com
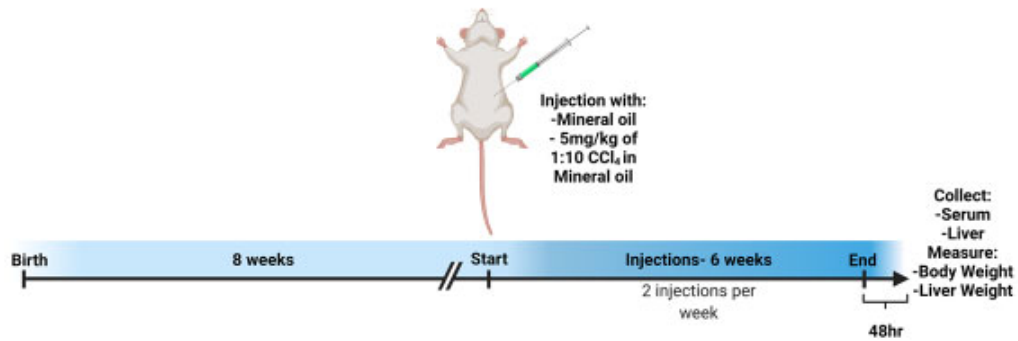
Figure 2.2 Experimental design for the Hfib1 study.

Mice selected for the Hfib1 experiment were maintained for 8 weeks until the start of the

injection series. Mice were then given either mineral oil or CCl$_4$ twice weekly for 6 weeks.

Forty-eight hours after the last injection, mice were euthanized, and tissues were collected.

Created on BioRender.com
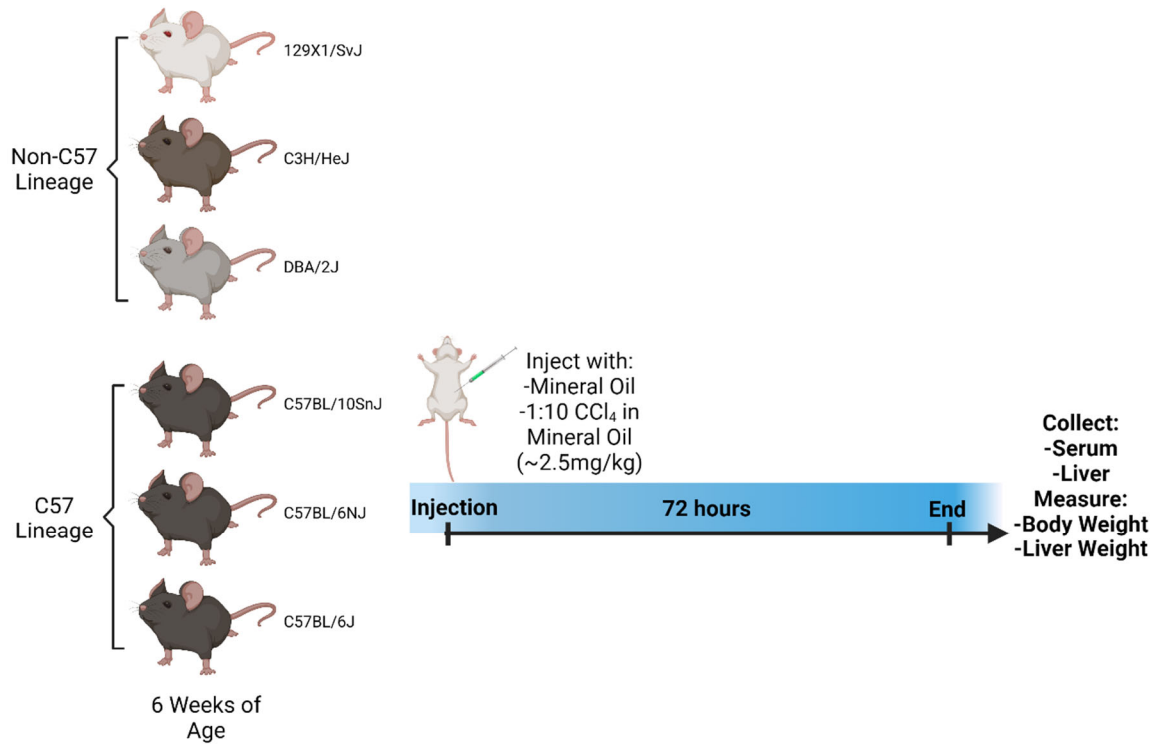
Figure 2.3 Experimental design for Afr2 pilot study.

Male mice from six mouse strains (129X1/SvJ, C3H/HeJ, DBA/2J, C57BL/10SnJ, C57BL/6NJ, and C57BL/6J) were injected once with either mineral oil or CCl_4. After 72 hours, mice were euthanized, and tissue was collected. Created on BioRender.com
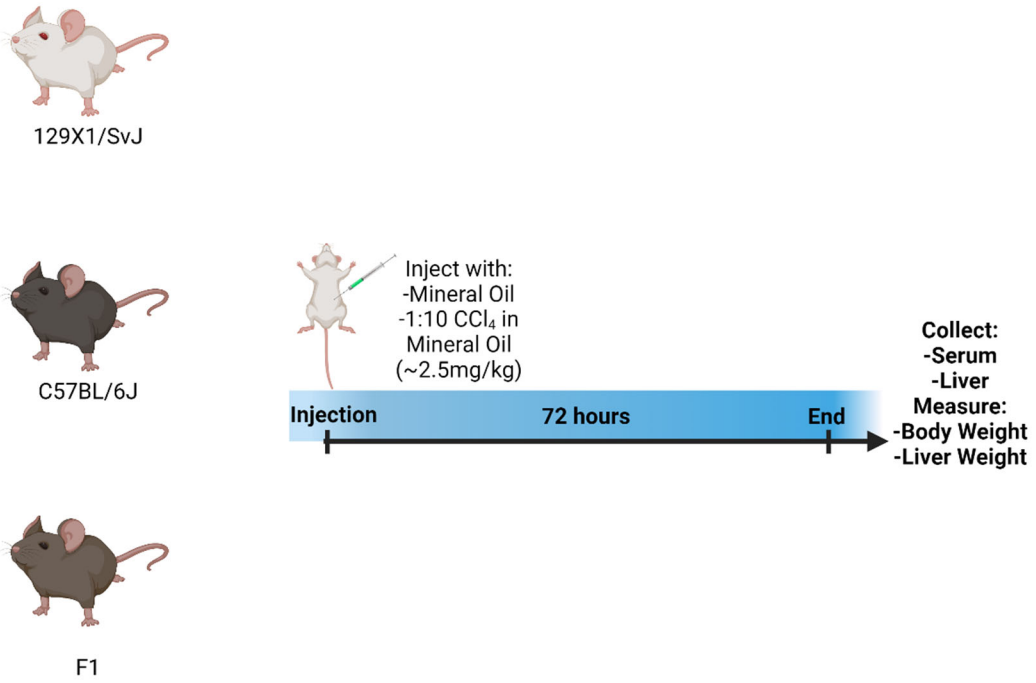
Figure 2.4 Experimental design for Afr2 full liver regeneration study.

129X1/SvJ, C57BL/6J, and F1 male and female mice were injected once with either mineral oil or CCl_4. After 72 hours, mice were euthanized, and tissue was collected. Created on BioRender.com

Table 2.1 Primers used for genotyping

Primer Number	Gene	Sequence
1651	Zhx25F	5' GGACCGAATCTCACTATTTAACTCA
1652	LAR3	5'ACAACGGGTTCTTCTGTTAGTCC
1654	Zhx25R	5' AGGCTGGCAGTGGGTTAGAAA
1043	Afr1	5' AACCCAAGTAGCAAGTGAGTGGTG
1044	Afr2	5' AACCCAAGTAGCAAGTGAGTGGTG
1045	Afr3	5' ATCTCTGGTCCAGTAGAAAGGTGC
1259	ETn3Flank	5' CCTATCTTGGTACCCTGATCAAGC

Primer number, gene names, and sequences of primers used for genotyping experimental

mice.

Table 2.2 Primers used for gene expression analysis

Primer Number	Gene	Sequence
1688	SFRS4f	5' CTCGCACAGAGTACAGACTTAT
1689	SFRS4r	5' TTGCGTCCCTTGTGAGCATCT
1588	Zhx2	5' GGACCGATATGATGCTTCCTGG
1589	Zhx2R	5' CGTTCAGGTTTTGCGTGGAGT
1806	Col1a1f	5' CATAAAGGGTCATCGTGGCT
1807	Col1a1r	5' TTGAGTCCGTCTTTGCCAG
2393	mCola1f	5' ACATGTTCAGCTTTGTGGACC
2394	mCola1r	5' TAGGCCATTGTGTATGCAGC
1775	SMAf	5' GTCCCAGACATCAGGGAGTAA
1776	SMAr	5' TCGGATACTTCAGCGTCAGGA
2624	mTimp1 F	5' CCCTTCGCATGGACATTTA
2625	mTimp1 R	5' AGATGCCAGAGATGCAAAG
1590	AFPrtF	5'CCGGAAGCCACCGAGGAGGA
1591	AFPrtR	5'TGGGACAGAGGCCGGAGCAG
1130	H19Ex2-U2	5'GGAGAGGACAGAAGGGCAGT
1131	H19Ex3-L3	5'GTTCAAGGTAGGGGGAGGAG
1604	LplrtF	5'TGGCTACACCAAGCTGGTGGGA
1605	LplrtR	5'GGTGGACGTTGTCTAGGGGGTAGT
1031	Gpc3URT	5'CTCCCAAGCAACGCCAATATAGAT
1032	Gpc3LRT	5'CTGATTCTTCATCCCGTTCCTTGC
1524	Cyp2E1F	5'CAAGTCTTTAACCAAGTTGGCAAA
1525	Cyp2E1R	5'CCACGATGCGCCTCTGA

Primer number, gene names, and sequences of primers used in qPCR gene expression analysis.

CHAPTER 3. THE INCREASED FIBROSIS PHENOTYPE, HFIB1, IN BALB/CJ MICE IS NOT DUE TO THE MUTATION IN ZHX2 (AFR1)

3.1 Introduction

Liver disease prevalence has a significant clinical impact, being the cause of two million deaths globally in 2010, with one million of those being due to liver cirrhosis [98]. Liver fibrosis and cirrhosis occur when harmful stimuli cause persistent damage, resulting in the production of extracellular matrix proteins. Fibrotic accumulation within the liver is initially triggered by hepatocyte damage. Studies have shown that in the case of lipotoxic injury, hepatocytes increase the release of vesicles that contains tumor necrosis factor apoptosis ligand (TRAIL), which activates macrophages [99]. These inflammatory cells then produce and release chemokines, including TGF-β, PDGF, and TNF-α [48, 49]. These chemokines bind to specific receptors on hepatic stellate cells to cause activation and promote the transition to myofibroblasts [100]. The activated extracellular matrix cells produce collagen 1a1 and α-SMA, contributing to the build-up of fibrosis in the liver [50]. As fibrotic tissue continues to accumulate in the liver, the organ may become cirrhotic, resulting in an increased amount of irreparable damage that disrupts the liver's normal functioning [51].

One specific mouse substrain, BALB/cJ, has been found to display several unique phenotypic traits. BALB/cJ mice exhibit persistent expression of fetal liver genes into adulthood [82, 84]. This trait is due to a hypomorphic mutation in the gene *Zinc fingers and homeoboxes 2* (*Zhx2*), located on chromosome 15, leading to significantly lower Zhx2 protein levels [82, 84]. BALB/cJ mice also display reduced atherosclerotic plaques than other mouse strains when fed a high-fat diet [87]. QTL analysis determined that this

33

trait, named Hyperlipidemia2 (Hyplip2), mapped to the same region on chromosome 15 as Zhx2. Further research using Zhx2 transgenic BALB/cJ mice determined that the Zhx2 mutation was responsible for the reduced atherosclerotic phenotype in BALB/cJ mice [88]. Although there were reductions in cardiovascular disease using the high-fat diet model, studies in our lab demonstrated that there was increased liver pathophysiology, including increased lipid accumulation and inflammation, in BALB/cJ mice fed a high-fat diet; this liver phenotype is due to the Zhx2 mutation [89]. Other traits in BALB/cJ mice, including altered expression of numerous Cyp and Major urinary proteins (Mup) genes, are due to the Zhx2 mutation in this strain [101, 102].

A screen for differences in liver fibrosis in a panel of mouse strains indicated that BALB/cJ mice exhibit increased liver fibrosis in a chemical-induced model of chronic liver damage. In this CCl_4 model, BALB/cJ mice were shown to have increased fibrotic histology and hydroxyproline levels compared to A/J and FVB/N mice [90, 91]. These studies found that when BALB/cJ mice were crossed with these other strains, the offspring had reduced fibrosis, indicative of a recessive mutation. QTL analysis revealed several loci that controlled increased fibrosis in BALB/cJ mice. The strongest of these QTLs, named Hepatic fibrosis 1 (Hfib1), mapped to the same region of chromosome 15 as Zhx2.

Although the Hfib1 region overlaps with Zhx2, the gene responsible for Hfib1 is unknown. Considering both the overlap of the Hfib1 interval with Zhx2 and the effect Zhx2 has on several liver phenotypes in BALB/cJ mice, we hypothesize that the Zhx2 mutation is responsible for the Hfib1 fibrosis phenotype in this mouse strain. To directly test this, I performed two complementation experiments using the chronic CCl_4-treated

34

liver fibrosis model. Although we hypothesized that there would be a difference in fibrosis markers between mice that did or did not express Zhx2, we observed no significant differences in fibrosis. This finding eliminates Zhx2 as a candidate Hfib1 gene and suggests that there is another gene in this region responsible for the increased fibrosis phenotype.

3.2 Results

As described in chapter 2, our lab obtained mice with a floxed allele of the Zhx2 gene from the KOMP. We have crossed this allele to C57BL/6J and to mice with the βactin-Cre transgene to delete Zhx2 exon 3 in all cells; the deleted allele will be referred to as Zhx2^{KO}.

Two complementation studies were performed. First, BALB/cJ mice (BALB/cJ$^{Afr1/Afr1}$) were bred to Zhx2$^{WT/KO}$ mice to generate offspring that were Zhx2$^{Afr1/WT}$ or Zhx2$^{Afr1/KO}$. We also bred BALB/cJ mice to BALB/cByJ, which is highly related to BALB/cJ but has a wild-type Zhx2 gene to obtain an F1. These F1 offspring were backcrossed to BALB/cJ to obtain F$_2$ offspring that were BALB/cJ$^{Afr1/WT}$ or BALB/cJ$^{Afr1/Afr1}$. PCR of genomic DNA was used to confirm the Zhx2 alleles in experimental animals. At 8 weeks of age, mice from each genotype received either MO or CCl$_4$ twice weekly for 6 weeks. Forty-eight hours after the final injection, livers and serum were collected. Analysis of liver RNA in both studies confirmed that Zhx2 mRNA levels in both male and female Zhx2$^{KO/Afr1}$ and BALB/cJ$^{Afr1/Afr1}$ mice were dramatically lower than Zhx2 levels in Zhx2$^{WT/Afr1}$ and BALB/cJ$^{WT/Afr1}$ littermates (Fig. 3.1 A-D). Zhx2 expression in male and female mice from both cohorts did not significantly change due to CCl$_4$ treatment (Fig. 3.1A-D).

With confirmation that Zhx2 expression was reduced in these mice as expected, liver damage was assessed using histological staining. The overall liver damage and fibrosis observed in CCl_4-treated mice was assessed using hematoxylin & eosin, Masson trichrome, and Sirius red staining (Fig. 3.2 A-D). Although it was seen that CCl_4-treated mice displayed increased liver damage and fibrosis, histological results show that differences in Zhx2 expression did not alter the fibrosis levels, as determined histologically, when mice were treated chronically with CCl_4 (Fig. 3.2 A-D). Initial quantification of Sirius Red staining revealed no significant difference in average fluorescence except female $Zhx2^{KO/Afr1}$ when compared to $Zhx2^{WT/Afr1}$ treated with CCl_4 (Figure 3.3 A-D). These results will further need to be confirmed by a pathologist and quantified using fluorescent microscopy.

In addition to histological assessment, mRNA expression levels of fibrosis markers associated with fibrosis were also analyzed. Alpha smooth muscle actin (Gene: ACTA2) mRNA expression levels were found to be substantially higher in CCl_4-treated compared to MO-treated mice in male and female mice of both cohorts (Fig. 3.4 A-D). A similar pattern was observed when Collagen1a1 mRNA levels were analyzed; levels increased in both male and female CCl_4-treated mice compared to MO controls but were not affected by Zhx2 levels (Fig 3.5. A-D). Timp1, which regulates matrix metalloproteinases, was also analyzed. Timp1 mRNA levels also increased in CCl_4-treated mice but were not affected by Zhx2 levels (Fig. 3.6 A-D). Hydroxyproline is a major component of collagen and can be used to measure collagen levels [103]. In previous studies identifying the Hfib1 region, hydroxyproline has been used as a marker of fibrosis [90]. Hydroxyproline levels were also assessed in these experimental mice

using a colorimetric kit, showing no significant changes regardless of treatment or Zhx2 expression (Figure 3.7).

Increased inflammation is a hallmark of liver disease, including liver fibrosis. We, therefore looked at several inflammatory cytokines in these experimental mice. Levels of Tumor Necrosis Factor α (TNFα) and Transforming Growth Factor-β (TGF-β) were assessed in all groups. In Zhx2$^{WT/Afr1}$ and Zhx2$^{KO/Afr1}$ mice, TNFα mRNA levels only differed between Zhx2$^{KO/Afr1}$ CCl4 and MO-treated male mice (Fig. 3.8 A-B). In BALB/cJ$^{WT/Afr1}$ and BALB/cJ$^{Afr1/Afr1}$ mice, there were no significant changes in TNFα expression regardless of treatment or sex (Fig. 3.8 C-D). However, TGF-β mRNA levels were higher in the male and female Zhx2$^{WT/Afr1}$, Zhx2$^{KO/Afr1}$, BALB/cJ$^{WT/Afr1}$, and BALB/cJ$^{Afr1/Afr1}$ mice treated with CCl4 than MO-treated mice, but only significantly in male and female Zhx2$^{WT/Afr1}$, male Zhx2$^{KO/Afr1}$, and male BALB/cJ$^{Afr1/Afr1}$ (Fig. 3.9 A-D). Zhx2 expression did not significantly change TGF-β mRNA levels. Serum levels of TGF-β were assessed using ELISA. Regardless of treatment or Zhx2 expression, TGF-β levels did not significantly differ for all mice (Fig. 3.10 A-D).

In addition to assessing fibrosis and inflammation, mouse serum was analyzed for alanine aminotransferase (ALT) levels. ALT levels serve as a serum biomarker for liver damage, being released from damaged hepatocytes into the bloodstream [104]. When the mouse serum was assayed for ALT levels, male and female Zhx2$^{WT/Afr1}$ and Zhx2$^{KO/Afr1}$ mice treated with CCl4 had significantly higher ALT levels than mice treated with MO (Fig. 3.11 A-B). Male BALBcJ$^{WT/Afr1}$ and BALBcJ$^{Afr1/Afr1}$ treated with CCl4 also have significantly higher ALT levels than mineral oil-treated (Fig. 3.11 C). Unexpectedly, Female BALBcJ$^{WT/Afr1}$ and BALBcJ$^{Afr1/Afr1}$ treated with mineral oil had significantly

higher ALT levels than the CCl$_4$-treated mice (Fig. 3.11 D). There was no significant

difference in ALT levels regardless of Zhx2 expression in male or female mice.

3.3 Discussion

Studies described in this chapter tested the hypothesis that Zhx2 was responsible

for the Hfib1 phenotype that was previously described in BALB/cJ mice. We used two

genetic complementation approaches to test this directly. The first used BALB/cJ and

C57BL/6J mice that have a null mutation in the Zhx2 gene. The second was a cross

between two highly related BALB/c substrains, one with a hypomorphic Zhx2 mutation

(BALB/cJ) and the second with a wild-type Zhx2 gene (BALB/cBYJ). Analysis of

mRNA levels confirmed that dramatically reduced Zhx2 levels were observed in

Zhx2$^{\text{Afr1/Afr1}}$ and Zhx2$^{\text{Afr1/KO}}$ mice compared to their Zhx2$^{\text{Afr1/WT}}$ littermates in both

cohorts. Chronic CCl$_4$ treatment did promote fibrosis in male and female mice in both

cohorts as determined by histological analysis, expression of the fibrotic genes ACTA2,

Col1a1 and TIMP1, TGFβ and TNFα levels, and serum ALT levels. However, the

presence or absence of Zhx2 did not impact the severity of fibrosis as judged by these

markers. Based on these results, we were not surprised that liver hydroxyproline levels

were not affected by the absence of Zhx2. However, we did anticipate that

hydroxyproline levels would be higher in CCl$_4$ treated mice than in MO controls and

cannot explain why there were no differences in these two treatment groups. Since there

are noticeable differences in liver histology, it is possible that the assay was not sensitive

enough to determine changes in hydroxyproline levels within the livers of control and

treated mice.

Data from this study indicate that the Afr1 mutation in Zhx2 is not responsible for the Hfib1 phenotype. This would suggest that another candidate gene within the Hfib1 region could account for the Hfib1 trait. This region houses several genes involved in liver disease, including Tnfrsf11b, Colec10, DEPTOR, A1bg, Col14a1, and Has2. Tnfrsf11b, or osteoprotegerin, was reduced in the circulating serum in individuals with NAFLD [105]. In HCC, collectin liver 1 (Colec10) and alpha-1-beta glycoprotein (A1bg) were found to be reduced [106] [107]. Poorer prognosis in HCC has also been linked to the expression of the inhibitor of mTOR signaling DEPTOR [108]. Increases in both collagen 14a1 (Col14a1) and hyaluronan synthase 2 (Has2) have been found in liver fibrosis [109, 110]. Further experiments looking at the expression of, or polymorphisms within, these other genes could be analyzed to determine if any are viable candidates for Hfib1. Additionally, the CCl4 data from this experiment is highly variable, which might make any slight difference we see between the wild-type and Zhx2 deficient mice from reaching significance. Modifications in CCl4 administration or altering the fibrosis model might lead to more consistent results.
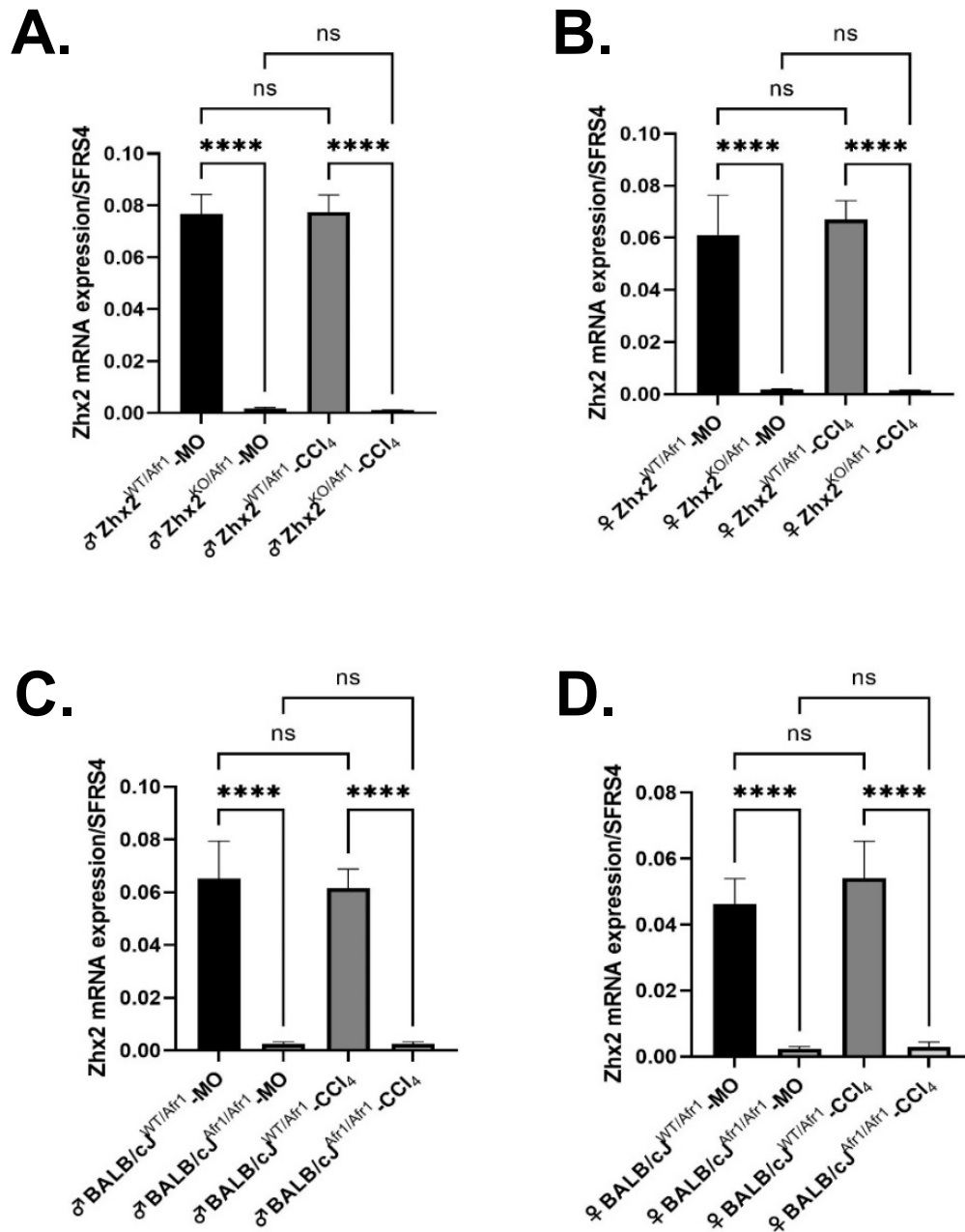
Figure 3.1 Mice homozygous for the Zhx2^{Afr1} mutation or heterozygous Zhx2$^{Afr1/KO}$ mice display reduced Zhx2 mRNA levels.

Zhx2 mRNA expression in male Zhx2$^{WT/Afr1}$ (n=6) or Zhx2$^{Afr1/Afr1}$ mice (CCl$_4$ n=5, MO n=6), treated with either CCl$_4$ or MO (A). Zhx2 mRNA expression in female Zhx2$^{WT/Afr1}$

(CCl$_4$ n=5, MO n=6) or Zhx2$^{Afr1/Afr1}$ mice (CCl$_4$ n=5, MO n=4), treated with either CCl$_4$ or MO (B). Zhx2 mRNA expression in male BALB/cJ$^{WT/Afr1}$ (CCl$_4$ n=6, MO n=5) or BALB/cJ$^{Afr1/Afr1}$ mice (n=6), treated with CCl$_4$ or MO (C). Zhx2 mRNA expression levels in female BALB/cJ$^{WT/Afr1}$ (n=5) or BALB/cJ$^{Afr1/Afr1}$ mice (CCl$_4$ n=5, MO n=6) (D). *p<0.05, **p<0.01.

A.

| ♂Zhx2^{WT/Afr1}-MO | ♂Zhx2^{KO/Afr1}-MO | ♂Zhx2^{WT/Afr1}-CCl$_4$ | ♂Zhx2^{KO/Afr1}-CCl$_4$ |

B.

| ♀Zhx2^{WT/Afr1}-MO | ♀Zhx2^{KO/Afr1}-MO | ♀Zhx2^{WT/Afr1}-CCl$_4$ | ♀Zhx2^{KO/Afr1}-CCl$_4$ |
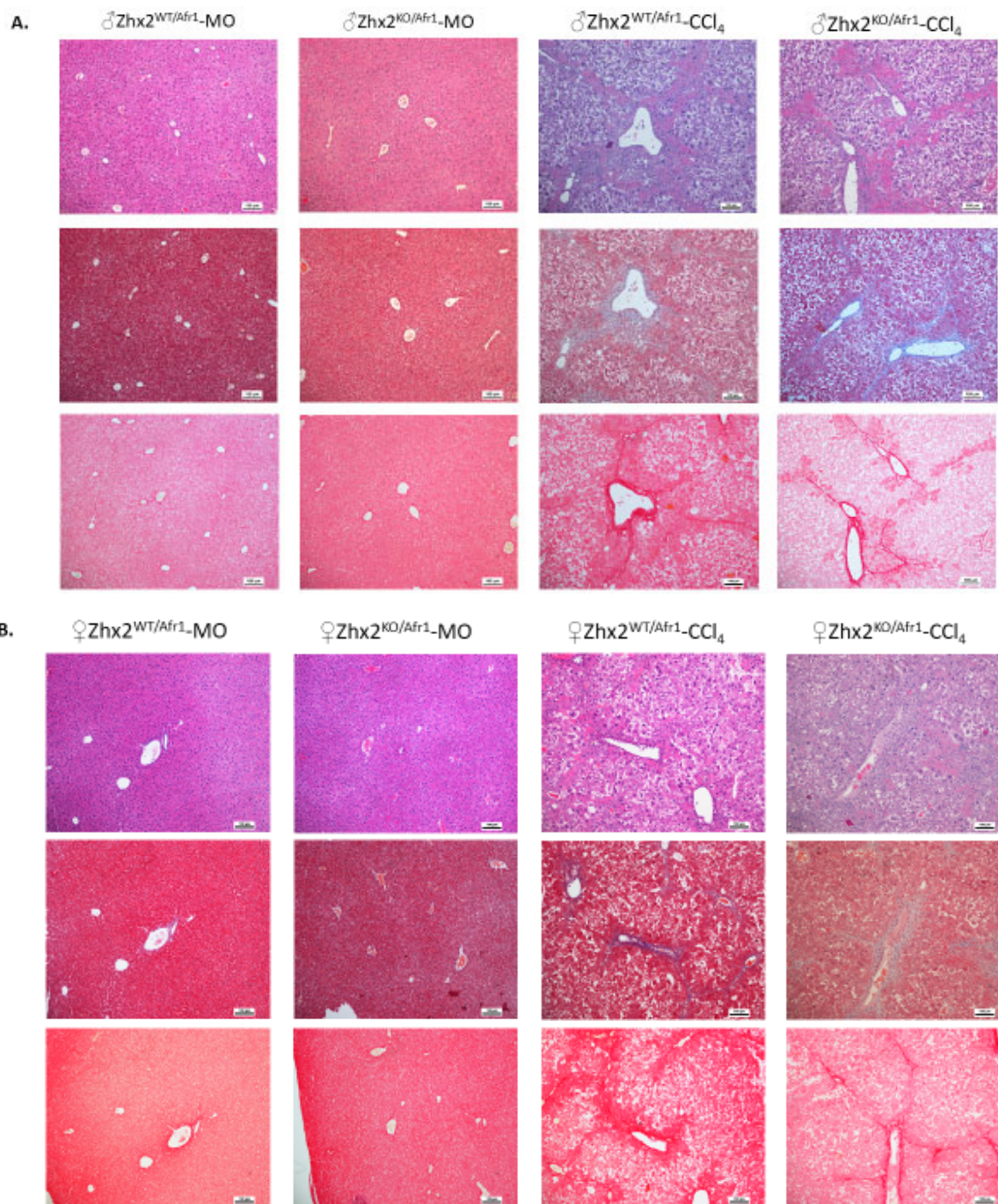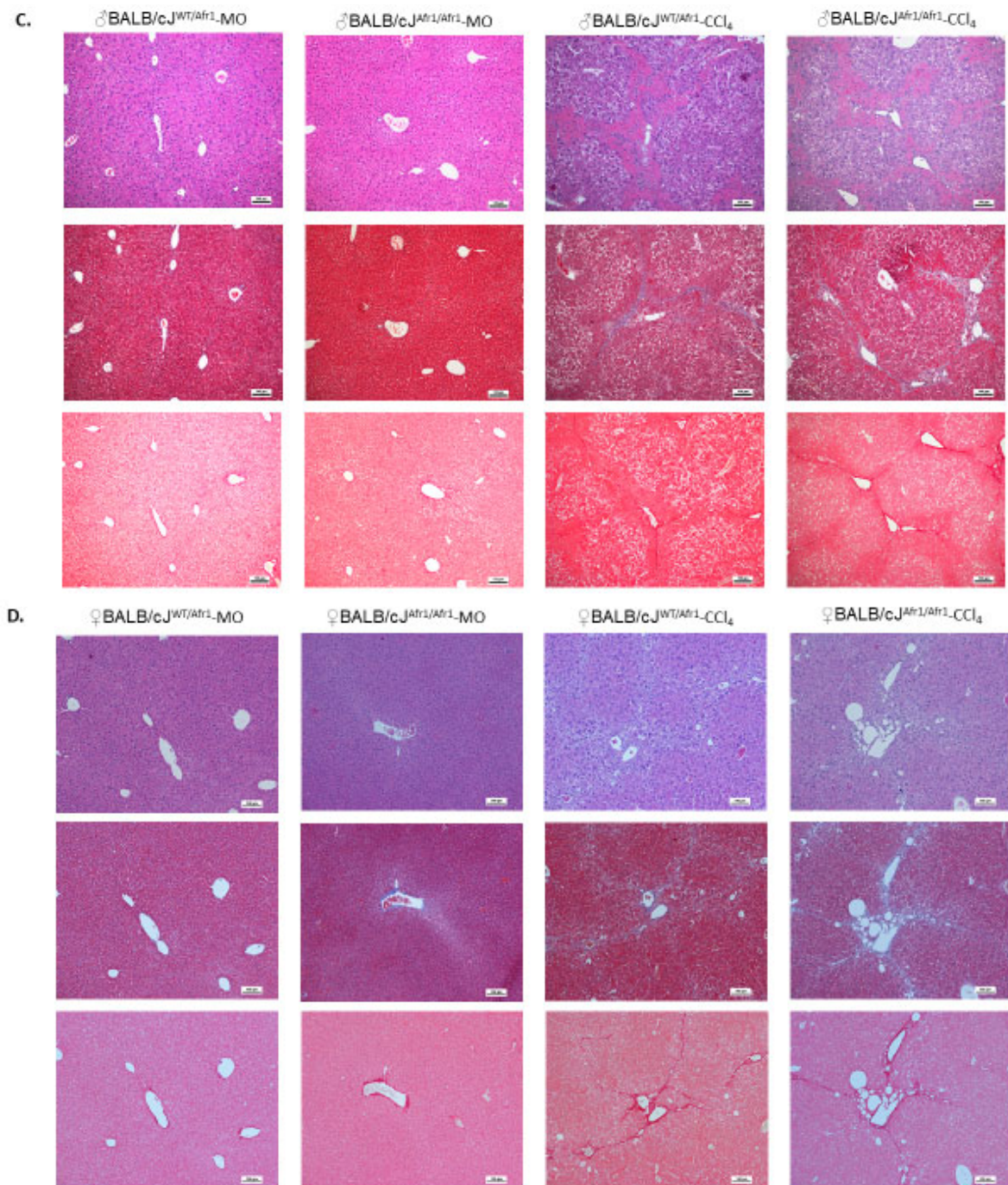
Figure 3.2 Histological analysis indicates that reduced Zhx2 expression does not alter fibrosis after CCl4 treatment.

Representative histology (10x) from male and female Zhx2$^{WT/Afr1}$ and Zhx2$^{KO/Afr1}$ mice (A, B) and male and female BALB/cJ$^{WT/Afr1}$ and BALB/cJ$^{Afr1/Afr1}$ mice (C, D) with either

WT or reduced Zhx2, treated with CCl$_4$ or MO for six weeks. Images shown are

Hematoxylin and Eosin (Top), Masson Trichrome (Middle), and Sirius Red (Bottom).
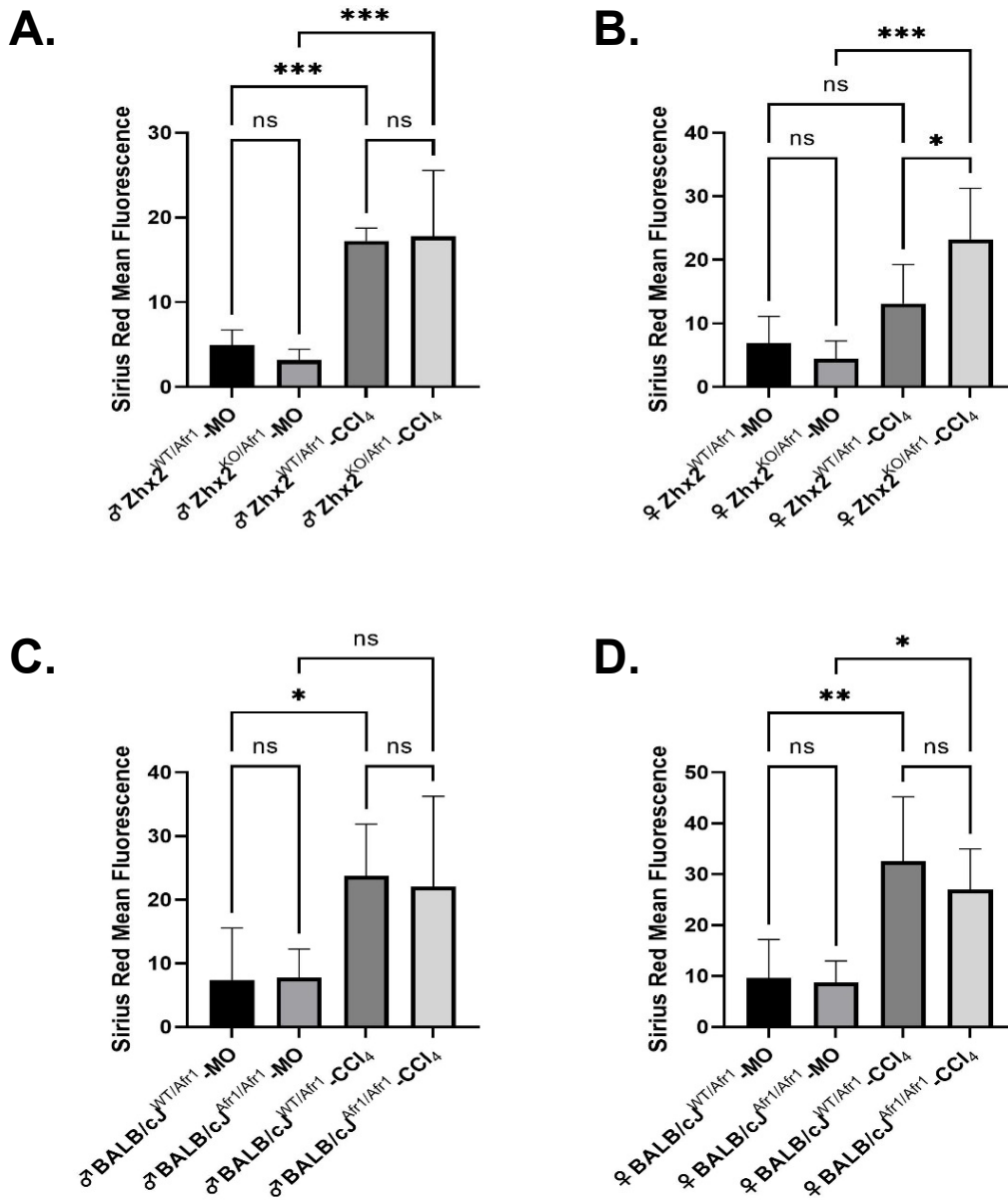
Figure 3.3 Sirius Red quantification indicates that Zhx2 expression does not alter fibrosis after CCl₄ treatment.

Histology (10x) from male and female $Zhx2^{WT/Afr1}$ and $Zhx2^{KO/Afr1}$ mice and $BALB/cJ^{WT/Afr1}$ and $BALB/cJ^{Afr1/Afr1}$ mice treated with CCl₄ or MO for six weeks were imaged for red fluorescence. Images were quantified using ImageJ. Sirius Red

fluorescence was quantified in male Zhx2$^{WT/Afr1}$ (MO n=5, CCl$_4$ n=6) or Zhx2$^{KO/Afr1}$ (n=6) mice, treated with CCl$_4$ or MO (A). Sirius Red fluorescence was quantified in female Zhx2$^{WT/Afr1}$ (n=6) or Zhx2$^{KO/Afr1}$ mice (MO n=4, CCl$_4$ n=5), treated with CCl$_4$ or MO (B). Sirius Red fluorescence was quantified in male BALB/cJ$^{Afr1/Afr1}$ (n=6) or BALB/cJ$^{WT/Afr1}$ (n=5) mice treated with CCl$_4$ or MO (C). Sirius Red fluorescence was quantified in female BALB/cJ$^{Afr1/Afr1}$ (MO n=6, CCl$_4$ n=5) or BALB/cJ$^{WT/Afr1}$ (n=5) mice, treated with CCl$_4$ or MO (D). *$p<0.05$, **$p<0.01$, ***$p<0.001$.
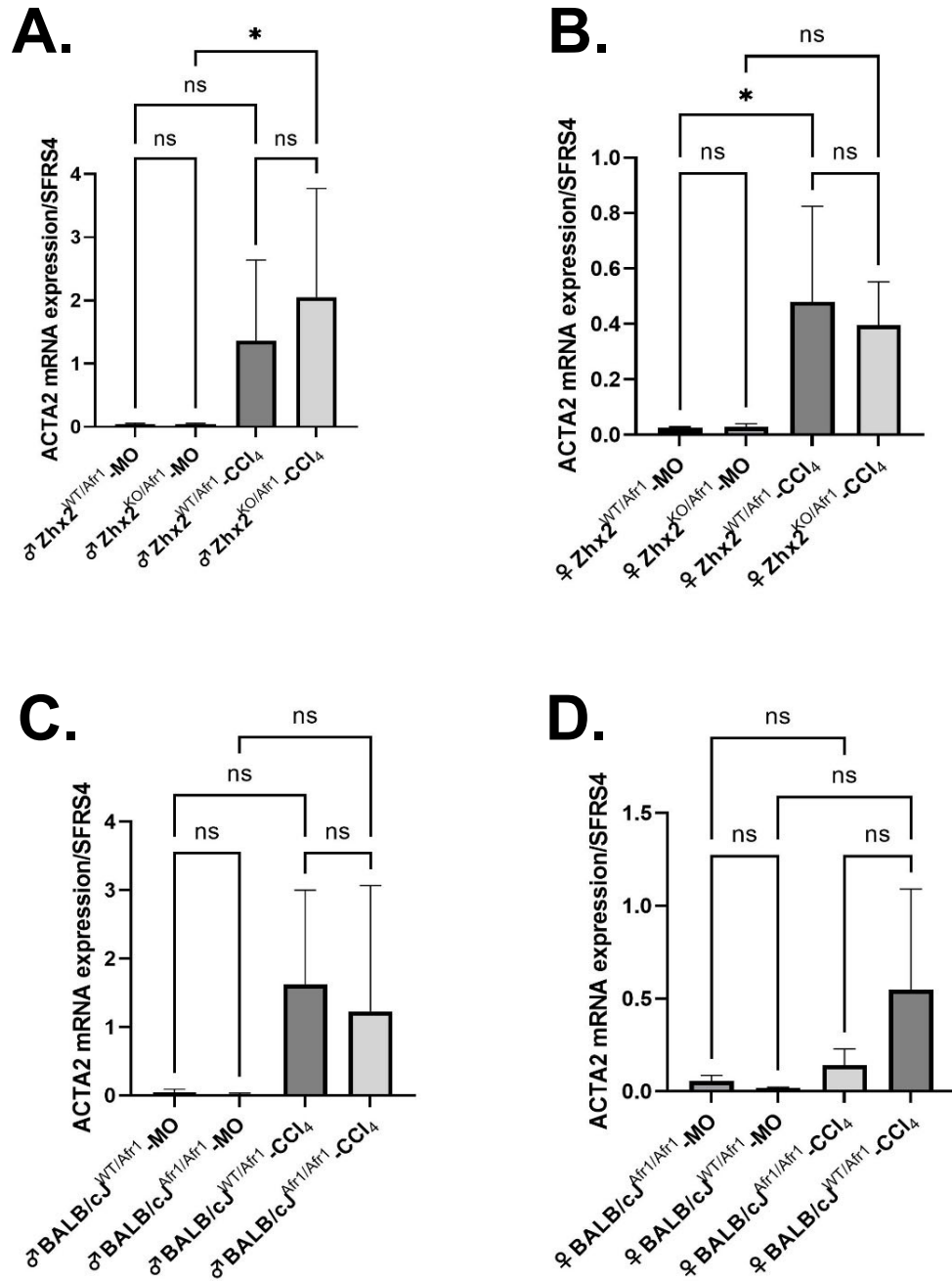
Figure 3.4 CCl₄-mediated increase in ACTA2 mRNA levels are not altered by the absence of Zhx2.

ACTA2 mRNA expression in male $Zhx2^{WT/Afr1}$ or $Zhx2^{KO/Afr1}$ mice, treated with CCl₄ or MO (n=6) (A). ACTA2 mRNA expression in female $Zhx2^{WT/Afr1}$ (CCl₄ n=5, MO n=4) or

Zhx2$^{KO/Afr1}$ mice (n=4), treated with CCl$_4$ or MO (B). ACTA2 mRNA expression in male BALBcJ$^{Afr1/Afr1}$ (CCl$_4$ n=6, MO n=5) or BALB/cJ$^{WT/Afr1}$ (n=6) mice, treated with CCl$_4$ or MO (C). ACTA2 mRNA expression in female BALB/cJ$^{Afr1/Afr1}$ (CCl$_4$ n=4, MO n=6) or BALB/cJ$^{WT/Afr1}$ (CCl$_4$ n=5, MO n=4) mice, treated with CCl$_4$ or MO (D). *p<0.05.
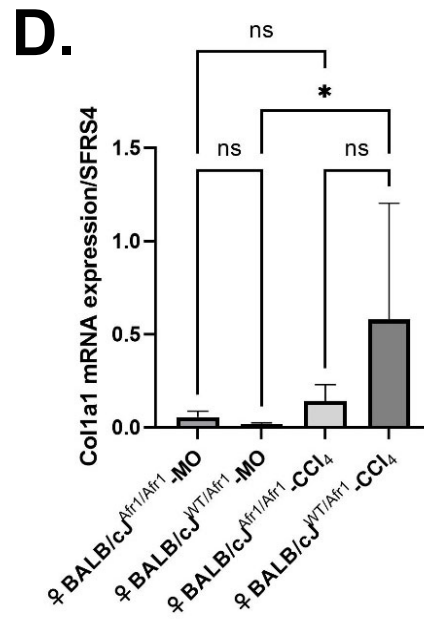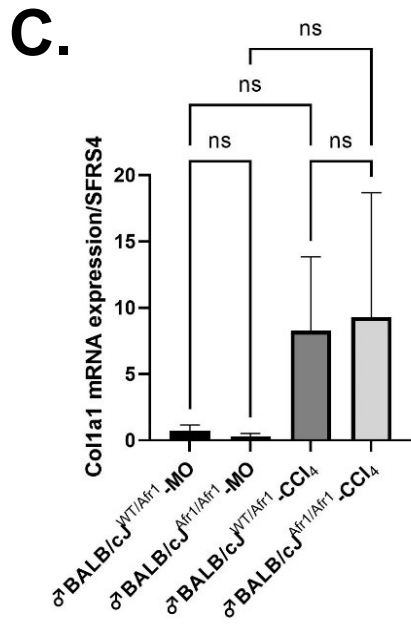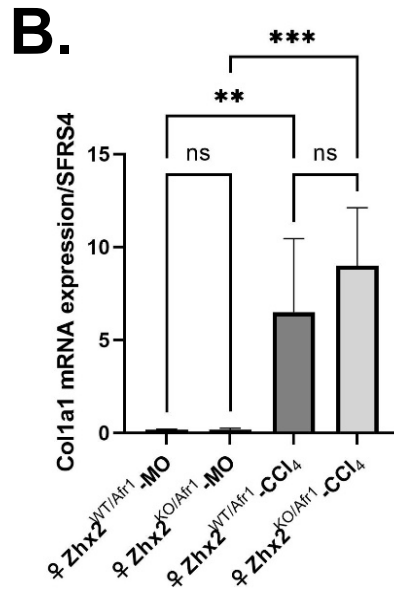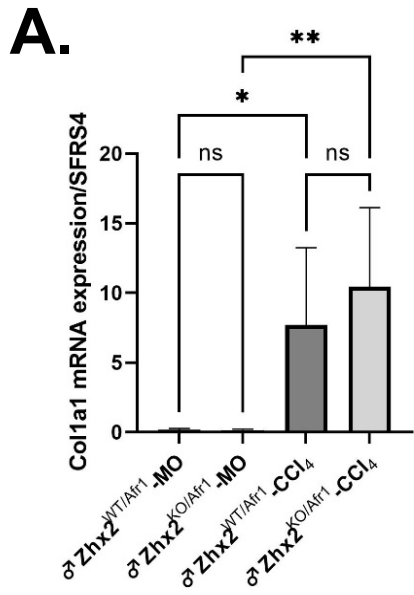
Figure 3.5 CCl$_4$-mediated increase in Col1a1 mRNA levels are not altered by the absence of Zhx2.

Col1a1 mRNA expression in male Zhx2$^{WT/Afr1}$ (n=6) or Zhx2$^{KO/Afr1}$ mice (CCl$_4$ n=5, MO n=6), treated with CCl$_4$ or MO (A). Col1a1 mRNA expression in female Zhx2$^{WT/Afr1}$ (CCl$_4$ n=6, MO n=5) or Zhx2$^{KO/Afr1}$ mice (CCl$_4$ n=5, MO n=4), treated with CCl$_4$ or MO (B). Col1a1 mRNA expression in male BALBcJ$^{Afr1/Afr1}$ (CCl$_4$ n=6, MO n=5) or BALB/cJ$^{WT/Afr1}$ mice (CCl$_4$ n=6, MO n=5), treated with CCl$_4$ or MO (C). Col1a1 mRNA expression in female BALB/cJ$^{Afr1/Afr1}$ (CCl$_4$ n=4, MO n=6) or BALBcJ$^{WT/Afr1}$ mice (CCl$_4$ n=4, MO n=5), treated with CCl$_4$ or MO (D). *p<0.05, **p<0.01, ***p<0.001.
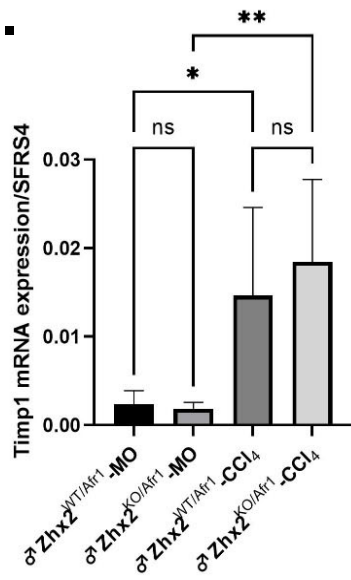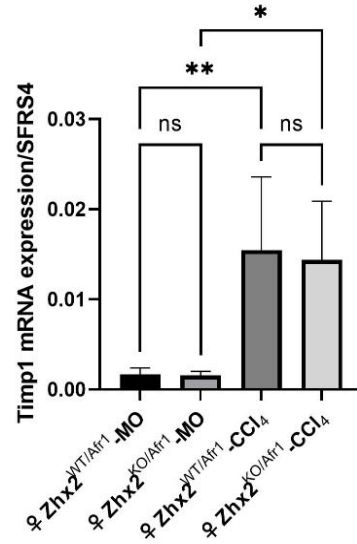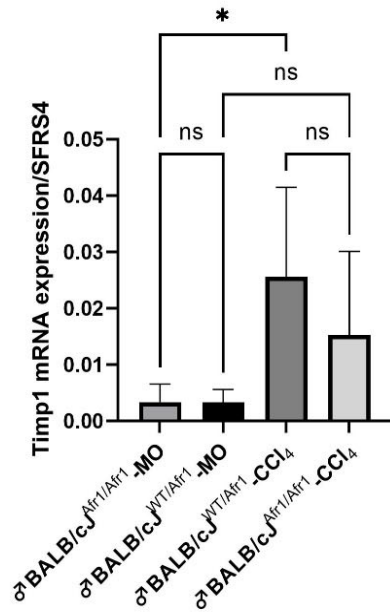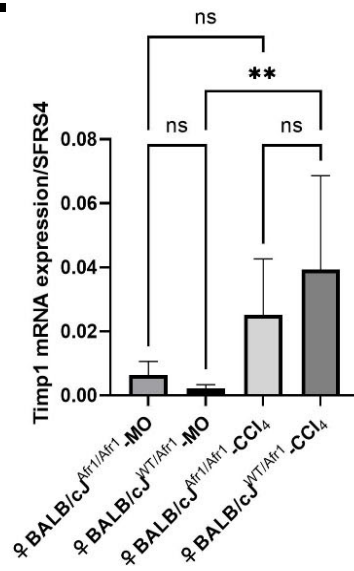
Figure 3.6 CCl₄-mediated increase in Timp1 mRNA levels are not altered by the absence of Zhx2.

Timp1 mRNA expression in male Zhx2$^{WT/Afr1}$ or Zhx2$^{KO/Afr1}$ mice, treated with CCl₄ or MO (n=6) (A). Timp1 mRNA expression in female Zhx2$^{WT/Afr1}$ (n=6) or Zhx2$^{KO/Afr1}$ (CCl₄ n=5, MO n=4) mice, treated with CCl₄ or MO (B). Timp1 mRNA expression in male BALB/cJ$^{Afr1/Afr1}$ (CCl₄ n=5, MO n=6) or BALB/cJ$^{WT/Afr1}$ (CCl₄ n=6, MO n=5) mice, treated with CCl₄ or MO (C). Timp1 mRNA expression in female BALB/cJ$^{Afr1/Afr1}$ or BALB/cJ$^{WT/Afr1}$ mice (n=6), treated with CCl₄ or MO (D). *p<0.05, **p<0.01.
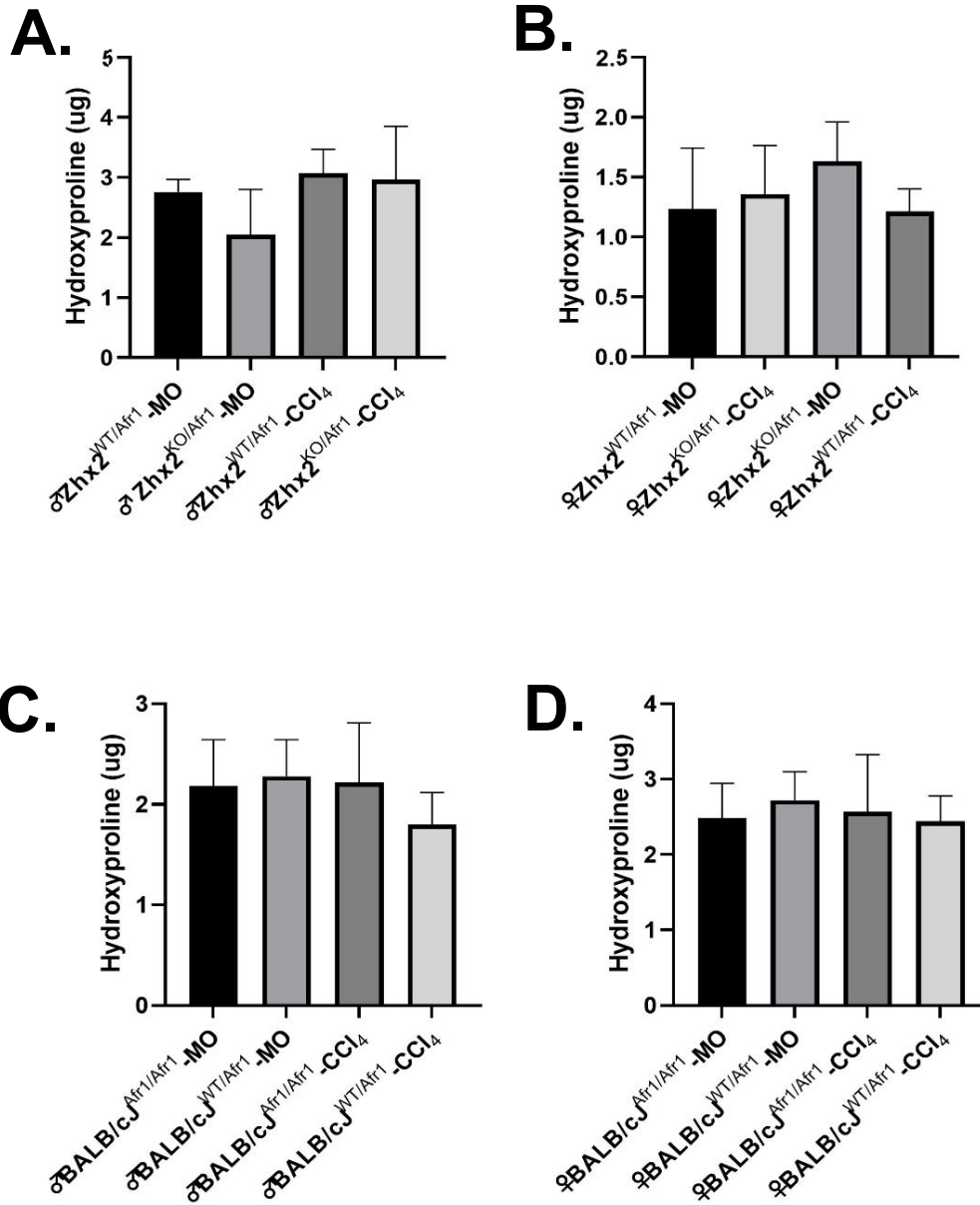
Figure 3.7 CCl$_4$ administration does not alter hydroxyproline levels in the liver, regardless of Zhx2 expression.

Hydroxyproline levels (ug) of hydrolyzed tissue homogenate in both Male Zhx2$^{WT/Afr1}$ and Zhx2$^{Afr1/Afr1}$ mice treated with CCl$_4$ or MO (n=6) (A). Hydroxyproline levels (ug) of hydrolyzed tissue homogenate in both Female Zhx2$^{WT/Afr1}$(CCl$_4$ n=5, MO n=4) and

Zhx2$^{Afr1/Afr1}$ (n=6) mice treated with CCl$_4$ or MO (B). Hydroxyproline levels (ug) of hydrolyzed tissue homogenate in male BALB/cJ$^{Afr1/Afr1}$ (CCl$_4$ n=5, MO n=6) and BALB/cJ$^{WT/Afr1}$ (n=6) given CCl$_4$ or MO (C). Hydroxyproline levels (ug) of hydrolyzed tissue homogenate in female BALB/cJ$^{Afr1/Afr1}$ (CCl$_4$ n=5, MO n=6) and BALB/cJ$^{WT/Afr1}$ (CCl$_4$ n=6, MO n=5) given CCl$_4$ or MO.
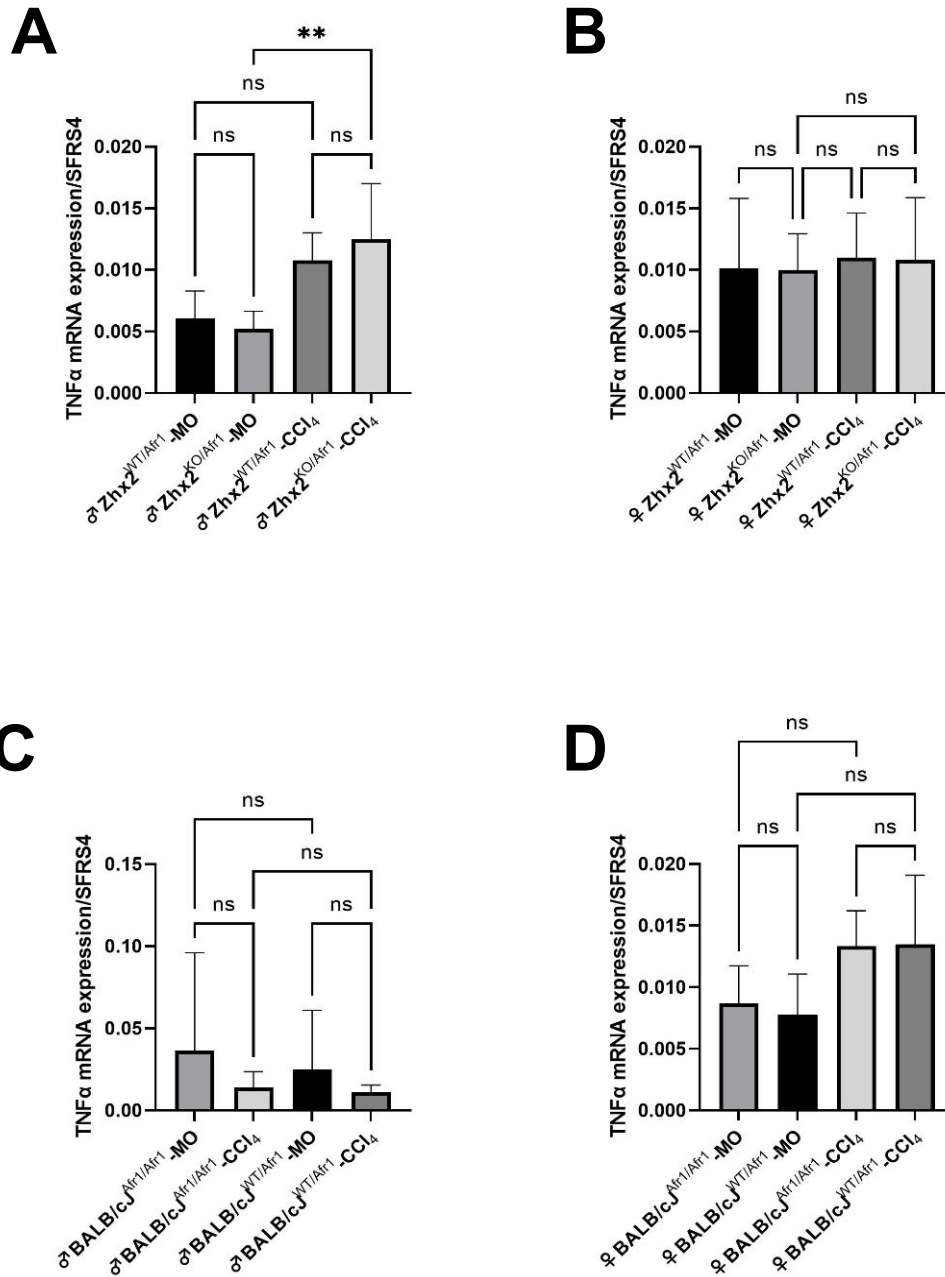
Figure 3.8 CCl₄ administration does not significantly alter TNFα mRNA expression in the liver, regardless of Zhx2 expression.

TNFα mRNA expression in male Zhx2$^{WT/Afr1}$(CCl₄ n=5, MO n=6) or Zhx2$^{KO/Afr1}$ (n=6) mice, treated with CCl₄ or MO (A). TNFα mRNA expression in female Zhx2$^{WT/Afr1}$ (n=6)

or Zhx2$^{KO/Afr1}$ (CCl$_4$ n=5, MO n=4) mice, treated with CCl$_4$ or MO (B). TNFα mRNA expression in male BALB/cJ$^{Afr1/Afr1}$ (n=6) or BALB/cJ$^{WT/Afr1}$ (CCl$_4$ n=6, MO n=5) mice, treated with CCl$_4$ or MO (C). TNFα mRNA expression in female BALB/cJ$^{Afr1/Afr1}$ (CCl$_4$ n=5, MO n=6) or BALB/cJ$^{WT/Afr1}$ (n=5) mice, treated with CCl$_4$ or MO (D). *p<0.05.
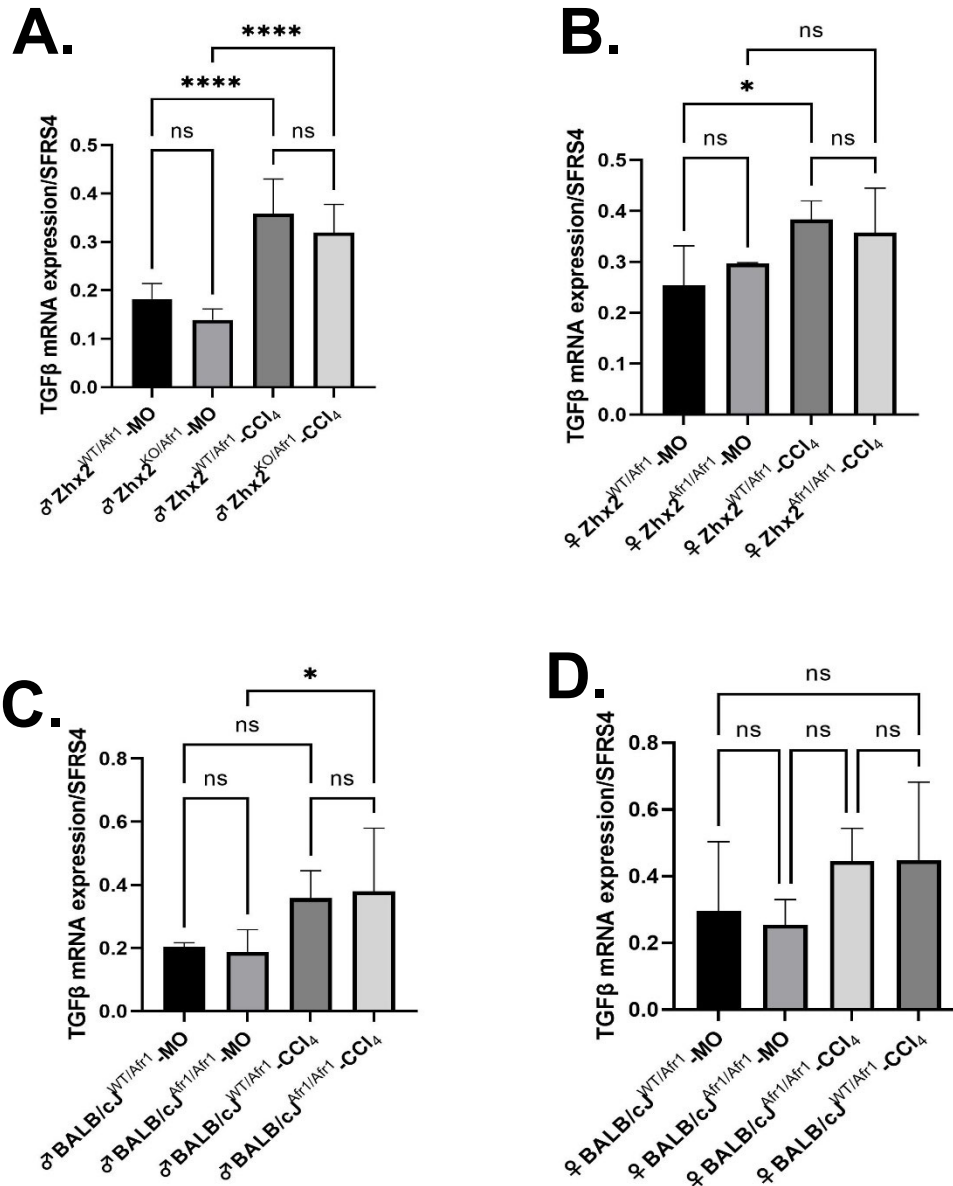
Figure 3.9 CCl₄ administration does alter TGF-β mRNA expression but does not alter with the absence of Zhx2.

TGF-β mRNA expression in male Zhx2$^{WT/Afr1}$ (CCl₄ n=6, MO n=5) or Zhx2$^{KO/Afr1}$ (n=6) mice, treated with CCl₄ or MO (A). TGF-β mRNA expression in female Zhx2$^{WT/Afr1}$ (n=6) or Zhx2$^{KO/Afr1}$ (CCl₄ n=5, MO n=3) mice, treated with CCl₄ or MO (B). TGF-β mRNA expression in male BALBcJ$^{Afr1/Afr1}$ (n=6) or BALBcJ$^{WT/Afr1}$ (CCl₄ n=6, MO n=5)

mice, treated with CCl$_4$ or MO (C). TGF-β mRNA expression in female BALBcJ$^{Afr1/Afr1}$ (CCl$_4$ n=5, MO n=6) or BALBcJ$^{WT/Afr1}$ (n=5) mice, treated with CCl$_4$ or MO (D). *p<0.05, ****p<0.0001.
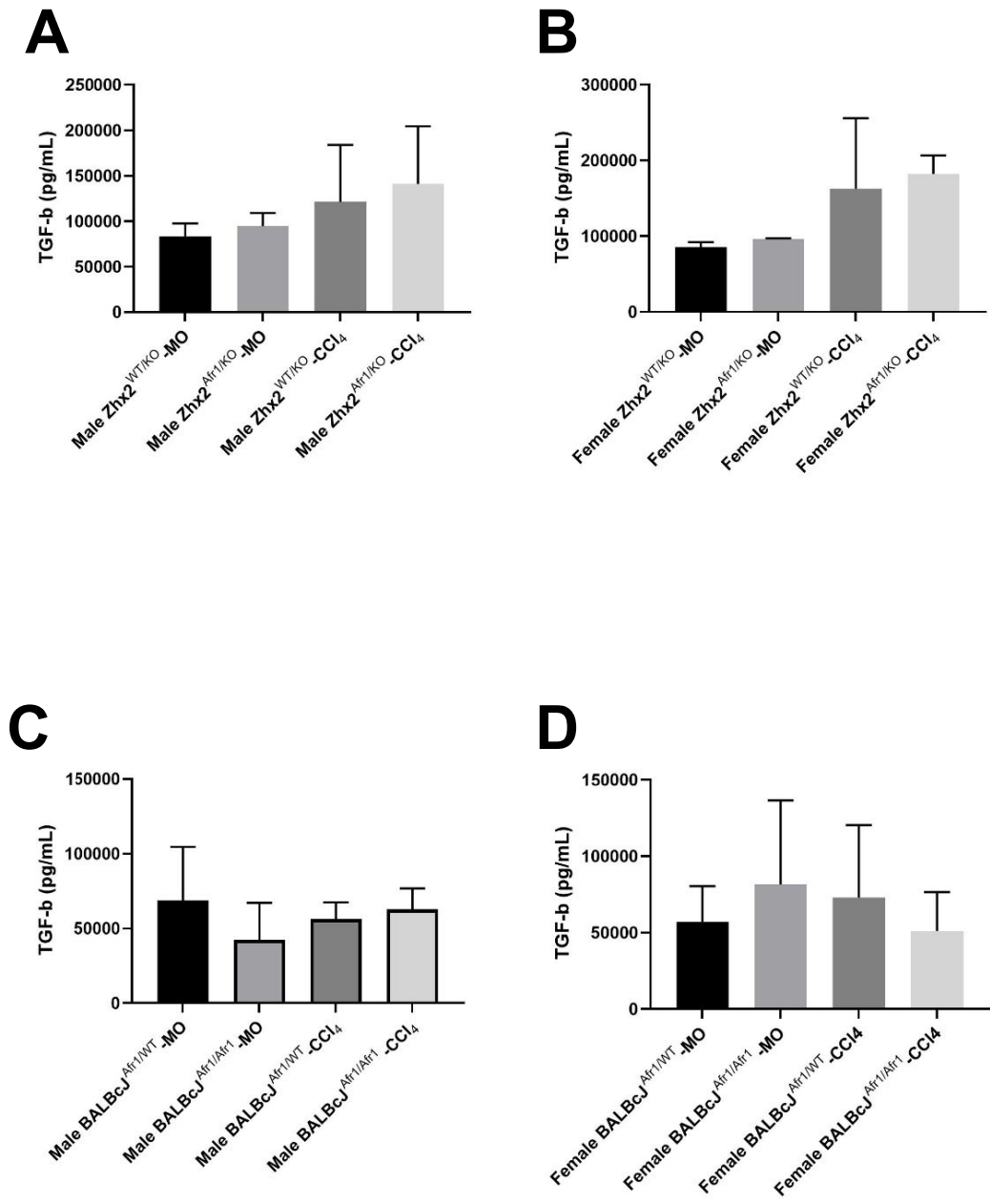
Figure 3.10 CCl_4 administration does not alter TGF-β serum levels, regardless of Zhx2 expression.

TGF-β serum levels in male $Zhx2^{WT/Afr1}$ or $Zhx2^{KO/Afr1}$ mice, treated with CCl_4 (n=6) or MO (n=4) (A). TGF-β serum levels in female $Zhx2^{WT/Afr1}$ or $Zhx2^{KO/Afr1}$ mice, treated

with CCl$_4$ (n=6) or MO (n=4) (B). TGF-β serum levels in male BALB/cJ$^{Afr1/Afr1}$ or BALBcJ$^{WT/Afr1}$ mice, treated with CCl$_4$ (n=6) or MO (n=4) (C). TGF-β serum levels in female BALBcJ$^{Afr1/Afr1}$ or BALBcJ$^{WT/Afr1}$ mice, treated with mineral oil (n=4, n=3) or carbon tetrachloride (n=6) (D).
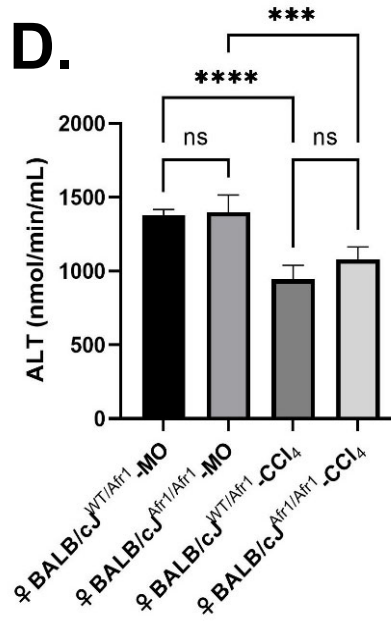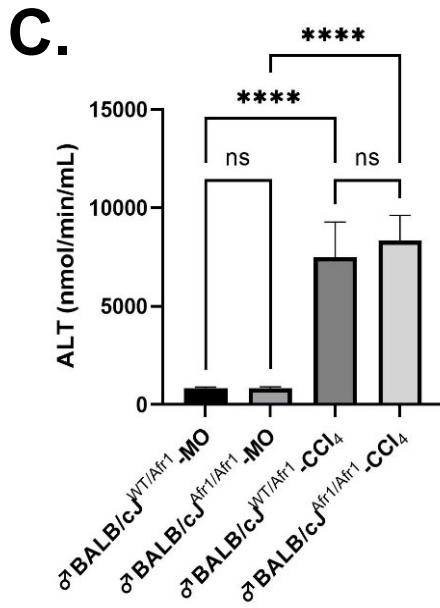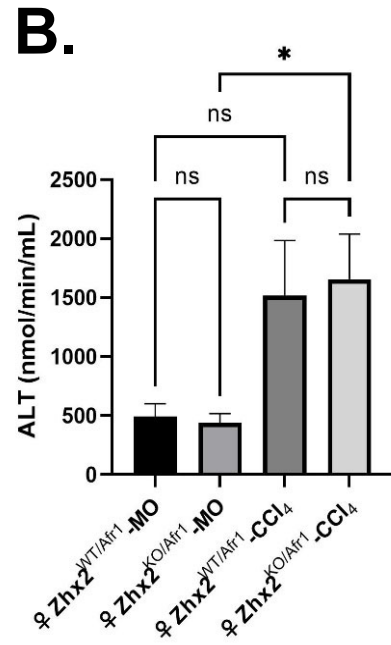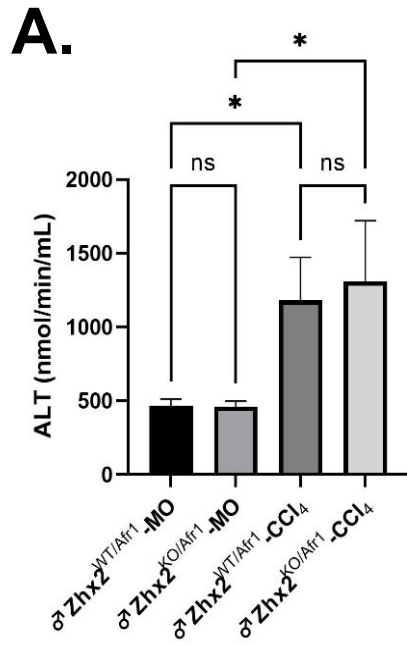
Figure 3.11 CCl$_4$ administration does alter ALT serum levels but does not worsen with reduced Zhx2 expression.

ALT serum levels in male Zhx2$^{WT/Afr1}$ (CCl$_4$ n=6, MO n=5) and Zhx2$^{KO/Afr1}$ (n=6) mice, treated with CCl$_4$ or MO for six weeks (A). ALT serum levels in female Zhx2$^{WT/Afr1}$ (CCl$_4$ n=5, MO n=4) and Zhx2$^{KO/Afr1}$ (CCl$_4$ n=5, MO n=6) mice, treated with CCl$_4$ or MO for six weeks (B). ALT serum levels in male BALB/cJ$^{WT/Afr1}$ (n=6) and BALB/cJ$^{Afr1/Afr1}$ (n=6) mice, treated with CCl$_4$ or MO for six weeks (C). ALT serum levels in female BALB/cJ$^{WT/Afr1}$ (n=6) and BALB/cJ$^{Afr1/Afr1}$ (CCl$_4$ n=5, MO n=4), treated with CCl$_4$ or MO for six weeks. *p<0.05, *** p<0.001, ****p<0.0001.

CHAPTER 4. CHARACTERIZATION OF THE ALPHA-FETOPROTEIN
REGULATOR 2 (AFR2) TRAIT IN RESPONSE TO LIVER REGENERATION

4.1 Introduction

The liver has a remarkable ability to repair and regenerate itself in response to damage. In most liver diseases, regeneration is required after hepatocyte damage, inflammation, and fibrosis. Subsequent to damage, remaining hepatocytes must be signaled to proliferate to regain liver mass. This proliferation process is accomplished by priming the hepatocytes, resulting from increased signaling of c-jun and c-myc and the production of inflammatory cytokines TNF-α and IL-6 [60, 61]. This signaling cascade makes it possible for the transition of quiescent hepatocytes to proliferative hepatocytes. After the initial priming phase, growth factors, including hepatocyte growth factor (HGF) and endothelial growth factor (EGF), are released [62, 63]. HGF binds to mesenchymal-epithelial transition factor (c-Met), activating downstream signaling to induce proliferation and decrease apoptosis [111]. EGF binds to the EGF receptor (EGFR), which is also required for activating proliferation [112]. The proliferation phase continues, in order to replace damaged or apoptotic cells, until the liver regains normal size; at this point, hepatocytes enter the termination phase. Although there are many unknowns regarding the termination of hepatocyte regeneration, TGF-β signaling has been found integral in blocking further hepatocyte proliferation [64]. Through this multi-phased process, the liver can orchestrate the regeneration and repair to recover from the loss of hepatocytes. Understanding regeneration signaling and regulation is beneficial in developing new treatments for liver disease.

Experimentally, liver regeneration can be initiated by a variety of methods. In rodents, two of the most commonly used methods are partial hepatectomy (PH) and treatment with the hepatotoxin CCl_4. PH is conducted by the removal of two-thirds of the liver lobes. Although these lobes do not grow back, the liver regenerates to make up for the loss of volume without causing any persistent liver tissue damage [113]. Metabolism of CCl_4 by hepatic *Cyp2e1* produces free radicals, which, when administered acutely, can cause necrosis, apoptosis, and ultimately regeneration of hepatocytes [67].

AFP, which is normally expressed at high levels in the fetal liver and silenced at birth, is transiently reactivated during liver regeneration. In fact, AFP has become a well-characterized marker of liver regeneration. Previous studies found that the C3H/HeJ mouse strain exhibited greater levels of AFP mRNA after CCl_4 treatment than C57BL/6J mice [82]. The high AFP induction in C3H/HeJ was found to be dominant to the low induction, and the locus controlling this trait was called alpha-fetoprotein regulator 2 (Afr2); C3H/HeJ and C57BL/6J mice were designated as having Afr2[a] and Afr2[b] alleles, respectively[82]. Further QTL analysis indicated that the gene responsible for the Afr2 trait was located on mouse chromosome 2 [92].

Although previous studies have provided insight regarding the Afr2 trait, the Afr2 gene has not been identified. Previous studies analyzed Afr2 in C3H/HeJ and C57BL/6J mice but not in other mouse strains. A better understanding of Afr2 in additional mouse strains could provide insight to identify the Afr2 gene. In particular, we were interested to know whether the Afr2[b] allele was unique to C57BL6/J mice or found in other C57BL substrains. Therefore, in this pilot study, I used CCl_4 to induce liver regeneration in mice of six strains: 129X1/SvJ, C3H/HeJ, DBA/2J, C57BL/10SnJ, C57BL/6NJ, and

C57BL/6J. My results indicated that the Afr2[b] allele was present in all C57BL substrains, based on low AFP induction after CCl4 treatment, whereas the other strains contained the Afr2[a] allele. Initial studies indicated that the Afr2[a] allele was dominant over the Afr2[b] allele; another study suggested that these two alleles were co-dominant [114]. To further explore this, we analyzed AFP expression in F1 mice that were generated from a cross between 129X1/SvJ and C57BL/6J parents. Male and female F1 offspring at eight weeks of age were injected with CCl4 to induce liver regeneration. I found that F1 mice had intermediate levels of AFP reactivation compared to 129X1/SvJ and C57BL/6J mice, consistent with the Afr2[a] and Afr2[b] alleles being co-dominant.

An additional regulator of AFP, initially called Afr1, was also found to be the cause of persistent AFP expression after birth in BALB/cJ mice [82]. In our lab, the Afr1 trait was found to be due to a hypomorphic mutation in the gene *Zhx2* [84]. Our lab has also shown that Zhx2 deficiency can significantly elevate several other genes, including H19, Gpc3, and LPL [84, 86, 89]. When looking at the Afr2 trait in C3H/HeJ and C57BL/6J mice, our lab and others have shown that both Zhx2 and Afr2 repress the same genes but are not genetically linked [82, 86]. We hypothesized that mice with high AFP reactivation would have elevated levels of Zhx2 targeted genes in this liver regeneration model. When looking at our data in a pilot study, H19, LPL, and Gpc3 were increased in mice with high AFP reactivation. Interestingly, even though eight-week-old F1 mice have an intermediate AFP reactivation, male mice do not have a fold increase in H19 and LPL while female mice do, suggesting that there might be additional sex-regulated factors involved in targeting their expression.

4.2 Results

In an initial pilot study, six-week-old male mice from six different strains were injected with either MO or CCl_4 in a model of liver regeneration. After 72 hours, livers were collected, and AFP mRNA levels were measured. 129X1/SvJ, C3H/HeJ, and DBA/2J exhibited significantly increased AFP levels after CCl_4 treatment, having a fold increase of approximately 42, 46, and 42 compared to MO controls, respectively (Fig. 4.1 A-C, Fig. 4.6 A). In contrast, much lower AFP induction was seen in C57BL/6J, C57BL/6NJ, and C57BL/10SnJ mice, which only had a fold increase of approximately 2, 5, and 3 compared to MO controls, respectively (Fig. 4.1 D-F, Fig. 4.6 A). This result was confirmed by analyzing serum AFP levels in 129X1/SvJ, C3H/HeJ, and C57BL/6J mice. Male 129X1/SvJ and C3H/HeJ mice had a 42-fold and 52-fold increase in AFP serum levels in CCl_4-treated mice compared to MO controls, respectively (Fig. 4.2). Male C57BL/6J mice treated with CCl_4 did have an increased serum AFP of 29-fold over MO treated mice, but the maximum levels remained much lower than the non-C57 lineage mice (Fig. 4.2).

The long non-coding RNA H19 was originally identified based on a screen for Zhx2-regulated genes and subsequently found to be regulated by Afr2 [114]. Additional genes that were identified in our lab to be targets of Zhx2, including Gpc3 and Lpl, also appeared to be controlled by Afr2 in C57BL/6J and C3H/HeJ mice. To test whether these three genes also showed the same response to Afr2 in the six strains used in my pilot study, their expression was analyzed. In 129X1/SvJ, C3H/HeJ, and DBA/2J mice, H19 mRNA expression was increased by 8-, 95-, and 2.3-fold, respectively, compared to MO controls (Fig. 4.3 A-C, Fig. 4.6 B). H19 levels in C57BL/6J, C57BL/6NJ, and

C57BL/10SnJ were increased by 1.6-, 1.5- and 0.9-fold, respectively, compared to MO controls (Fig. 4.3 D-F, Fig. 4.6 B). The same trend was observed for Lpl; levels were significantly increased in the 129X1/SvJ, C3H/HeJ, and DBA/2J mice roughly 3-fold after CCl4 treatment (Fig. 4.4 A-C, Fig. 4.6 C). In contrast, Lpl mRNA levels in C57BL/6J, C57BL/6NJ, and C57BL/10SnJ increased 1.6-, 1.5-, and 0.8-fold, respectively (Fig. 4.4 D-F, Fig. 4.6 C). Gpc3 mRNA levels increased roughly 7- and 9-fold in 129X1/SvJ and C3H/HeJ mice, respectively, although there was no significant difference in Gpc3 levels between CCl4- and MO-treat DBA/2J mice (Fig. 4.5 A-C, Fig. 4.6 D). C57BL/6J, C57BL/6NJ, and C57BL/10SnJ exhibited slightly decreased Gpc3 levels after CCl4 treatment compared to MO controls (Fig. 4.5 D-F, Fig. 4.6 D).

Cyp2e1 is the major CCl4-metabolizing enzyme in the liver and is responsible for generating radicals that cause liver damage. A simple explanation for the mouse strain differences in AFP induction after CCl4 treatment could be differences in *Cyp2e1* levels. We, therefore, analyzed *Cyp2e1* levels in all six strains after MO treatment, in which no liver damage occurred. We found no significant differences in *Cyp2e1* mRNA levels between the six groups in the pilot study (Fig. 4.7 A). Modest differences in *Cyp2e1* mRNA levels were found after CCl4 treatment, but these differences did not correlate with the expression of Afr2 target genes (Fig. 4.7 B). This data suggests that differences in *Cyp2e1* levels cannot account for the Afr2 phenotype.

Previous studies provided conflicting data regarding the dominance of the Afr2 alleles; initial studies indicated that Afr2[a] was dominant over Afr2[b], whereas a second study indicated that these two alleles were co-dominant [82, 92]. Since 129X1/SvJ mice showed a robust increase in AFP levels after CCl4 treatment, we used this strain,

C57BL/6J, and F1 offspring between these two strains to further investigate dominance of the Afr2 alleles in a full liver regeneration study. Analysis was performed in mice that were 8 weeks of age since we found that these mice exhibited a more robust AFP activation than 6-week-old mice used in the pilot study. Seventy-two hours after CCl_4 or MO treatment, male and female mice were killed, and serum and liver tissue were collected. Liver mRNA analysis showed that AFP mRNA levels in 129X1/SvJ mice had an 89-fold increase in males and a 68-fold increase in females (Figure 4.7 A, B). C57BL/6J mice exhibited lower AFP activation in regenerating livers, increasing 11-fold in males and 5-fold in females (Figure 4-7 C, D). When F1 mice were injected with CCl_4, the activation of AFP was 26-fold in males and 28-fold in females (Figure 4-7 E, F). Serum AFP levels were also measured in the 8-week-old liver regeneration mice (Figure 4-8 A-B). For both male and female mice, the increase in serum AFP levels was intermediate between 129X1/SvJ mice (high induction) and C57BL/6J mice (low induction). Taken together, these data from the full liver regeneration study indicate that the $Afr2^a$ and $Afr2^b$ alleles are co-dominant.

As with the six-week-old pilot study mice, the full study male and female 129X1/SvJ, F1, and C57BL/6J were analyzed for gene expression of Zhx2 targets. When we analyzed H19, we saw a robust increase in 129X1/SvJ mice of 9-fold in males and 8-fold in females (Fig. 4.11 A-B, Fig. 4.12 A-B). In C57BL/6J mice, H19 expression was minimal and increased around 2-fold for males and 3-fold for females in the liver regeneration model (Fig. 4.11 C-D, Fig. 4.12 A-B). Interestingly, we expected to see intermediate H19 expression in the F1 mice. However, we saw a pattern that differed between male and female mice. Male F1 mice had a minimal increase of 2-fold in H19

68

expression, similar to C57BL/6J mice (Fig. 4.11 E, Fig. 4.12 A). Females had a robust increase in H19 mRNA expression of 29-fold, which was even greater than the increase we saw in 129X1/SvJ mice. (Fig. 4.11 F, Fig. 4.12 B). When we look at LPL mRNA expression, we see a similar pattern. 129X1/SvJ mice had a robust increase of around 10-fold in males and 7-fold in females mice during liver regeneration (Fig. 4.13 A-B, Fig 4.14 A-B). C57BL/6J mice also had a minimal increase in LPL mRNA levels of 3-fold in males and remained the same in females (Fig. 4.13 C-D, Fig. 4.14 A-B). In F1 male mice, we see LPL expression that minimally increases by 3-fold, like C57BL/6J mice (Fig. 4.13 E, Fig. 4.14 A). F1 females had a more robust increase of LPL of 9-fold, which was more similar to the 129X1/SvJ mice (Fig. 4.13 F, Fig 4.14 B). When looking at Gpc3 mRNA expression, we saw expression changes that matched the pattern of AFP expression. 129X1/SvJ male and female mice had a Gpc3 mRNA expression increase of around 10.6 and 8-fold (Fig. 4.15 A-B, Fig. 4.16 A-B). C57BL/6J male and female mice had a much lower increase of Gpc3 expression that was 4.6- and 1.43-fold greater (Fig. 4.15 C-D, Fig. 4.16 A-B). F1 male and female mice had fold increases and expression of Gpc3 that were more intermediate at 7.4- and 3-fold (Fig. 4.15 E-F, Fig. 4.16 A-B).

An transient increased liver weight:body weight ratio is observed in the CCl_4 in a model of liver regeneration [115]. The full liver regeneration study was analyzed for liver weight:body weight ratio to determine if different strains of mice responded to CCl_4 treatment. Both male and female mice in all three strains had similar liver weight: body weight ratio increases when undergoing CCl_4 treatment (Figure 4.17 A-F).

4.3 <u>Discussion</u>

Results in this chapter provide new insight regarding the Afr2 phenotype. My data from the pilot study showed that male mice from 129X1/SvJ, C3H/HeJ, and DBA/2J strains displayed robust AFP activation in a regeneration model, while the mice from the C57BL lineage (C57BL/6J, C57BL/6NJ, and C57BL/10SnJ) show minimal AFP reactivation. When doing a full study using an 8-week-old mouse model of liver regeneration with 129X1/SvJ and C57BL/6J mice, we were able to see that 129X1/SvJ mice displayed robust AFP activation. In contrast, C57BL/6J mice displayed much lower AFP levels after CCl$_4$ injection. When F1 mice, a cross of both pairings, were injected, they displayed an intermediate activation of AFP.

From the 6-week-old initial pilot study, we determined that mice from the C57BL lineage (C57BL/6J, C57BL/6NJ, and C57BL/10SnJ) have the Afr2^b phenotype, while other strains across several other lineages (129X1/SvJ, C3H/HeJ, and DBA/2J) have the Afr2^a phenotype. This finding confirms previous literature showing that C3H/HeJ mice have significantly higher AFP reactivation over the C57BL/6J mice [82]. Our data from the pilot study additionally shows that other strains outside of C3H/HeJ mice also display the Afr2^a trait, while other mice in the C57BL lineage continue to display the Afr2^b. Serum AFP levels also confirmed that mice with the Afr2^a trait have significantly higher reactivation in liver regeneration than mice from the C57BL lineage. This data supports that both 129X1/SvJ and C57BL/6J mice served as a suitable choice for both the Afr2^a and Afr2^b for a full 8-week-old mouse liver regeneration study, respectively.

It is known that Zhx2 (Afr1) and Afr2 are not genetically linked both regulate AFP independently of each other along with other essential liver genes [82, 86]. Our pilot

study data confirmed that C3H/HeJ and 129X1/SvJ mice both have increases H19, LPL, and Gpc3 levels, but DBA/2J mice only have an increase in LPL. This might suggest that the gene responsible for Afr2 might not be sufficient to alter these gene's expression alone in these strains of mice and also might rely on other gene changes.

With the full liver regeneration study, we were able to determine that F1 mice have intermediate AFP activation, suggesting that the two Afr2 alleles are co-dominant. The AFP mRNA ΔΔCT average for 129X1/SvJ mice was 3.38, whereas C57BL/6J mice were 0.22. The F1 mice have an average of 1.23, falling in between those two strains. This data supports a previous finding that F1 offspring from C3H/HeJ and C57BL/6J mice have an intermediate AFP response in a model of liver regeneration [114]. Our data additionally shows that using other strains that have the Afr2[a] trait for the F1 breeding also results in intermediate AFP reactivation.

The data from the pilot study suggests that the Afr2[b] trait is unique to the mice from the C57BL lineage. Identifying the point in the evolution of different inbred mouse strains when the Afr2[b] allele first appeared could help identify the causal Afr2 gene. Future experiments could focus on repeating the liver regeneration model with mouse strains closer to the branching that led to the C57 lineage, including YBR/EiJ and C58/J mice, to determine if this trait is present in these mice. Combined knowledge gained from this experiment and available sequencing might determine potential genes that could result in AFP regulation.

The full liver regeneration data suggests that the Afr2[a] and Afr2[b] alleles are co-dominant. F1 offspring from 129X1/SvJ and C57BL/6J parental mice have an intermediate expression of AFP mRNA and serum levels. Using what we know from

these data, we potentially can breed F1 mice to map and identify the gene responsible for Afr2. Previous studies bred C3H/HeJ and C57BL/6J mice mapped the potential Afr2 gene to a region on chromosome 2, but the gene responsible was never identified [92]. Using 129X1/SvJ and C57BL/6J mice, the offspring of two F1 mice should display AFP reactivation at high, intermediate, and low levels at a frequency of 25%:50%:25% [114]. Like the previous study, we could identify these high, intermediate, and low AFP activators with serum AFP and perform QTL analysis to determine a region of interest in the Afr2 trait.

Our pilot mouse data looking at H19 and LPL, and Gpc3 suggest that Afr2 does increase Zhx2 targets. Although DBA/2J mice do not have an increase in H19 and Gpc3, which might suggest additional genes that might be involved in targeting these gene's expression. The data from our full mouse study suggest that 129X1/SvJ with the Afr2^a allele have robust increases in H19, LPL, and Gpc3 levels, while C57BL/6J mice with the Afr2^b allele have lower fold increases of these genes. F1 male and female mice with both alleles have intermediate levels of Gpc3. Interestingly, F1 male mice have minimal increases in H19 and LPL levels, where females have more significant increases. Our data could suggest that there could be additional sex-dependent factors that might affect H19 and LPL levels.
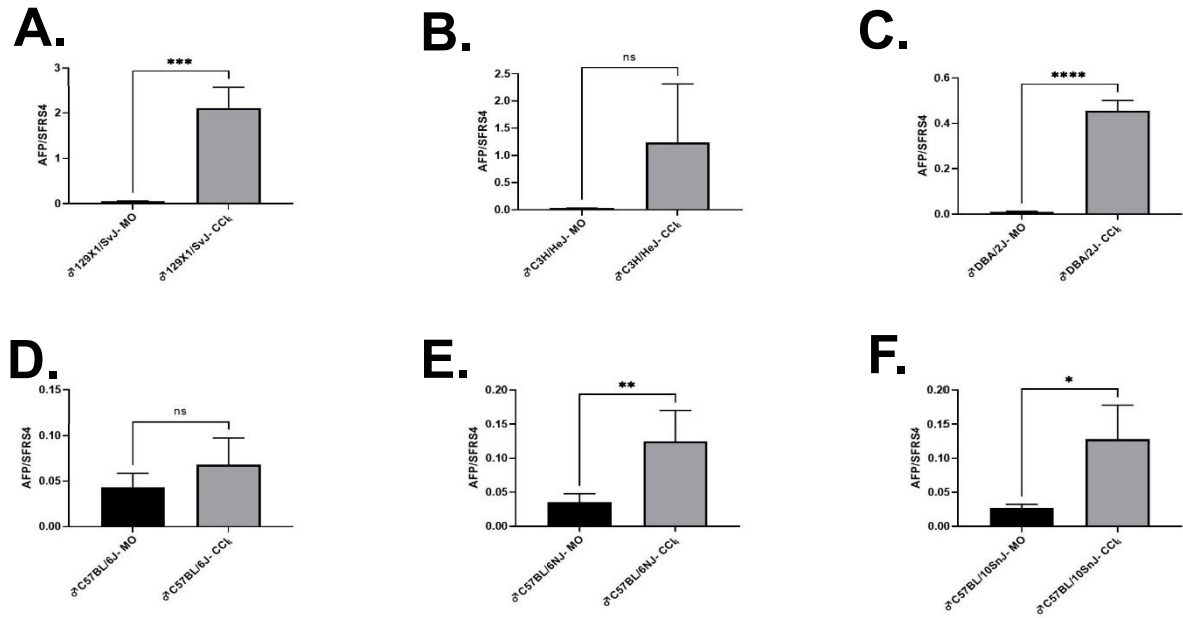
Figure 4.1 AFP activation during regeneration is reduced in the mice from the C57 lineage compared to other mouse strains.

AFP mRNA expression in six-week-old male 129X1/SvJ mice treated with one MO or CCl4 injection (n=4) (A). AFP mRNA expression in six-week-old male C3H/HeJ mice treated with one MO (n=4) or CCl4 injection (n=6) (B). AFP mRNA expression in six-week-old male DBA/2J mice with one MO (n=3) or CCl4 injection (n=5) (C). AFP mRNA expression in six-week-old male C57BL/6J mice treated with one MO (n=3) or CCl4 injection (n=6) (D). AFP mRNA expression in six-week-old male C57BL/6NJ mice treated with one MO (n=4) or CCl4 injection (n=6) (E). AFP mRNA expression in six-week-old male C57BL/10SnJ mice treated with one MO (n=3) or CCl4 injection (n=6) (F). *p<0.05, **p<0.01, ****p<0.0001.

Figure 4.2 Afr2ᵃ trait in non-C57 strains of mice significantly increases serum AFP levels compared to C57BL/6J mice.

AFP serum levels male six-week-old 129X1/SvJ, C3H/HeJ, and C57BL/6J (n=4, C57BL/6J-MO n=3) were treated acutely with either MO or CCl_4 in a model of liver regeneration. $**p<0.01$, $****p<0.0001$.
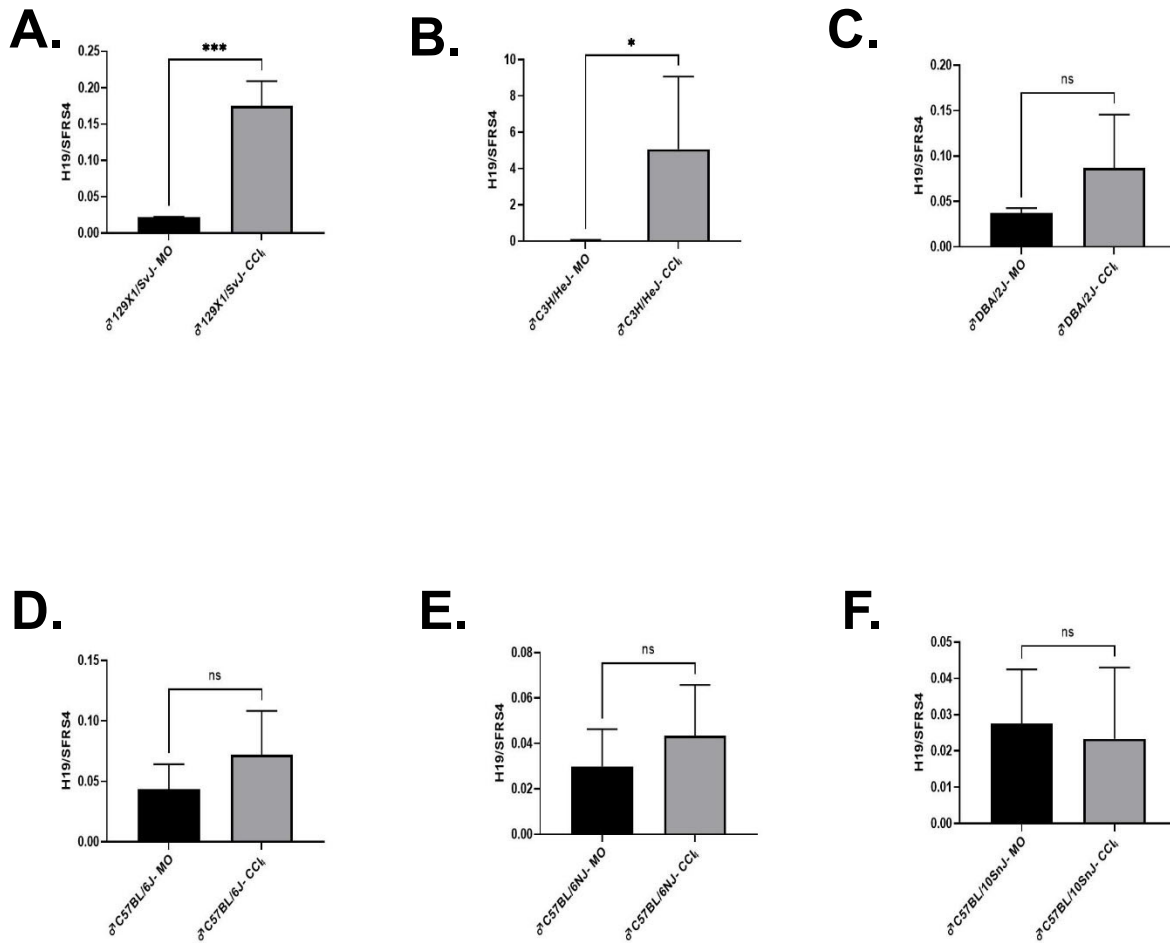
Figure 4.3 Afr2ᵃ trait increases H19, a target gene of Zhx2, in a model of liver regeneration.

H19 mRNA expression in six-week-old male 129X1/SvJ mice treated with one MO (n=4) or CCl4 injection (n=5) (A). H19 mRNA expression in six-week-old male C3H/HeJ mice treated with one MO (n=4) or CCl4 injection (n=6) (B). H19 mRNA expression in six-week-old male DBA/2J mice treated with one MO (n=4) or CCl4 injection (n=6) (C). H19 mRNA expression in six-week-old male C57BL/6J mice treated with one MO (n=3) or CCl4 injection (n=5) (D). H19 mRNA expression in six-week-old male C57BL/6NJ mice treated with one MO (n=4) or CCl4 injection (n=6) (E). H19 mRNA expression in six-

week-old male C57BL/10SnJ mice treated with one MO (n=4) or CCl$_4$ injection (n=6)

(F). *p<0.05, **p<0.01.
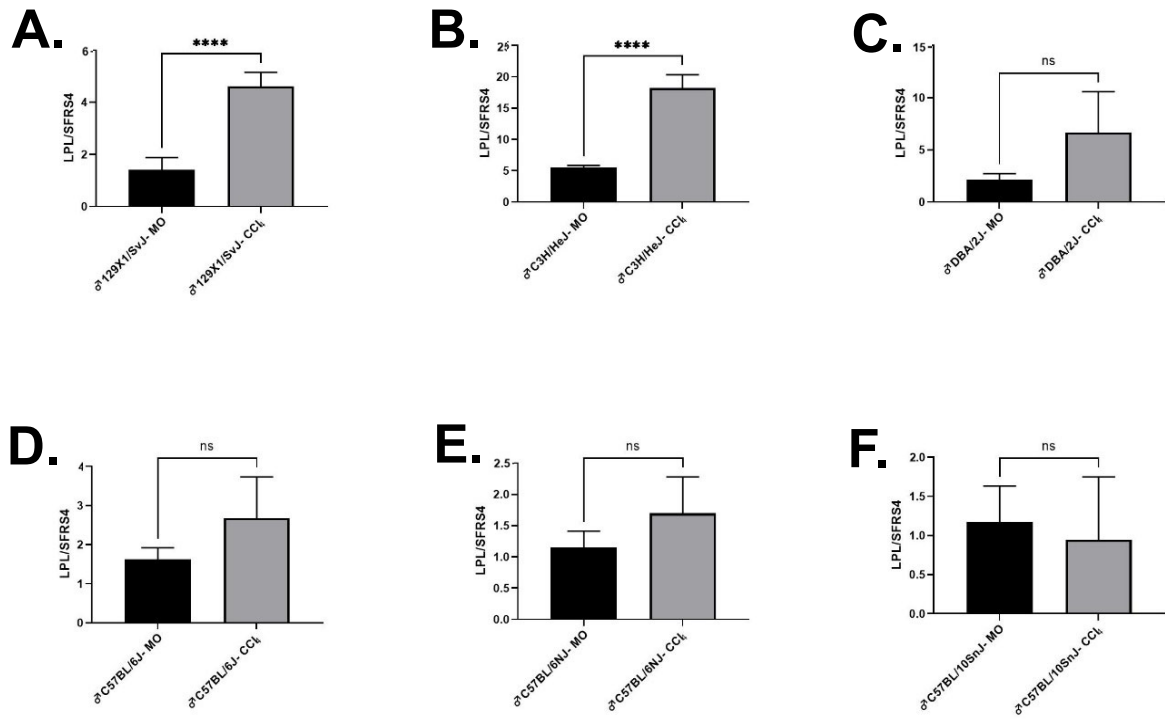
Figure 4.4 Afr2ᵃ trait increases LPL, a target gene of Zhx2, in a model of liver regeneration.

LPL mRNA expression in six-week-old male 129X1/SvJ mice treated with one MO (n=4) or CCl₄ injection (n=5) (A). LPL mRNA expression in six-week-old male C3H/HeJ mice treated with one MO (n=4) or CCl₄ injection (n=6) (B). LPL mRNA expression in six-week-old male DBA/2J mice treated with one MO (n=4) or CCl₄ injection (n=6) (C). LPL mRNA expression in six-week-old male C57BL/6J mice treated with one MO (n=3) or CCl₄ injection (n=6) (D). LPL mRNA expression in six-week-old male C57BL/6NJ mice treated with one MO (n=4) or CCl₄ injection (n=6) (E). LPL mRNA expression in six-week-old male C57BL/10SnJ mice treated with one MO (n=4) or CCl₄ injection (n=6) (F). *p<0.05, **p<0.01.
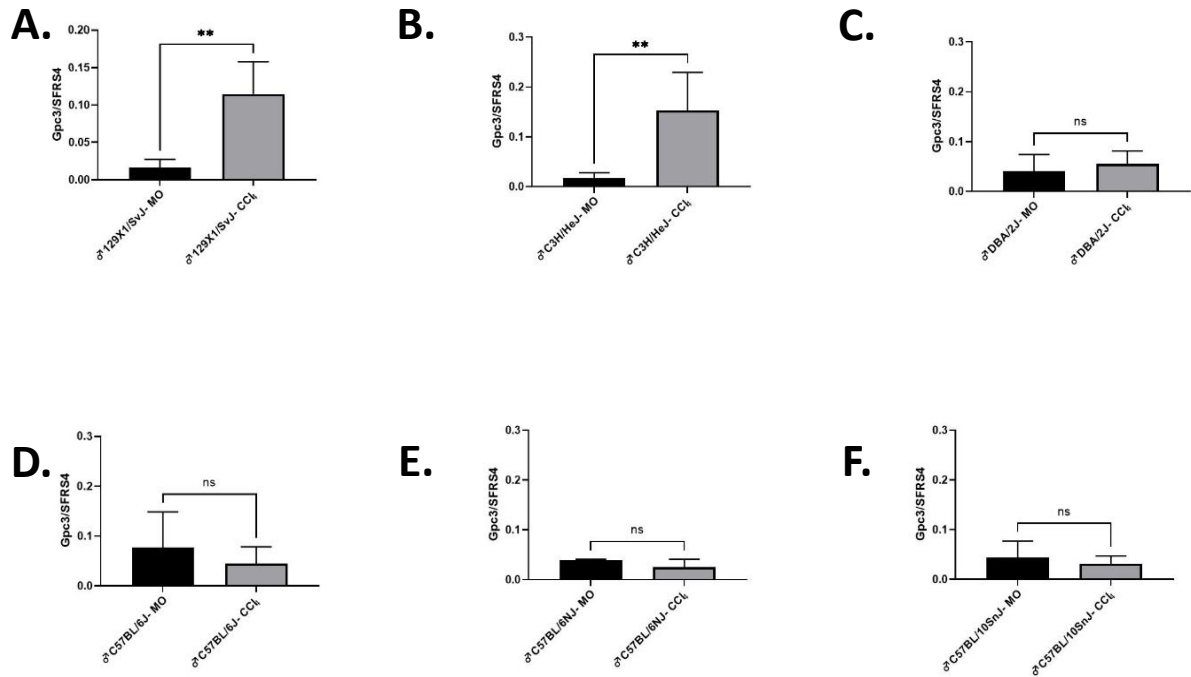
Figure 4.5 Afr2ᵃ trait increases Gpc3, a target gene of Zhx2, in a model of liver regeneration.

Gpc3 mRNA expression in six-week-old male 129X1/SvJ mice treated with one MO (n=4) or CCl$_4$ injection (n=5) (A). Gpc3 mRNA expression in six-week-old male C3H/HeJ mice treated with one MO (n=4) or CCl$_4$ injection (n=6) (B). Gpc3 mRNA expression in six-week-old male DBA/2J mice treated with one MO (n=4) or CCl$_4$ injection (n=5) (C). Gpc3 mRNA expression in six-week-old male C57BL/6J mice treated with one MO (n=4) or CCl$_4$ injection (n=6) (D). Gpc3 mRNA expression in six-week-old male C57BL/6NJ mice treated with one MO (n=3) or CCl$_4$ injection (n=6) (E). Gpc3 mRNA expression in six-week-old male C57BL/10SnJ mice treated with one MO (n=4) or CCl$_4$ injection (n=6) (F). *p<0.05, **p<0.01.
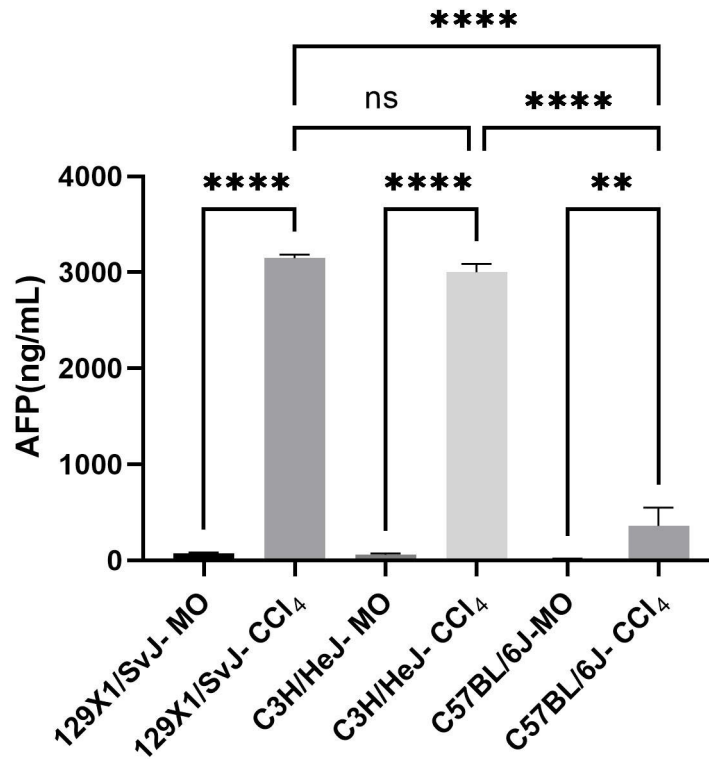
A.

B.

C.

D.
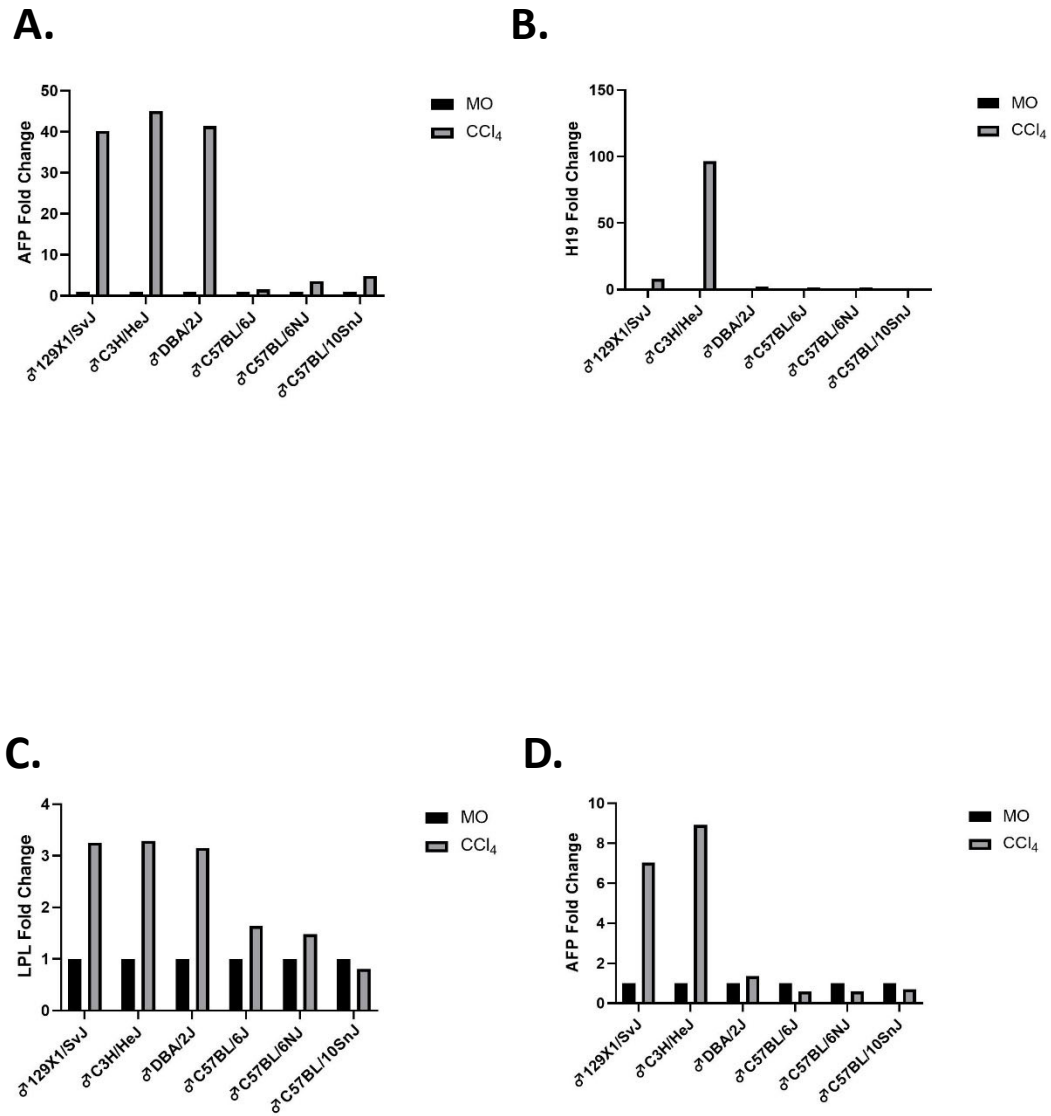
Figure 4.6 Afr2ᵃ trait increases AFP and target genes of Zhx2 in a model of liver regeneration.

AFP mRNA expression fold change in six-week-old male 129X1/SvJ, C3H/HeJ, DBA/2J, C57BL/6J, C57BL/6NJ, and C57BL/10SnJ mice treated with one MO or CCl₄ injection (A). H19 mRNA expression fold change in six-week-old male 129X1/SvJ, C3H/HeJ, DBA/2J, C57BL/6J, C57BL/6NJ, and C57BL/10SnJ mice treated with one MO or CCl₄

injection (B). LPL mRNA expression fold change in six-week-old male 129X1/SvJ,

C3H/HeJ, DBA/2J, C57BL/6J, C57BL/6NJ, and C57BL/10SnJ mice treated with one

MO or CCl$_4$ injection (C). Gpc3 mRNA expression fold change in six-week-old male

129X1/SvJ, C3H/HeJ, DBA/2J, C57BL/6J, C57BL/6NJ, and C57BL/10SnJ mice treated

with one MO or CCl$_4$ injection (D).
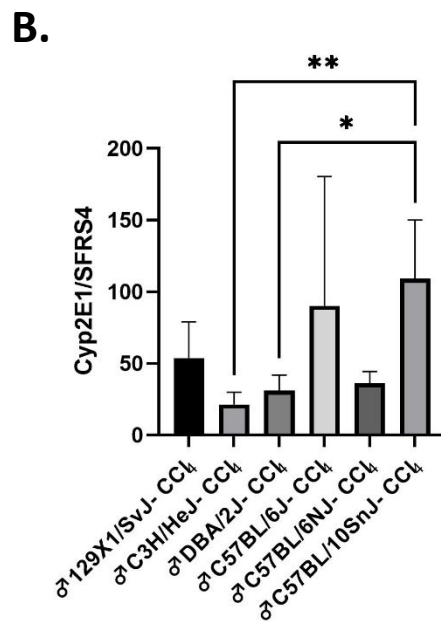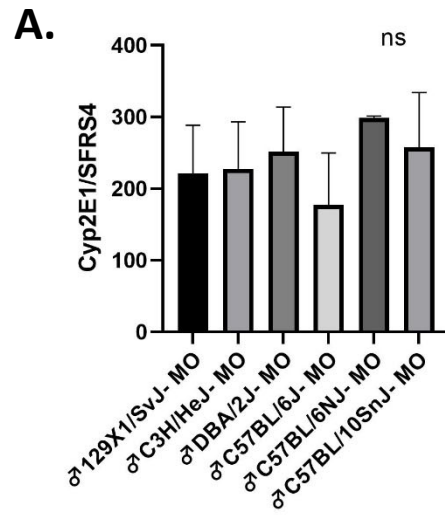
Figure 4.7 AFP reactivation through Afr2 is not dependent on Cyp2E1.

Cyp2E1 mRNA expression of six-week-old male 129X1/SvJ, C3H/HeJ, DBA/2J,

C57BL/6J, C57BL/6NJ, and C57BL/10SnJ treated with MO (n=4, C57BL/6NJ n=3) (A).

Cyp2E1 mRNA expression of male 129X1/SvJ, C3H/HeJ, DBA/2J, C57BL/6J, C57BL/6NJ, and C57BL/10SnJ treated with CCl4 (n=6, 129X1/SvJ, C3H/HeJ, C57BL/6NJ n=5). *p<0.05, **p<0.01.

Figure 4.8 F1 mice display an intermediate activation of AFP in liver regeneration.

AFP mRNA expression in eight-week-old male 129X1/SvJ mice injected with MO (n=5) or CCl_4 (n=7) (A). AFP mRNA expression in eight-week-old female 129X1/SvJ mice injected with MO (n=6) or CCl4 (n=6) (B). AFP mRNA expression in eight-week-old male C57BL/6J mice injected with MO (n=5) or CCl_4 (n=6) (C). AFP mRNA expression

in female eight-week-old C57BL/6J mice injected with MO (n=6) or CCl$_4$ (n=9)(D). AFP

mRNA expression in eight-week-old male F1 mice injected with MO (n=5) or CCl$_4$

(n=7)(E). AFP mRNA expression in female F1 mice injected with MO (n=7) or CCl$_4$

(n=8) (F). *p<0.05, **p<0.01, ***p<0.001.
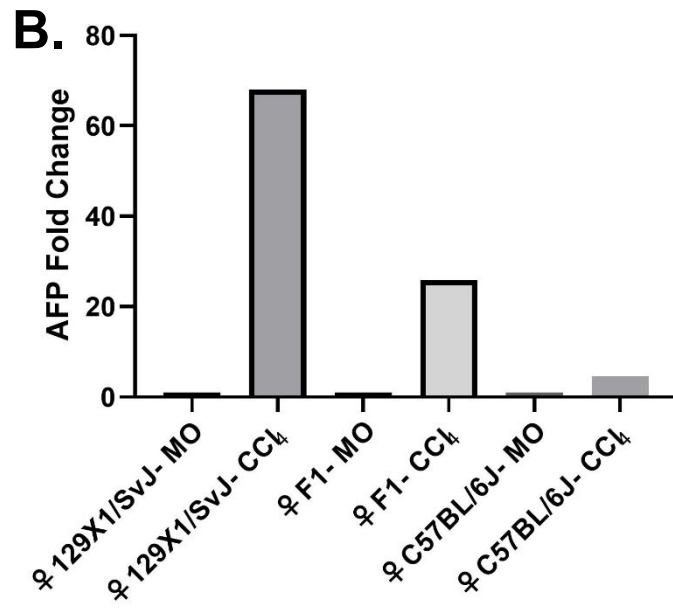
Figure 4.9 F1 mice display an intermediate activation AFP in a model of liver regeneration.

AFP mRNA fold change in eight-week-old male 129X1/SvJ, F1, and C57BL/6J mice injected with MO or CCl$_4$ (A). AFP mRNA fold change in eight-week-old female 129X1/SvJ, F1, and C57BL/6J mice injected with MO or CCl$_4$ (B).

Figure 4.10 F1 mice display intermediate AFP serum reactivation levels in a model of liver regeneration.

AFP serum levels of eight-week-old male 129X1/SvJ, C57BL/6J, and F1 mice were assayed after acute treatment with mineral oil (n=5) or CCl_4 (n=7, C57BL/6J CCl4 n=6) (A). AFP serum levels of eight-week-old female 129X1/SvJ, C57BL/6J, and F1 mice measured after acute treatment with mineral oil (129X1/SvJ n=6, C57BL/6J n=4, F1 n=7) or CCl4 (129X1/SvJ n=6, C57BL/6J n=9, F1 n=8). *p<0.05, ****p<0.0001.
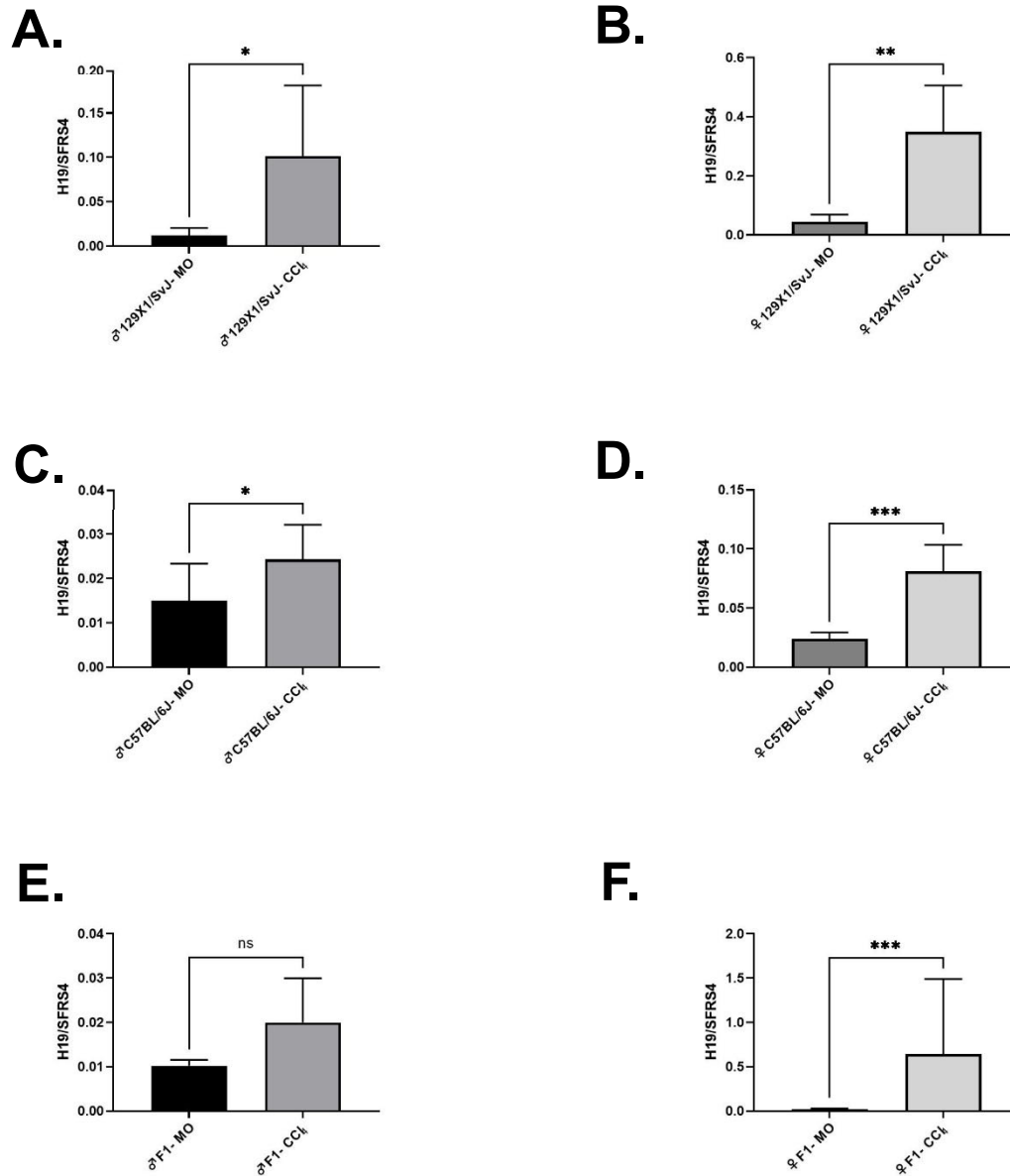
Figure 4.11 F1 mice display an intermediate activation H19, a target of Zhx2.

H19 mRNA expression in eight-week-old male 129X1/SvJ mice injected with MO (n=5)

or CCl4 (n=6) (A). H19 mRNA expression in eight-week-old female 129X1/SvJ mice

injected with MO (n=5) or CCl4 (n=6) (B). H19 mRNA expression in eight-week-old

male C57BL/6J mice injected with MO (n=6) or CCl4 (n=7) (C). H19 mRNA expression

in eight-week-old female C57BL/6J mice injected with MO (n=5) or CCl4 (n=8) (D).

H19 mRNA expression in eight-week-old male F1 mice injected with MO (n=5) or CCl$_4$

(n=7) (E). H19 mRNA expression in eight-week-old female F1 mice injected with MO

(n=7) or CCl4 (n=9) (F). *p<0.05, **p<0.01, ***p<0.001.
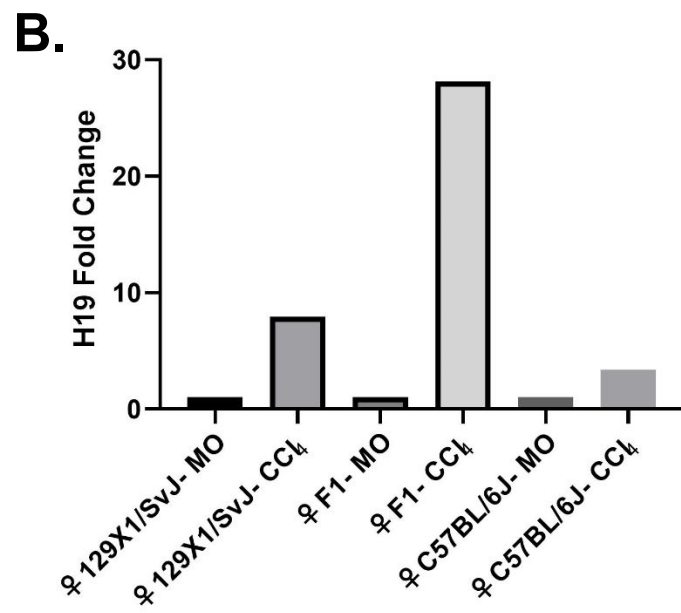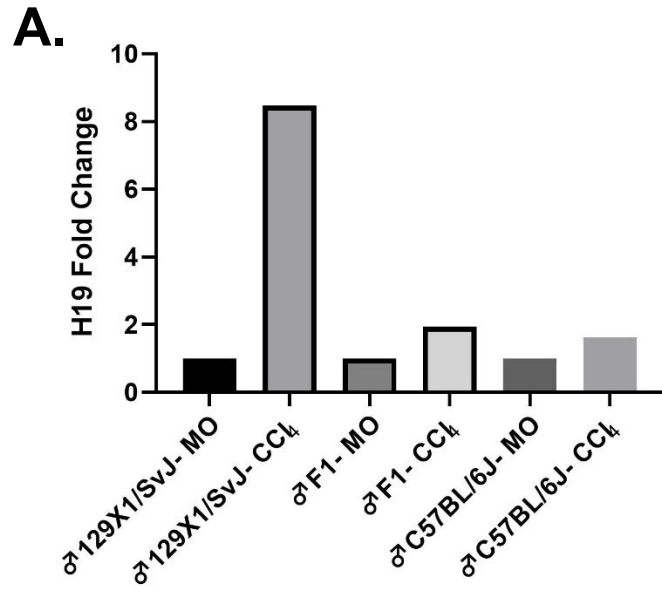
Figure 4.12 F1 female mice display an increase in H19 expression in a model of liver regeneration.

H19 mRNA fold change in eight-week-old male 129X1/SvJ, F1, and C57BL/6J mice injected with MO or CCl_4 (A). H19 mRNA fold change in eight-week-old female 129X1/SvJ, F1, and C57BL/6J mice injected with MO or CCl_4 (B).
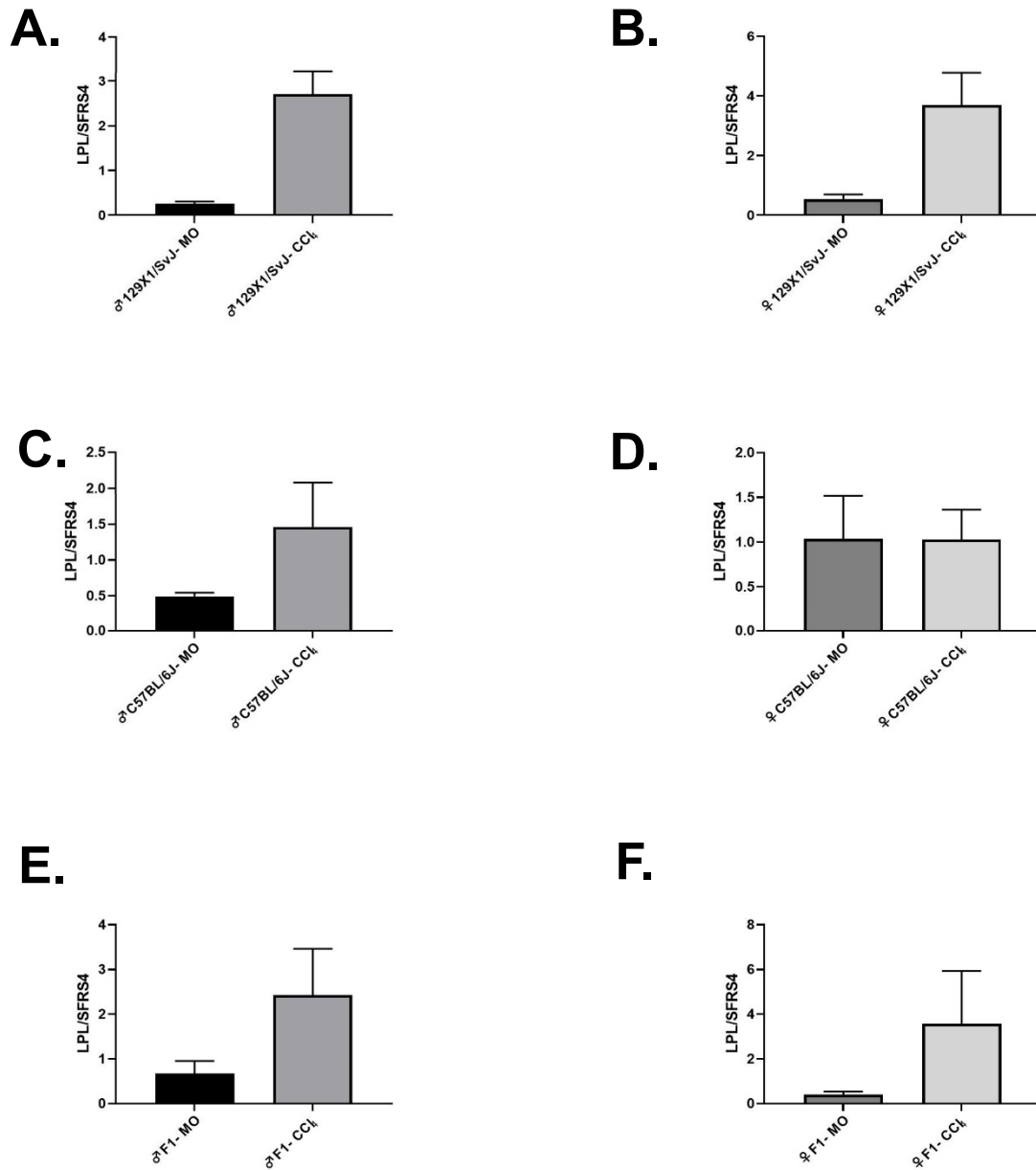
Figure 4.13 F1 mice display an intermediate activation of LPL, a target of Zhx2.

LPL mRNA expression in eight-week-old male 129X1/SvJ mice injected with MO (n=5)

or CCl$_4$ (n=6) (A). LPL mRNA expression in eight-week-old female 129X1/SvJ mice

injected with MO (n=5) or CCl$_4$ (n=7) (B).LPL mRNA expression in eight-week-old

male C57BL/6J mice injected with MO (n=5) or CCl$_4$ (n=7) (C). LPL mRNA expression

in eight-week-old female C57BL/6J mice injected with MO (n=6) or CCl4 (n=9) (D). LPL mRNA expression in eight-week-old male F1 mice injected with MO (n=5) or CCl4 (n=7) (E). LPL mRNA expression in female F1 mice injected with MO or CCl4 after injection at 8-weeks of age (n=6, n=9)(F). **p<0.01, ***p<0.001, ****p<0.0001.
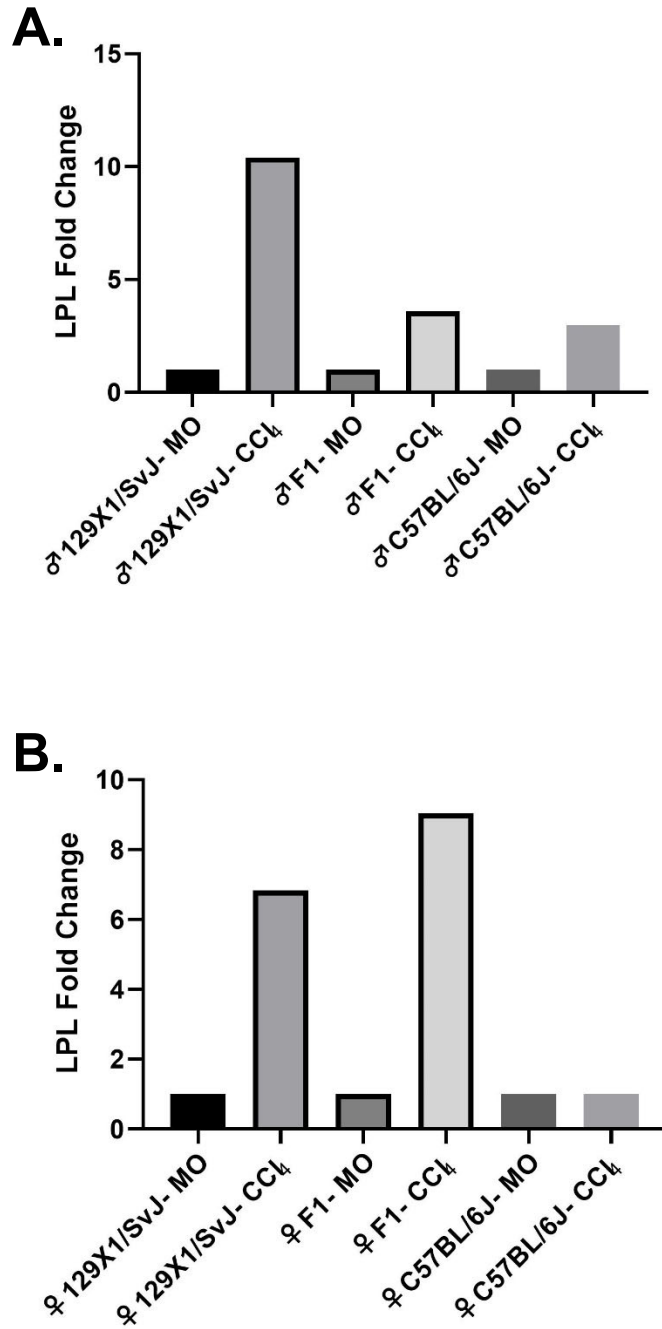
Figure 4.14 F1 female mice have an increase in LPL expression in a model of liver regeneration.

LPL mRNA fold change in eight-week-old male 129X1/SvJ, F1, and C57BL/6J mice injected with MO or CCl$_4$ (A). LPL mRNA fold change in eight-week-old female 129X1/SvJ, F1, and C57BL/6J mice injected with MO or CCl$_4$ (B).
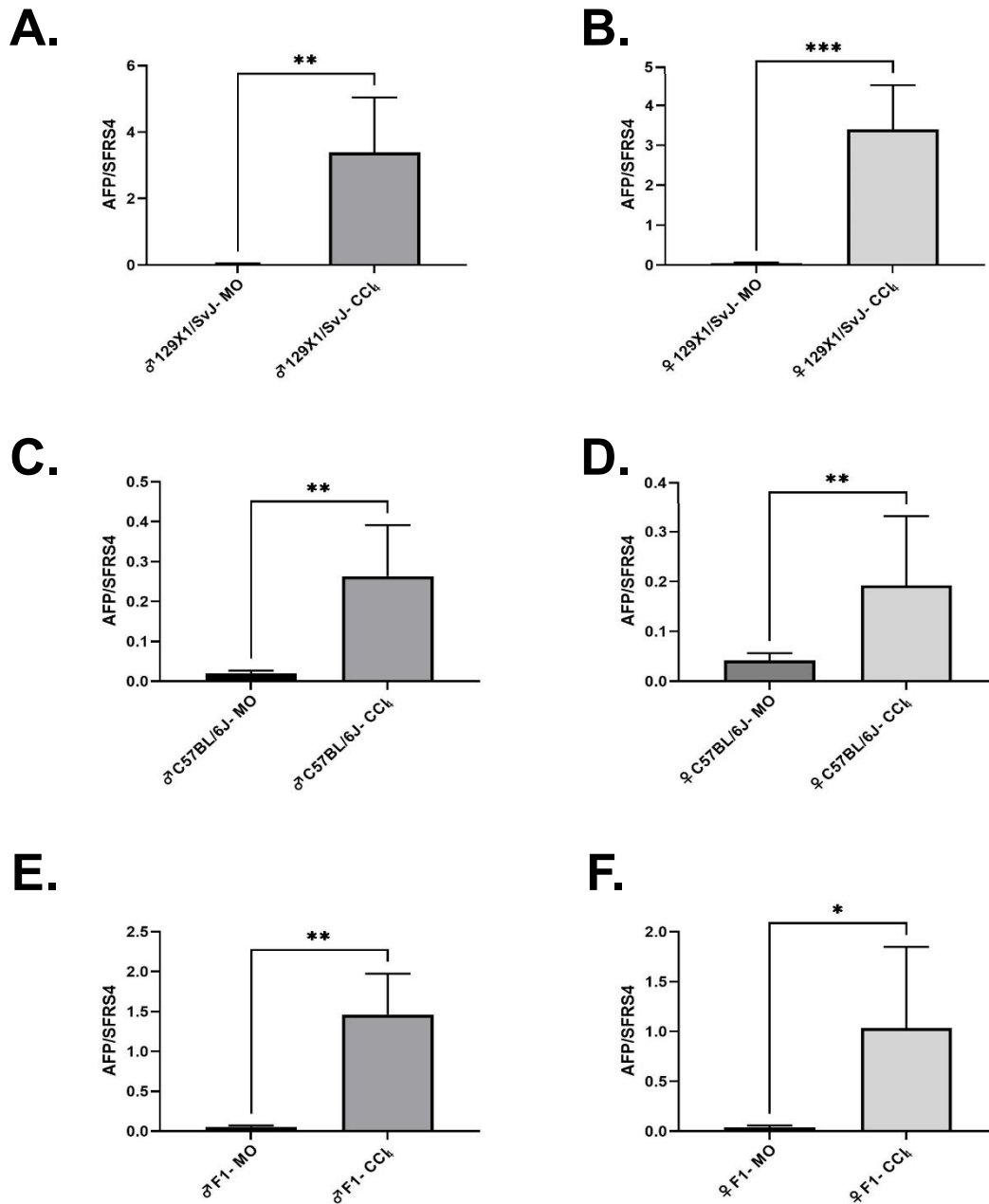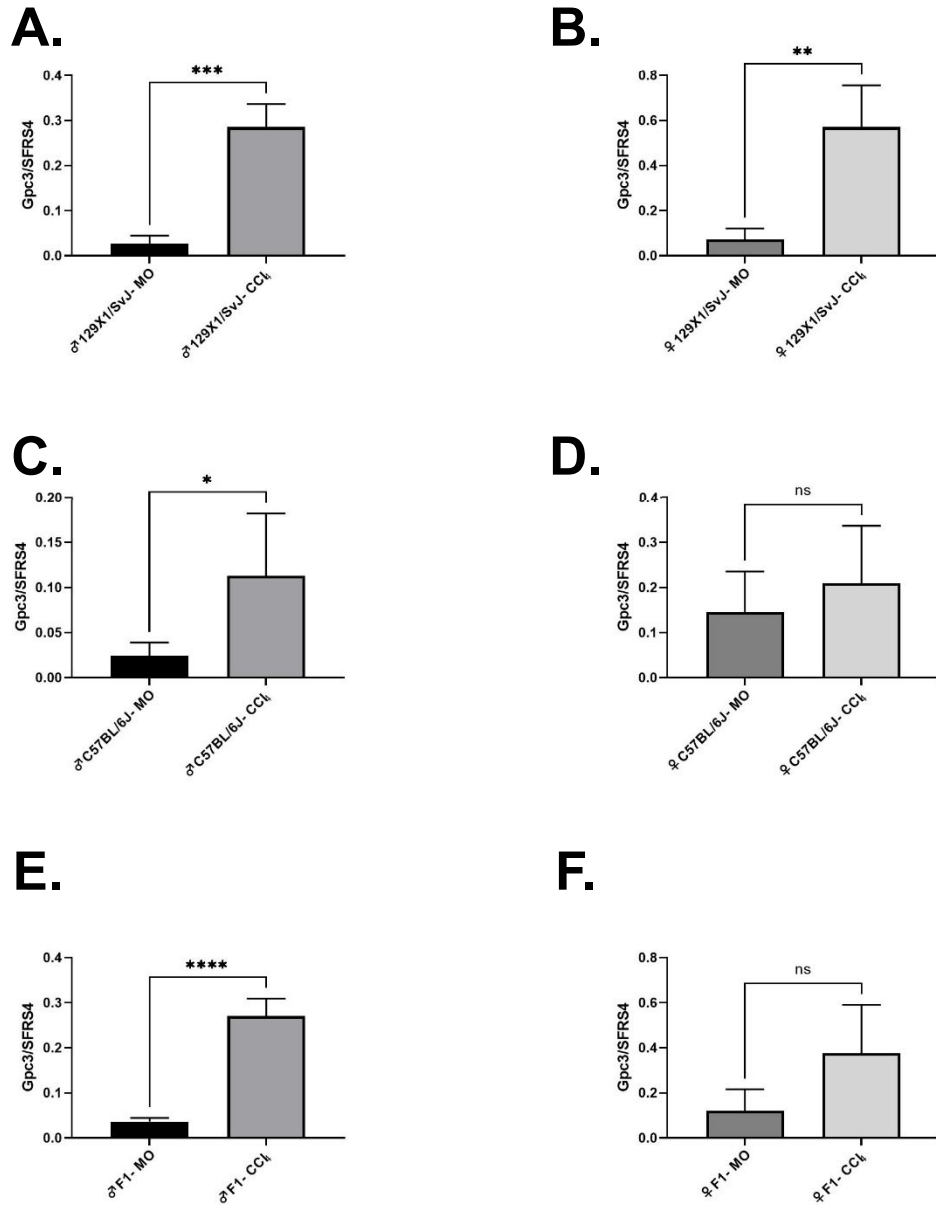
Figure 4.15 F1 mice display an intermediate activation of Gpc3, a target of Zhx2.

Gpc3 mRNA expression in eight-week-old male 129X1/SvJ mice injected with MO (n=3) or CCl$_4$ (n=5) (A). Gpc3 mRNA expression in eight-week-old female 129X1/SvJ mice injected with MO (n=3) or CCl$_4$ (n=4) (B). Gpc3 mRNA expression in eight-week-old male C57BL/6J mice injected with MO (n=3) or CCl$_4$ (n=5) (C). Gpc3 mRNA expression in eight-week-old female C57BL/6J mice injected with MO (n=3) or CCl$_4$ (n=4) (D).

Gpc3 mRNA expression in eight-week-old male F1 mice injected with MO (n=3) or CCl_4 (n=6) (E). Gpc3 mRNA expression in female F1 mice injected with MO (n=3) or CCl_4 (n=5) after injection at 8-weeks of age (F). $*p<0.05$, $**p<0.01$, $***p<0.001$, $****p<0.0001$.
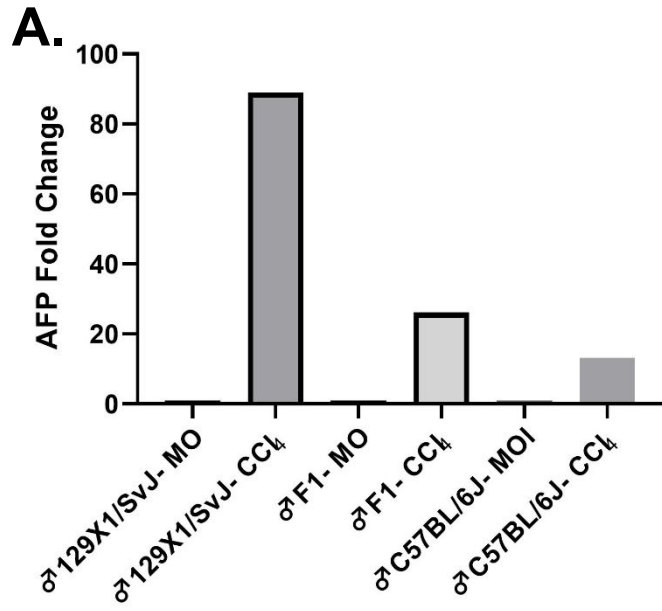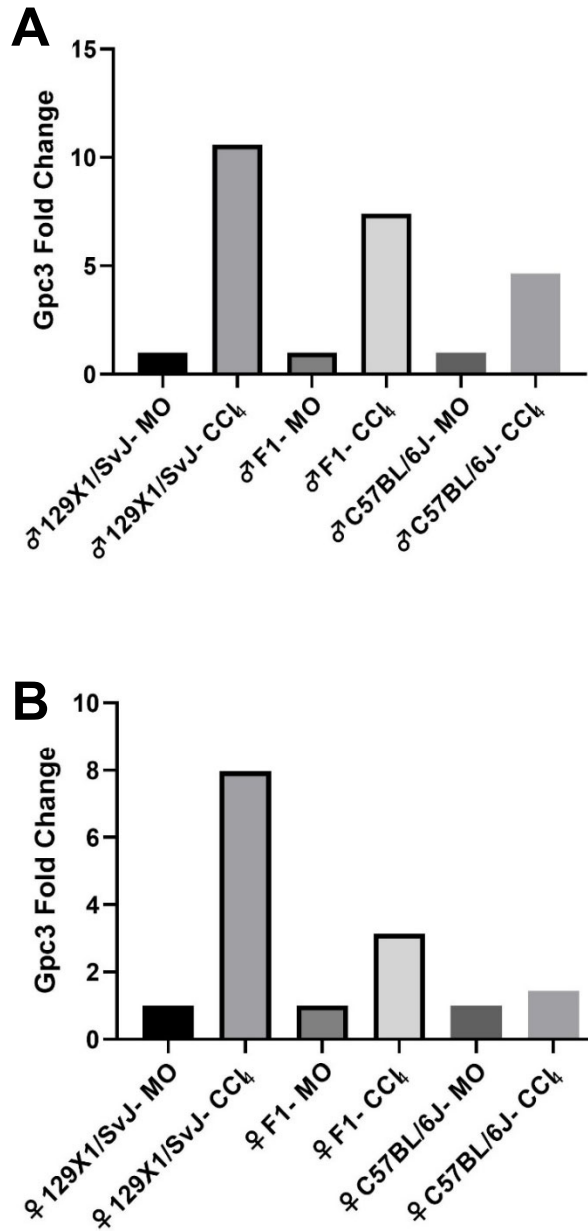
Figure 4.16 F1 mice display an intermediate increase in Gpc3 expression in a model of liver regeneration.

Gpc3 mRNA fold change in eight-week-old male 129X1/SvJ, F1, and C57BL/6J mice injected with MO or CCl₄ (A). Gpc3 mRNA fold change in eight-week-old female 129X1/SvJ, F1, and C57BL/6J mice injected with MO or CCl₄ (B).
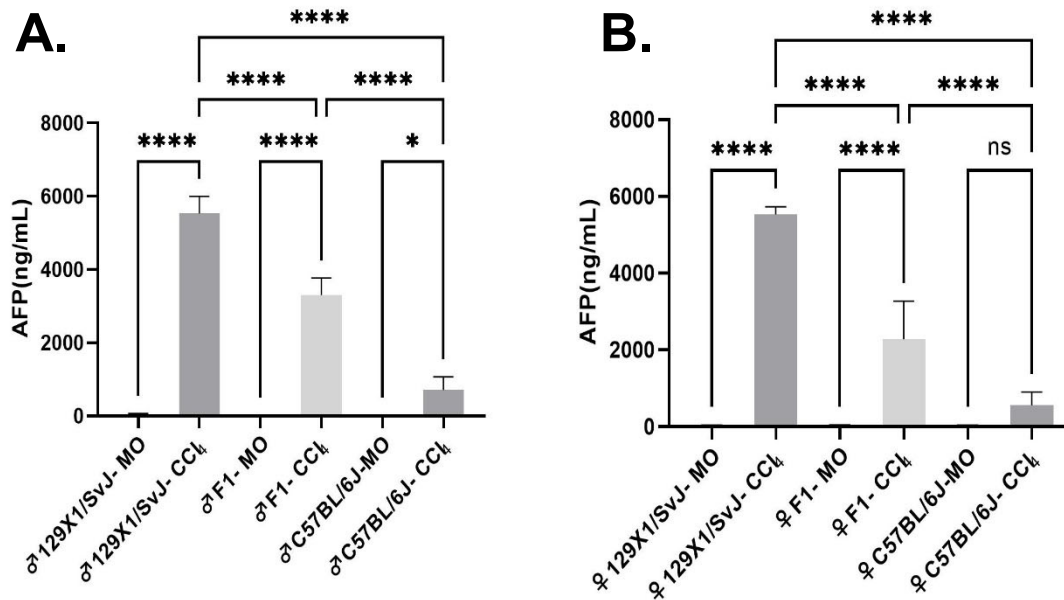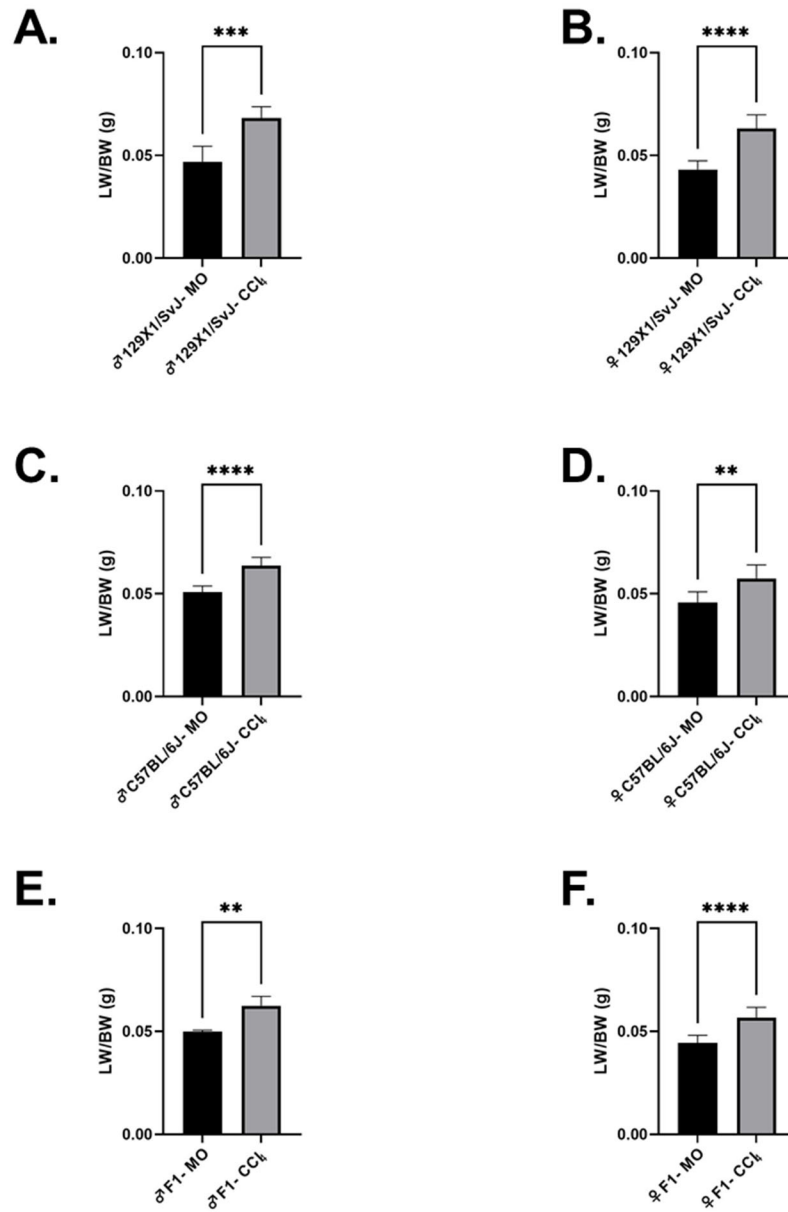
Figure 4.17 129X1/SvJ, C57BL/6J, and F1 mice respond to liver regeneration with CCl$_4$.

Liver weight/body weight ratio in eight-week-old male 129X1/SvJ mice injected with MO (n=5) or CCl$_4$ (n=7) (A). Liver weight/body weight ratio in eight-week-old female 129X1/SvJ mice injected with MO (n=6) or CCl$_4$ (n=7) (B). Liver weight/body weight ratio in eight-week-old male C57BL/6J mice injected with MO (n=6) or CCl$_4$ (n=7) (C).

Liver weight/body weight ratio in eight-week-old female C57BL/6J mice injected with MO (n=6) or CCl_4 (n=9) (D). Liver weight/body weight ratio in eight-week-old male F1 mice injected with MO (n=4) or CCl_4 (n=7) (E). Liver weight/body weight ratio in female F1 mice injected with MO (n=7) or CCl_4 (n=9) after injection at 8-weeks of age (F). **$p<0.01$, ***$p<0.001$, ****$p<0.0001$.

CHAPTER 5. SUMMARY AND FUTURE DIRECTIONS

Inbred mice have been kept as pets and bred for their interesting phenotypes, including coat color, for thousands of years [70]. However, since their use in biomedical research, many genetic differences between different inbred strains have been observed. For example, well documented differences have been found between the frequently used substrains C57BL/6J and C57BL/6N mice. Research has shown many genetic and phenotypic differences between these two substrains, including differences in glucose tolerance and insulin secretion, making them suited for different experimentation models [72, 73]. Outside these substrains, many additional unique phenotypes have been discovered. Identifying and using genetic and phenotypic differences across strains and substrains of mice can be a helpful tool to gain insight into signaling pathways and disease.

The data reported in this dissertation focuses on showing how two genes involved in AFP regulation, Zhx2 (Afr1) and Afr2, can impact liver physiology over the mouse species. Chapter 3 focuses on determining if the hypomorphic mutation of Zhx2 in BALB/cJ mice is responsible for the Hfib1 liver fibrosis phenotype. Previous research identified a region on chromosome 15 in BALB/cJ mice leading to increased liver fibrosis, overlapping with Zhx2 [84, 90]. Based on my results, I eliminated Zhx2 as the causal gene involved in increased fibrosis in BALB/cJ mice. Mice having diminished Zhx2 levels did not differ in fibrosis, inflammation, or damage markers. Chapter 4 focuses on identifying if AFP reactivation during liver regeneration due to the Afr2 trait is dominant and present across different mouse strains. Previous work identified that AFP levels are significantly higher in response to liver regeneration in C3H/HeJ mice than

C57BL/6J [82]. It was determined that this was due to the monogenic Afr2 trait, which had two different alleles, Afr2^a and Afr2^b, leading to high and low levels of AFP, respectively [92]. My data shows that the allele responsible for diminished AFP mRNA and serum reactivation in a 6-week-old liver regeneration model, Afr2^b, was expressed in mice across three strains in the C57BL lineage. The Afr2^a allele leads to significant AFP mRNA and serum level increases in 129X1/SvJ, C3H/HeJ, and DBA/2J mice. This data suggests that the gene responsible for Afr2 might be mutated within the C57BL lineage, leading to low AFP reactivation in response to CCl$_4$ treatment . This finding was further validated by conducting an 8-week- old liver regeneration model in 129X1/SvJ, C57BL/6J, and F1 mice that were a cross of these two strains. As expected, 129X1/SvJ mice had robust AFP reactivation while C57BL/6J mice did not. Interestingly, the F1 mice displayed an intermediate level of AFP reactivation, suggesting that the both Afr2^a and Afr2^b alleles are co-dominant. Overall, this data suggests that both regulators of AFP have an impact on liver functioning and pathophysiology.

5.1 Hfib1

The data collected during the Hfib1 study suggests that the Zhx2 mutation found in BALB/cJ mice is not responsible for the increased fibrosis phenotype seen in this strain. Although, the severity of disease in the treated groups was highly variable, which could lead to a masking of the effect. It is possible that the variation we see is due to samples being taken from different lobes of the liver. In a paper from 1997, expression of fibrinogen genes were found to be different in each lobe [116]. In other CCl$_4$ studies, inbred rat models were found to have a high level of variation between individuals [117, 118]. A study reported that gene expression differences in pathways involved in

immunity, steroid metabolism, and lipid metabolism could lead to variation between mice in CCl4 treatment models [119]. In my study, I found that many mRNA fibrosis markers were varied; for example, male Zhx2$^{KO/Afr1}$ treated with CCl4 had an ACTA2 mRNA expression average of 2.05 with a standard deviation of 1.72. With such a high standard deviation, the data is unreliable, and other analysis should be done. If there was a minor effect, the variation of this data could potentially conceal it. Several other methods for administration of CCl4 induce liver damage, including oral gavage, subcutaneous injection, and inhalation [120-122]. Unfortunately, it seems that these methods of administration also see variation and have more significant mortality. Treating mice with a lower amount of CCl4 might allow us to determine differences between the treatment groups. If there was some protection in mice with wild-type Zhx2, it might be overwhelmed by high prolonged CCl4 doses. Smaller studies looking at lower CCl4 dosing could be potentially done in these mice to determine if there is a small effect. It is also possible that the number of mice (n) used in CCl4- treated groups was too small. Some studies have n values up to 10 to minimize variability [123]. Another option for reducing variability would be to change the liver fibrosis model entirely. Bile duct ligation (BDL) is another model for promoting liver fibrosis that is commonly used. In a study looking at various models for liver fibrosis induction, BDL is a consistent way of inducing fibrosis and liver failure within two months of surgery [124]. Although more invasive, this might be a better model for observing any effect that Zhx2 might have on the fibrosis seen in mice.

With such high mRNA variability of fibrosis markers, additional protein analysis should be performed. Dr. Shirley Qiu analyzed levels of αSMA in the livers of these mice

but found that there were no significant differences between CCl_4-treated mice (data not shown). Protein levels of collagen 1a1 and Timp1 could also be analyzed to determine any differences in fibrosis markers.

In addition to Zhx2, many genes fall within the Hfib1 region on Chromosome 15. Potentially, one of these genes may be responsible for the increased fibrosis phenotype previously seen in BALB/cJ mice. As previously discussed, several genes within this region can play a role in liver fibrosis, including Col14a1 and Has2. Col14a1 (Undulin) is increased during liver fibrosis, found in areas of concentrated fibrosis [125]. In addition, Hyaluronan Synthase 2 (Has2) has been frequently observed in liver disease, with it being produced by the hepatic stellate cells during fibrosis. Further studies looking into the candidate genes in the region might determine which is responsible for the Hfib1 phenotype.

5.2 Afr2

My results from the Afr2 study show that C57BL lineage mice have display low AFP reactivation in response to CCl_4. In contrast, the other strains used in the study have a robust increase of AFP during liver regeneration. This finding confirms previous studies but further shows AFP reactivation differences across several strains [82, 92]. Although it is known that this Afr2 trait is involved in liver regeneration, the mechanism involved remains unknown. Liver regeneration is a process that happens over a few days and activates many pathways required for proliferation and inflammation [126]. We could further investigate the Afr2 trait and its mechanism of action by looking at 129X1/SvJ and C57BL/6J mice throughout liver regeneration. Mice could have blood collected before the initial injection and one, three, five, and seven days post-injection to

monitor AFP levels in the serum. mRNA expression of markers involved in the initial priming process of liver regeneration, including TNF-α and IL-6, can be assessed in the livers of these mice soon after injection [127]. Factors associated with hepatocyte proliferation, including HGF and EGF, could also be assessed throughout liver regeneration [62]. Measuring early differences in liver damage markers, such as ALT, might also be informative in how much damage is occurring in these mice in the first several days of liver regeneration.

In my Afr2 study looking at F1 mice, I was able to show these mice had an intermediate level of reactivation of AFP during liver regeneration. This data would suggest that $Afr2^a$ and $Afr2^b$ are co-dominant. Although it was previously thought that $Afr2^a$ was dominant, my data supports more recent findings that $Afr2^{a/b}$ mice have an intermediate phenotype [82, 92]. We could further use this information to map and determine the gene responsible for Afr2. Two F1 mice can be bred to obtain offspring that are $Afr2^{a/a}$, $Afr2^{b/b}$, and $Afr2^{a/b}$. These high, low, and intermediate mice can be used to map the possible position of the gene responsible for Afr2. Previous studies looking at Afr2 using C3H/HeJ and C57BL/6J mice mapped the potential gene responsible for AFP reactivation in this model to a region on Chromosome 2 [92]. However, the causal gene was never identified. Using both the 129X1/SvJ mice and a less invasive way to screen large amounts of offspring through serum AFP, we should be able to remap the Afr2 region.

My data also found that there might be additional factors involved in the extent to whicgh Afr2 alters expression of genes that are also targets of Zhx2. H19 expression fold change was not as robust in 129X1/SvJ and DBA/2J mice compared to C3H/HeJ mice,

while their AFP reactivation was similar. This finding would suggest that regulation of H19 might require regulation besides Afr2. When looking at the 8-week-old study, H19 and Lpl were not significantly different in the F1 male mice but were in females. This result might also suggest that a sex-dependent mechanism regulates these target genes. In previous studies, H19 was found to be female-biased in the mouse eye [128]. It has also been seen that increases in steroid hormones, like estrogen, cause increase H19 expression within the tissues and were diminished in ovariectomized mice [129]. Thus, H19 activation in the liver in response to injury might result from an estrogen-regulated mechanism in this model of liver regeneration. Studies could be done to look at estrogen levels before, during, and after liver regeneration to test if increases in estrogen might play a role in increasing H19 and Lpl levels in female mice.

5.3 <u>Summary</u>

Both Zhx2 (Afr1) and Afr2 have been found to play a role within different mouse strains in regulating AFP expression in development and during liver injury. Zhx2 seems to affect the whole range of liver disease, including diet-induced fatty liver and hepatocellular carcinoma [89, 130]. Although my studies suggest Zhx2 is not involved in the extent of liver fibrosis, many other genes within the region might be responsible for Hfib1. AFP reactivation during liver injury is caused by the Afr2 trait [82, 92]. Although the gene has not been identified, my findings confirmed that the C57BL lineage has lower AFP activation levels than other strains and that this trait is co-dominant [92]. In future studies, identifying the gene responsible for the Afr2 could be of benefit. As with the case of Zhx2, the gene responsible for Afr2 could play a potential role in human liver disease. In addition, understanding more about the possible mechanisms involved in

Zhx2 and Afr2's regulation of liver function might help develop new targets in treating liver disease.

REFERENCES

1.	Han, H.S., et al., *Regulation of glucose metabolism from a liver-centric perspective.* Exp Mol Med, 2016. **48**: p. e218.
2.	Pilkis, S.J. and D.K. Granner, *Molecular physiology of the regulation of hepatic gluconeogenesis and glycolysis.* Annu Rev Physiol, 1992. **54**: p. 885-909.
3.	Rui, L., *Energy metabolism in the liver.* Compr Physiol, 2014. **4**(1): p. 177-97.
4.	Rothschild, M.A., M. Oratz, and S.S. Schreiber, *Serum albumin.* Hepatology, 1988. **8**(2): p. 385-401.
5.	Drugan, A., et al., *Alpha-fetoprotein.* Curr Opin Obstet Gynecol, 1991. **3**(2): p. 230-4.
6.	Canbay, A., L. Bechmann, and G. Gerken, *Lipid metabolism in the liver.* Z Gastroenterol, 2007. **45**(1): p. 35-41.
7.	Hellerstein, M.K., J.M. Schwarz, and R.A. Neese, *Regulation of hepatic de novo lipogenesis in humans.* Annu Rev Nutr, 1996. **16**: p. 523-57.
8.	Guengerich, F.P., *Mechanisms of Cytochrome P450-Catalyzed Oxidations.* ACS Catal, 2018. **8**(12): p. 10964-10976.
9.	Almazroo, O.A., M.K. Miah, and R. Venkataramanan, *Drug Metabolism in the Liver.* Clin Liver Dis, 2017. **21**(1): p. 1-20.
10.	Rendic, S. and F.P. Guengerich, *Survey of Human Oxidoreductases and Cytochrome P450 Enzymes Involved in the Metabolism of Xenobiotic and Natural Chemicals.* Chem Res Toxicol, 2015. **28**(1): p. 38-42.
11.	Wienkers, L.C. and T.G. Heath, *Predicting in vivo drug interactions from in vitro drug discovery data.* Nature Reviews Drug Discovery, 2005. **4**(10): p. 825-833.
12.	Connor, H.D., et al., *The formation of a novel free radical metabolite from CCl4 in the perfused rat liver and in vivo.* J Biol Chem, 1986. **261**(10): p. 4542-8.
13.	Tolba, R., et al., *Diethylnitrosamine (DEN)-induced carcinogenic liver injury in mice.* Lab Anim, 2015. **49**(1 Suppl): p. 59-69.
14.	McGregor, D. and M. Lang, *Carbon tetrachloride: genetic effects and other modes of action.* Mutat Res, 1996. **366**(3): p. 181-95.
15.	Guengerich, F.P., *Cytochrome P450 2E1 and its roles in disease.* Chemico-Biological Interactions, 2020. **322**: p. 109056.
16.	Jancova, P., P. Anzenbacher, and E. Anzenbacherova, *Phase II drug metabolizing enzymes.* Biomed Pap Med Fac Univ Palacky Olomouc Czech Repub, 2010. **154**(2): p. 103-16.
17.	Xu, C., C.Y. Li, and A.N. Kong, *Induction of phase I, II and III drug metabolism/transport by xenobiotics.* Arch Pharm Res, 2005. **28**(3): p. 249-68.
18.	Nigam, S.K., *What do drug transporters really do?* Nat Rev Drug Discov, 2015. **14**(1): p. 29-44.
19.	Kmiec, Z., *Cooperation of liver cells in health and disease.* Adv Anat Embryol Cell Biol, 2001. **161**: p. III-XIII, 1-151.
20.	Dixon, L.J., et al., *Kupffer cells in the liver.* Compr Physiol, 2013. **3**(2): p. 785-97.
21.	Li, P.-z., et al., *An efficient method to isolate and culture mouse Kupffer cells.* Immunology Letters, 2014. **158**(1): p. 52-56.
22.	Li, N. and J. Hua, *Immune cells in liver regeneration.* Oncotarget, 2017. **8**(2): p. 3628-3639.

23. Higashi, T., S.L. Friedman, and Y. Hoshida, *Hepatic stellate cells as key target in liver fibrosis.* Advanced Drug Delivery Reviews, 2017. **121**: p. 27-42.

24. Sorensen, K.K., et al., *Liver Sinusoidal Endothelial Cells.* Compr Physiol, 2015. **5**(4): p. 1751-74.

25. LeSage, G., S. Glaser, and G. Alpini, *Regulation of cholangiocyte proliferation.* Liver, 2001. **21**(2): p. 73-80.

26. Fu, X., et al., *Modeling of xenobiotic transport and metabolism in virtual hepatic lobule models.* PLOS ONE, 2018. **13**(9): p. e0198060.

27. Brunt, E.M., et al., *Pathology of the liver sinusoids.* Histopathology, 2014. **64**(7): p. 907-20.

28. Ben-Moshe, S., et al., *Spatial sorting enables comprehensive characterization of liver zonation.* Nature Metabolism, 2019. **1**(9): p. 899-911.

29. Jungermann, K., *Metabolic zonation of liver parenchyma.* Semin Liver Dis, 1988. **8**(4): p. 329-41.

30. Kietzmann, T., *Metabolic zonation of the liver: The oxygen gradient revisited.* Redox Biol, 2017. **11**: p. 622-630.

31. Christoffels, V.M., et al., *A mechanistic model for the development and maintenance of portocentral gradients in gene expression in the liver.* Hepatology, 1999. **29**(4): p. 1180-1192.

32. Yang, J., et al., *Beta-catenin signaling in murine liver zonation and regeneration: A Wnt-Wnt situation!* Hepatology, 2014. **60**(3): p. 964-976.

33. Benhamouche, S., et al., *Apc Tumor Suppressor Gene Is the "Zonation-Keeper" of Mouse Liver.* Developmental Cell, 2006. **10**(6): p. 759-770.

34. Jungermann, K. and T. Kietzmann, *Zonation of parenchymal and nonparenchymal metabolism in liver.* Annu Rev Nutr, 1996. **16**: p. 179-203.

35. Hijmans, B.S., et al., *Zonation of glucose and fatty acid metabolism in the liver: mechanism and metabolic consequences.* Biochimie, 2014. **96**: p. 121-9.

36. Wei, Y., et al., *Liver homeostasis is maintained by midlobular zone 2 hepatocytes.* Science, 2021. **371**(6532): p. eabb1625.

37. Collaboration, G.B.o.D.L.C., *The Burden of Primary Liver Cancer and Underlying Etiologies From 1990 to 2015 at the Global, Regional, and National Level: Results From the Global Burden of Disease Study 2015.* JAMA Oncology, 2017. **3**(12): p. 1683-1691.

38. Yoon, Y.a.C., C. M., *Surveillance Report #114: Liver Cirrhosis Mortality in the United States: National, State, and Regional Trends, 2000-2017.* 2019.

39. Lazo, M. and J.M. Clark, *The epidemiology of nonalcoholic fatty liver disease: a global perspective.* Semin Liver Dis, 2008. **28**(4): p. 339-50.

40. Himoto, T. and M. Nishioka, *Autoantibodies in liver disease: important clues for the diagnosis, disease activity and prognosis.* Auto Immun Highlights, 2013. **4**(2): p. 39-53.

41. Manns, M.P. and A. Vogel, *Autoimmune hepatitis, from mechanisms to therapy.* Hepatology, 2006. **43**(2 Suppl 1): p. S132-44.

42. Idilman, I.S., I. Ozdeniz, and M. Karcaaltincaba, *Hepatic Steatosis: Etiology, Patterns, and Quantification.* Semin Ultrasound CT MR, 2016. **37**(6): p. 501-510.

43. Marchesini, G., et al., *Association of nonalcoholic fatty liver disease with insulin resistance.* The American Journal of Medicine, 1999. **107**(5): p. 450-455.

44. Jelenik, T., et al., *Mechanisms of Insulin Resistance in Primary and Secondary Nonalcoholic Fatty Liver.* Diabetes, 2017. **66**(8): p. 2241.

45. Spahis, S., et al., *Oxidative Stress as a Critical Factor in Nonalcoholic Fatty Liver Disease Pathogenesis.* Antioxidants & Redox Signaling, 2017. **26**(10): p. 519-541.

46. Seitz, H.K., et al., *Alcoholic liver disease.* Nature Reviews Disease Primers, 2018. **4**(1): p. 16.

47. Miele, L., et al., *Fatty liver and drugs: the two sides of the same coin.* Eur Rev Med Pharmacol Sci, 2017. **21**(1 Suppl): p. 86-94.

48. Bataller, R. and D.A. Brenner, *Liver fibrosis.* The Journal of Clinical Investigation, 2005. **115**(2): p. 209-218.

49. van Dijk, F., et al., *Design of a Gene Panel to Expose the Versatile Role of Hepatic Stellate Cells in Human Liver Fibrosis.* Pharmaceutics, 2020. **12**(3).

50. Friedman, S.L., *Hepatic stellate cells: protean, multifunctional, and enigmatic cells of the liver.* Physiological reviews, 2008. **88**(1): p. 125-172.

51. Smith, A., K. Baumgartner, and C. Bositis, *Cirrhosis: Diagnosis and Management.* Am Fam Physician, 2019. **100**(12): p. 759-770.

52. Sia, D., et al., *Liver Cancer Cell of Origin, Molecular Class, and Effects on Patient Prognosis.* Gastroenterology, 2017. **152**(4): p. 745-761.

53. Galle, P.R., et al., *Biology and significance of alpha-fetoprotein in hepatocellular carcinoma.* Liver Int, 2019. **39**(12): p. 2214-2229.

54. Lafaro, K.J., A.N. Demirjian, and T.M. Pawlik, *Epidemiology of Hepatocellular Carcinoma.* Surgical Oncology Clinics of North America, 2015. **24**(1): p. 1-17.

55. Siegel, R.L., et al., *Cancer Statistics, 2021.* CA Cancer J Clin, 2021. **71**(1): p. 7-33.

56. Rahib, L., et al., *Projecting cancer incidence and deaths to 2030: the unexpected burden of thyroid, liver, and pancreas cancers in the United States.* Cancer Res, 2014. **74**(11): p. 2913-21.

57. Kohler, C., et al., *Expression of Notch-1 and its ligand Jagged-1 in rat liver during liver regeneration.* Hepatology, 2004. **39**(4): p. 1056-65.

58. Stolz, D.B., et al., *Growth factor signal transduction immediately after two-thirds partial hepatectomy in the rat.* Cancer Res, 1999. **59**(16): p. 3954-60.

59. Michalopoulos, G.K. and B. Bhushan, *Liver regeneration: biological and pathological mechanisms and implications.* Nat Rev Gastroenterol Hepatol, 2021. **18**(1): p. 40-55.

60. Webber, E.M., P.J. Godowski, and N. Fausto, *In vivo response of hepatocytes to growth factors requires an initial priming stimulus.* Hepatology, 1994. **19**(2): p. 489-97.

61. Kang, L.I., W.M. Mars, and G.K. Michalopoulos, *Signals and cells involved in regulating liver regeneration.* Cells, 2012. **1**(4): p. 1261-92.

62. Michalopoulos, G., et al., *Control of hepatocyte replication by two serum factors.* Cancer Res, 1984. **44**(10): p. 4414-9.

63. Runge, D.M., et al., *Epidermal growth factor- and hepatocyte growth factor-receptor activity in serum-free cultures of human hepatocytes.* J Hepatol, 1999. **30**(2): p. 265-74.

64. Romero-Gallo, J., et al., *Inactivation of TGF-beta signaling in hepatocytes results in an increased proliferative response after partial hepatectomy.* Oncogene, 2005. **24**(18): p. 3028-41.

65.   Jahn, D., et al., *Animal models of NAFLD from a hepatologist's point of view.* Biochim Biophys Acta Mol Basis Dis, 2019. **1865**(5): p. 943-953.

66.   Lamas-Paz, A., et al., *Alcoholic liver disease: Utility of animal models.* World J Gastroenterol, 2018. **24**(45): p. 5063-5075.

67.   Weber, L.W., M. Boll, and A. Stampfl, *Hepatotoxicity and mechanism of action of haloalkanes: carbon tetrachloride as a toxicological model.* Crit Rev Toxicol, 2003. **33**(2): p. 105-36.

68.   Georgiev, P., et al., *Characterization of time-related changes after experimental bile duct ligation.* Br J Surg, 2008. **95**(5): p. 646-56.

69.   Yanguas, S.C., et al., *Experimental models of liver fibrosis.* Arch Toxicol, 2016. **90**(5): p. 1025-1048.

70.   Beck, J.A., et al., *Genealogies of mouse inbred strains.* Nat Genet, 2000. **24**(1): p. 23-5.

71.   Petkov, P.M., et al., *An efficient SNP system for mouse genome scanning and elucidating strain relationships.* Genome Res, 2004. **14**(9): p. 1806-11.

72.   Simon, M.M., et al., *A comparative phenotypic and genomic analysis of C57BL/6J and C57BL/6N mouse strains.* Genome Biol, 2013. **14**(7): p. R82.

73.   Toye, A.A., et al., *A genetic and physiological study of impaired glucose homeostasis control in C57BL/6J mice.* Diabetologia, 2005. **48**(4): p. 675-86.

74.   Kioussis, D., et al., *The evolution of alpha-fetoprotein and albumin. II. The structures of the alpha-fetoprotein and albumin genes in the mouse.* J Biol Chem, 1981. **256**(4): p. 1960-7.

75.   Gitlin, D., A. Perricelli, and G.M. Gitlin, *Synthesis of -fetoprotein by liver, yolk sac, and gastrointestinal tract of the human conceptus.* Cancer Res, 1972. **32**(5): p. 979-82.

76.   Tilghman, S.M. and A. Belayew, *Transcriptional control of the murine albumin/alpha-fetoprotein locus during development.* Proc Natl Acad Sci U S A, 1982. **79**(17): p. 5254-7.

77.   Bai, D.S., et al., *The prognostic correlation of AFP level at diagnosis with pathological grade, progression, and survival of patients with hepatocellular carcinoma.* Sci Rep, 2017. **7**(1): p. 12870.

78.   Smuckler, E.A., M. Koplitz, and S. Sell, *alpha-Fetoprotein in toxic liver injury.* Cancer Res, 1976. **36**(12): p. 4558-61.

79.   Li, M.S., et al., *The promoting molecular mechanism of alpha-fetoprotein on the growth of human hepatoma Bel7402 cell line.* World J Gastroenterol, 2002. **8**(3): p. 469-75.

80.   Vibert, E., et al., *Progression of alphafetoprotein before liver transplantation for hepatocellular carcinoma in cirrhotic patients: a critical factor.* Am J Transplant, 2010. **10**(1): p. 129-37.

81.   Olsson, M., G. Lindahl, and E. Ruoslahti, *Genetic control of alpha-fetoprotein synthesis in the mouse.* J Exp Med, 1977. **145**(4): p. 819-27.

82.   Belayew, A. and S.M. Tilghman, *Genetic analysis of alpha-fetoprotein synthesis in mice.* Mol Cell Biol, 1982. **2**(11): p. 1427-35.

83.   Blankenhorn, E.P., et al., *Chromosomal location of the regulator of mouse alpha-fetoprotein, Afr-1.* Genetics, 1988. **119**(3): p. 687-91.

84. Perincheri, S., et al., *Hereditary persistence of alpha-fetoprotein and H19 expression in liver of BALB/cJ mice is due to a retrovirus insertion in the Zhx2 gene.* Proc Natl Acad Sci U S A, 2005. **102**(2): p. 396-401.

85. Peyton, D.K., et al., *The alpha-fetoprotein promoter is the target of Afr1-mediated postnatal repression.* Genomics, 2000. **63**(2): p. 173-80.

86. Morford, L.A., et al., *The oncofetal gene glypican 3 is regulated in the postnatal liver by zinc fingers and homeoboxes 2 and in the regenerating liver by alpha-fetoprotein regulator 2.* Hepatology, 2007. **46**(5): p. 1541-7.

87. Wang, X., et al., *Hyplip2, a new gene for combined hyperlipidemia and increased atherosclerosis.* Arterioscler Thromb Vasc Biol, 2004. **24**(10): p. 1928-34.

88. Gargalovic, P.S., et al., *Quantitative trait locus mapping and identification of Zhx2 as a novel regulator of plasma lipid metabolism.* Circ Cardiovasc Genet, 2010. **3**(1): p. 60-7.

89. Clinkenbeard, E.L., et al., *Liver size and lipid content differences between BALB/c and BALB/cJ mice on a high-fat diet are due, in part, to Zhx2.* Mamm Genome, 2019. **30**(7-8): p. 226-236.

90. Hillebrandt, S., et al., *Genome-wide analysis of hepatic fibrosis in inbred mice identifies the susceptibility locus Hfib1 on chromosome 15.* Gastroenterology, 2002. **123**(6): p. 2041-51.

91. Hall, R.A., S. Hillebrandt, and F. Lammert, *Exploring multiple quantitative trait loci models of hepatic fibrosis in a mouse intercross.* Mamm Genome, 2016. **27**(1-2): p. 70-80.

92. Jin, D.K. and M.H. Feuerman, *Genetic mapping of Afr2 (Rif): regulator of gene expression in liver regeneration.* Mamm Genome, 1998. **9**(3): p. 256-8.

93. Livak, K.J. and T.D. Schmittgen, *Analysis of relative gene expression data using real-time quantitative PCR and the 2(-Delta Delta C(T)) Method.* Methods, 2001. **25**(4): p. 402-8.

94. Waxman, S. and E. Wurmbach, *De-regulation of common housekeeping genes in hepatocellular carcinoma.* BMC Genomics, 2007. **8**: p. 243.

95. Junqueira, L.C.U., G. Bignolas, and R.R. Brentani, *A simple and sensitive method for the quantitative estimation of collagen.* Analytical Biochemistry, 1979. **94**(1): p. 96-99.

96. Iezzoni, J.C., *Diagnostic histochemistry in hepatic pathology.* Semin Diagn Pathol, 2018. **35**(6): p. 381-389.

97. Vogel, B., et al., *Determination of collagen content within picrosirius red stained paraffin-embedded tissue sections using fluorescence microscopy.* MethodsX, 2015. **2**: p. 124-134.

98. Mokdad, A.A., et al., *Liver cirrhosis mortality in 187 countries between 1980 and 2010: a systematic analysis.* BMC Med, 2014. **12**: p. 145.

99. Hirsova, P., et al., *Lipid-Induced Signaling Causes Release of Inflammatory Extracellular Vesicles From Hepatocytes.* Gastroenterology, 2016. **150**(4): p. 956-67.

100. Alegre, F., P. Pelegrin, and A.E. Feldstein, *Inflammasomes in Liver Fibrosis.* Semin Liver Dis, 2017. **37**(2): p. 119-127.

101.   Creasy, K.T., et al., *Zinc Fingers and Homeoboxes 2 (Zhx2) Regulates Sexually Dimorphic Cyp Gene Expression in the Adult Mouse Liver.* Gene Expr, 2016. **17**(1): p. 7-17.

102.   Jiang, J., et al., *Zhx2 (zinc fingers and homeoboxes 2) regulates major urinary protein gene expression in the mouse liver.* J Biol Chem, 2017. **292**(16): p. 6765-6774.

103.   Gould, B.S. and J.F. Woessner, *Biosynthesis of collagen; the influence of ascorbic acid on the proline, hydroxyproline, glycine, and collagen content of regenerating guinea pig skin.* J Biol Chem, 1957. **226**(1): p. 289-300.

104.   McGill, M.R., *The past and present of serum aminotransferases and the future of liver injury biomarkers.* EXCLI J, 2016. **15**: p. 817-828.

105.   Yilmaz, Y., et al., *Serum levels of osteoprotegerin in the spectrum of nonalcoholic fatty liver disease.* Scand J Clin Lab Invest, 2010. **70**(8): p. 541-6.

106.   Zhang, B. and H. Wu, *Decreased expression of COLEC10 predicts poor overall survival in patients with hepatocellular carcinoma.* Cancer Manag Res, 2018. **10**: p. 2369-2375.

107.   Sugihara, T., et al., *Screening of biomarkers for liver adenoma in low-dose-rate gamma-ray-irradiated mice.* Int J Radiat Biol, 2018. **94**(4): p. 315-326.

108.   Chen, J., et al., *DEPTOR induces a partial epithelial-to-mesenchymal transition and metastasis via autocrine TGFbeta1 signaling and is associated with poor prognosis in hepatocellular carcinoma.* J Exp Clin Cancer Res, 2019. **38**(1): p. 273.

109.   Knittel, T., et al., *Distribution and cellular origin of undulin in rat liver.* Lab Invest, 1992. **67**(6): p. 779-87.

110.   Yang, Y.M., et al., *Hyaluronan synthase 2-mediated hyaluronan production mediates Notch1 activation and liver fibrosis.* Sci Transl Med, 2019. **11**(496).

111.   Giebeler, A., et al., *c-Met confers protection against chronic liver tissue damage and fibrosis progression after bile duct ligation in mice.* Gastroenterology, 2009. **137**(1): p. 297-308, 308 e1-4.

112.   Natarajan, A., B. Wagner, and M. Sibilia, *The EGF receptor is required for efficient liver regeneration.* Proc Natl Acad Sci U S A, 2007. **104**(43): p. 17081-6.

113.   Michalopoulos, G.K. and M.C. DeFrances, *Liver regeneration.* Science, 1997. **276**(5309): p. 60-6.

114.   Pachnis, V., A. Belayew, and S.M. Tilghman, *Locus unlinked to alpha-fetoprotein under the control of the murine raf and Rif genes.* Proc Natl Acad Sci U S A, 1984. **81**(17): p. 5523-7.

115.   Arioka, Y., et al., *Pre-stimulated Mice with Carbon Tetrachloride Accelerate Early Liver Regeneration After Partial Hepatectomy.* Dig Dis Sci, 2015. **60**(6): p. 1699-706.

116.   Zhang, J., et al., *Two variants of quantitative reverse transcriptase PCR used to show differential expression of alpha-, beta- and gamma-fibrinogen genes in rat liver lobes.* Biochem J, 1997. **321 (Pt 3)**: p. 769-75.

117.   Xu, D., et al., *Protective effect of verapamil on multiple hepatotoxic factors-induced liver fibrosis in rats.* Pharmacol Res, 2007. **55**(4): p. 280-6.

118.   Zhu, W. and P.C. Fung, *The roles played by crucial free radicals like lipid free radicals, nitric oxide, and enzymes NOS and NADPH in CCl(4)-induced acute liver injury of mice.* Free Radic Biol Med, 2000. **29**(9): p. 870-80.

119. Yun, J.W., et al., *Determination of the key innate genes related to individual variation in carbon tetrachloride-induced hepatotoxicity using a pre-biopsy procedure.* Toxicol Appl Pharmacol, 2009. **239**(1): p. 55-63.

120. Shi, Z., A.E. Wakil, and D.C. Rockey, *Strain-specific differences in mouse hepatic wound healing are mediated by divergent T helper cytokine responses.* Proc Natl Acad Sci U S A, 1997. **94**(20): p. 10663-8.

121. Bhathal, P.S., et al., *Strain differences in mice in carbon tetrachloride-induced liver injury.* Br J Exp Pathol, 1983. **64**(5): p. 524-33.

122. Domenicali, M., et al., *A novel model of CCl4-induced cirrhosis with ascites in the mouse.* J Hepatol, 2009. **51**(6): p. 991-9.

123. Scholten, D., et al., *The carbon tetrachloride model in mice.* Laboratory Animals, 2015. **49**(1_suppl): p. 4-11.

124. Chang, M.L., et al., *Comparison of murine cirrhosis models induced by hepatotoxin administration and common bile duct ligation.* World J Gastroenterol, 2005. **11**(27): p. 4167-72.

125. Milani, S., et al., *Undulin RNA and protein expression in normal and fibrotic human liver.* Hepatology, 1994. **20**(4 Pt 1): p. 908-16.

126. Campana, L., et al., *Liver regeneration and inflammation: from fundamental science to clinical applications.* Nat Rev Mol Cell Biol, 2021.

127. Ozaki, M., *Cellular and molecular mechanisms of liver regeneration: Proliferation, growth, death and protection of hepatocytes.* Semin Cell Dev Biol, 2020. **100**: p. 62-73.

128. Reinius, B. and C. Kanduri, *Elevated expression of H19 and Igf2 in the female mouse eye.* PLoS One, 2013. **8**(2): p. e56611.

129. Adriaenssens, E., et al., *Steroid hormones modulate H19 gene expression in both mammary gland and uterus.* Oncogene, 1999. **18**(31): p. 4460-73.

130. Yue, X., et al., *Zinc fingers and homeoboxes 2 inhibits hepatocellular carcinoma cell proliferation and represses expression of Cyclins A and E.* Gastroenterology, 2012. **142**(7): p. 1559-70 e2.

VITA

COURTNEY P. TURPIN

EDUCATION

PhD   University of Kentucky, Nutritional Sciences

Dissertation: *Genetic Mouse Models Of Liver Disease:*
Potential Roles of Zhx2 (Afr1) and Afr2 in Damage and Regeneration   2018-Present
Committee: Drs. Brett Spear (chair), Nancy Webb,
Subbarao Bondada and Sean Thatcher

Committee: Drs. Shuxia Wang (chair), Brett Spear,   2015-2017
Nancy Webb and Subbarao Bondada

MS   Eastern Kentucky University, Biology   July 2015
Thesis: *"The effects of bacteriocin on the molecular*
mechanisms of Pseudomonas Aeruginosa biofilm production"
Advisor: Dr. Marcia Pierce

BS   Eastern Kentucky University, Biology   December 2012

Honors and Awards

ASBMB Graduate and Postdoctoral Travel Award   2020
Awarded travel grant to attend the 2020 Experimental Biology Meeting in San Diego.
Travel award enabled awardees to attend a day-long career development workshop.
Canceled due to COVID-19

NIH Training Grant T32 DK007778   2017
Awarded a two-year training grant that focuses on pharmacological
and nutritional approaches to prevent and treat metabolic-based disorders

NIH Bridging the Gap Grant R25 GM102776   2013
Awarded a two-year grant that focuses on increasing participation
of underrepresented students in science disciplines

Research Experience

University of Kentucky, Lexington, KY   2015 - present
    Advisor: Dr. Brett Spear (2017-present)

    Advisor: Dr. Shuxia Wang (2015-2017)

Eastern Kentucky University, Richmond, KY   2013 - 2015
    Advisor: Dr. Marcia Pierce

Eastern Kentucky University, Richmond, KY   2012
    Advisor: Dr. Rebekah Waikel

Teaching Experience

Eastern Kentucky University, Richmond, KY   2013
Instructor, Latino Leadership and College Experience Camp
- Developed, organized, and led activities involving laboratory techniques

Eastern Kentucky University, Richmond, KY   2013
Instructor, STEM Gifted and Talented Summer Camp
- Developed, organized, and led activities involving laboratory techniques

Eastern Kentucky University, Richmond, KY   2013
Lab Instructor, Cell and Molecular Biology
- Lectured during lab activities
- Administered grades

Publications

Peer-reviewed Publications

Clinkenbeard, EL, **Turpin, C**, Jiang, J, Peterson, ML and Spear BT. *Liver size and lipid content differences between BALB/c and BALB/cJ mice on a high-fat diet are due, in part, to Zhx2.* Mammalian Genome. 30(6-7): 226-236. 2019. PMID: 31321500; PMCID: PMC6761023.

Jain A, Tripathi R, **Turpin CP**, Wang C, Plattner R. *Abl kinase regulation by BRAF/ERK and cooperation with Akt in melanoma.* Oncogene. 36(32):4585-4596. 2017. PMID: 28368422; PMCID: PMC5552414.

Li Y, **Turpin CP**, Wang S. *Role of thrombospondin 1 in liver diseases.* Hepatology Research. 47(2):186-193. 2017. PMID: 27492250; PMCID: PMC5292098.

Additional Publications

Ghoweri, A, **Turpin, CP** and Police, S. 3 Tips to Increase Mental Acuity. Health and Wellness Magazine. December 2019.

Turpin, CP and Police, S. 4 Nutrition Tips for Weight Management in 2020. Health and Wellness Magazine. December 2019.

Peng, H, **Turpin, CP,** Xia, M. Vitamins and Minerals that Help Painful Periods. Health and Wellness Magazine. June 2019.

Schnell, D. **Turpin, CP,** Larian, N. Performance Nutrition: 3 Tips for Any Athlete. Health and Wellness Magazine. February 2019.

Presentations

Poster (presenter): *"Zinc Fingers and Homeoboxes 2 (Zhx2) deficiency modulates adiposity when fed a western diet"* Barnstable Brown Obesity & Diabetes Research Day, 2019.

Seminar: *"A Potential Role for Zhx2 in Adipose Tissue in Lipid Homeostasis"* Department of Pharmacology and Nutritional Sciences Seminar Series, 2019.

Poster (co-author): *"Role of transcription factor zinc fingers and homeoboxes 2 (Zhx2) in diethylnitros-amine (DEN)-induced liver cancer development"* Markey Cancer Center Research Day, 2019.

Oral Presentation: *"Thrombospondin 1 (TSP1) Deficiency Protects Against Diet-induced Fatty Liver Disease"* Saha Cardiovascular Research Day, 2017.

Poster (presenter): "*Thrombospondin 1 (TSP1) Deficiency Protects Against Diet-induced Fatty Liver Disease"* Saha Cardiovascular Research Day, 2017.

Seminar: *"The Role of Thrombospondin 1 (TSP1) in Diet-induced Fatty Liver"* Department of Pharmacology and Nutritional Sciences Seminar Series, 2017.

Poster (presenter): *"Thrombospondin 1 (TSP1) Deficiency Protects Against Diet-induced Fatty Liver"*Barnstable Brown Obesity and Diabetes Research Day, 2017.

Oral Presentation: *"Role of CD47 in Brown Adipose Tissue Function"* Department of Pharmacology and Nutritional Sciences Retreat, 2017

Poster (co-author): *"CD47 deficiency protected mice form non-alcoholic fatty liver disease"* Barnstable Brown Obesity and Diabetes Research Day, 2016.

Poster (co-author): *"Role of macrophage-derived TSP1 in Obesity and insulin resistance: A study with tissue specific TSP1 deletion model"* Barnstable Brown Obesity & Diabetes Research Day, 2016.

Poster (presenter): *"The role of myocyte-enriched calcineurin-inhibiting protein (MCIP1) in estrogen mediated repression of cardiac hypertrophy"* Annual Biomedical Research Conference for Minority Students, Nashville, TN, 2013.

Professional Training

NIH Career Symposium
National Institutes of Health, Webinar, 2020.

Integration of Toxicology and Pathology in Drug Development and Discovery
Eli Lilly Global Headquarters, Indianapolis, IN, 2019.

South East Lipid Conference
Lexington, KY, 2017, 2018

Life Sciences Career Bootcamp at the Annual Derby Partnering Summit
Hotel Covington, Covington, KY, 2017.

Preparing Science Professionals
University of Kentucky, Lexington, KY, 2017.

Good Research Practices Certification, UK GRP, 2016.

Professional Affiliations

Vice-President, Nutritional Sciences and Pharmacology Student Association, 2020-Present
    Organized professional development, outreach, and social events for its members.

President, Nutritional Sciences and Pharmacology Student Association, 2019-2020
    Organized professional development, outreach, and social events for its members.

Secretary, Nutritional Sciences and Pharmacology Student Association, 2018-2019
    Maintained minutes and led correspondence for the student association.

American Association for Biochemistry and Molecular Biology (ASBMB), 2013-2015, 2020

American Society for Microbiology (ASM), 2014-2015

Professional Service

Webinar and Q&A regarding the Strategic Plan for NIH Nutrition Research with Dr. Christopher Lynch (Director, Office of Nutrition Research, NIDDK and Executive Secretary, NIH Nutrition Research Task Force), Conference Organizer and Webinar Leader, 2019

Community Service

FoodChain
Chat n' Chow Server, Lexington, KY, 2019

UK SURES Program
Poster Judge, Lexington, KY, 2018; Near Peer Mentor, University of Kentucky, 2019

Fayette County Science Fair
Science Fair Judge, Lexington, KY, February 2019, February 2018, February 2017

Lexington March of Science
Booth Presenter, Lexington, KY, 2017

Stonewall Elementary Science Night
Presenter and organizer, Lexington, KY, 2017

Daniel Boone Elementary Career Day
Presenter, 2016